Mainstreaming multi-mission satellite observations in operational water resources management

Nishan Kumar Biswas

A dissertation

submitted in partial fulfillment of the

requirements for the degree of

Doctor of Philosophy

University of Washington

2021

Reading Committee:

Faisal Hossain, Chair

David Butman

Hyongki Lee

Program Authorized to Offer Degree:
Department of Civil and Environmental Engineering

University of Washington

Abstract

Mainstreaming multi-mission satellite observations in operational water resources management

Nishan Kumar Biswas

Chair of the Supervisory Committee:
Professor Faisal Hossain
Department of Civil and Environmental Engineering

Effective water management depends on the accuracy of three key components: monitoring, forecasting, and quantification of human impacts. Understanding complex hydrological processes and the vast amount of data are prerequisites for monitoring and prediction of water resources. Although ground-based measurement is the best way to monitor, it is impossible to measure all relevant geophysical variables at the required spatiotemporal scale. As a complementary source, satellite remote sensing has proven its application potential during the last decade. A single satellite's observation capability was further enhanced by using the compound eye view afforded by multiple satellites. A combination of multi-mission platforms, numerical modeling, and advances in computational resources facilitated the way of better water management. The

overarching goal of this dissertation was to provide a proof-of-concept of mainstreaming the application of multi-satellite observation-based water management in data-limited regions.

Among the three primary water management components, a compound-eye satellite-based monitoring method was developed to improve river height from the altimeter satellite in the second chapter. In the proposed method, river morphology information from ancillary satellites (Landsat and Sentinel 1-SAR) was extracted and applied to get the altimeter height based on derived morphology. The accuracy of the method was tested over river locations with diverse hydraulic characteristics. It was found that the river-morphology based method can improve the conventional altimeter height estimation method in dynamically changing rivers. The forecasting component of water management was studied by applying satellite observations and numerical weather prediction (NWP) model outputs in extreme event forecasting and presented in the third chapter. Nowcast and forecast meteorological parameters (without applying computationally expensive downscaling methods) and land-surface variables were forced in a hydrologic-hydrodynamic framework to generate skillful forecasts for up to 5 days. The method was globally scalable and economically feasible for developing nations. In the fourth chapter, the quantification of the human impacts component of water management was studied. A global reservoir monitoring framework was built to investigate the impact of existing and proposed dams. A satellite data-based mass balance approach was used to quantify reservoir outflow. In the last chapter, this framework was used to study the impact of existing reservoirs and to optimize the benefits of future dams/reservoirs. This tool helped the user community understand the global picture of how dams and reservoirs are impacting natural flow.

The ability to quantify human impacts has broad implications on water management decisions. This dissertation promoted societal applications of satellites among water managers and policymakers through the four studies over three critical water management components. The greater transparency in water resources management and operations from this study allowed for more informed decisions regarding flood management and water supply security. The collection of completed works on water management showed how the vantage of space could “level the playing field” between nations and stakeholders competing for limited water resources, ultimately leading to greater cooperation.

Table of Contents

List of Figures

List of Tables

Acknowledgments

I would like to express my sincere gratitude to my academic advisor Dr. Faisal Hossain for his continuous support, encouragement, and patience. His dynamism, guidance, thoughtful insights, and enthusiasm over the last five years helped me accomplish my research objective. His motivation to do the greater good for the human being rather than just doing research and publishing articles inspired me to carry out my current doctoral research. I am greatly indebted to my advisor for giving me the opportunity to research with him and pursue my goal.

I would like to thank my dissertation committee members, Dr. David Butman and Dr. Hyongki Lee, for their valuable time, interest, energy and for providing their feedback that immensely helped improve the dissertation's content. Also, I would like to thank Dr. Erkan Istanbulluoglu and Dr. Bart Nijssen for their time and support during my Ph.D. qualifying exam.

It has been a pleasure working with the Sustainability, Satellites, Water and Environment (SASWE) Research Group members. A special thanks to all the members for their kind cooperation, continuous support, and encouragement during this study. I also appreciate all the help and support from the former SASWE members Dr. Matthew Bonnema, Dr. Safat Sikder, Dr. Xiaodong Chen, and Asif Mahmood.

I am grateful to all my family members, especially my parents, for their great inspiration and for reminding me of who I am. I also want to mention my father-in-law Prokash Chandra Sharma for his encouragement to pursue a doctoral degree.

I thank the following funding institutions for making this work possible:

- Ivanhoe Foundation
- NASA Applied Sciences Program
- Jet Propulsion Laboratory

Finally, while writing this dissertation, chapter 2 has been published in the Remote Sensing of Environment. Chapter 3 has been published in the Journal of Hydroinformatics, Chapter 4 is under review in Environmental Modelling and Software, and Chapter 5 is under review in Earth's Future. These chapters are:

Chapter 2:

Biswas, N. K., Hossain, F., Bonnema, M., Okeowo, M. A., & Lee, H. (2019). An altimeter height extraction technique for dynamically changing rivers of South and South-East Asia. Remote Sensing of Environment, 221, 24–37. https://doi.org/10.1016/j.rse.2018.10.033

Chapter 3:

Biswas, N. K., Hossain, F., Bonnema, M., Aminul Haque, A. M., Biswas, R. K., Bhuyan, A., & Hossain, A. (2020). A computationally efficient flash flood early warning system for a mountainous and transboundary river basin in Bangladesh. Journal of Hydroinformatics, 22(6), 1672-1692. https://doi.org/10.2166/hydro.2020.202

Chapter 4:

Biswas, N.K., Hossain, F., Bonnema, M., Lee, H., Chishtie, F. (2020). A Global Reservoir Assessment Tool for Predicting Hydrologic Impact and Operating Pattern of Existing and Planned Reservoirs, Environmental Modeling and Software (In revision).

Chapter 5:

Biswas, N.K., Hossain, F. (2021). A multi-decadal Analysis of Impact on Water availability due to Reservoir Operation in Ungauged Regions, Earth's Future (In revision).

DEDICATION

To Maumita, Arindam, and Anindya, for their unwavering love and support.

Chapter 1 Introduction

1.1 Background of the study

The scarcity of water resources is growing day-by-day as a result of expanding population demand, environmental concerns, and climate change effects. Effective water management is necessary for satisfying the growing demands and addressing the human impacts on these resources. An example of how human activities (such as dam development) impact river fragmentation and flow regulation is shown in figure 1.1. Figure 1.1 illustrates the combined impacts of all the current and planned hydropower reservoirs (Grill et al., 2015).

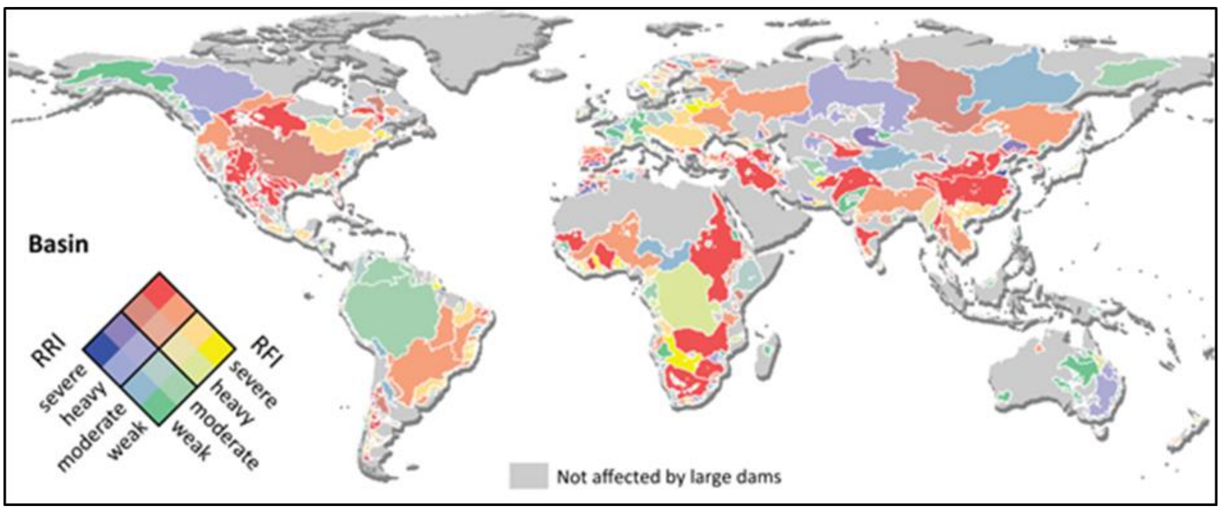

Figure 1.1 Combined impacts of the dams of 2030 in which all large hydropower dams currently planned or under construction are built (RFI and RRI means River fragmentation index and river regulation index) (Source: Grill et al., 2015)

Quantifying human impacts on the natural hydrologic cycle is necessary for short and long term decision making, maximizing stakeholder benefits, and managing water-related hazards such as floods and droughts, public safety, and infrastructure resilience (Lauri et al., 2012; Pokhrel et al., 2012; Woldemichael et al., 2012). To quantify the impact, water managers need to monitor the state of the resources in nowcast and forecast settings. Understanding of a complex hydrologic system, a vast amount of data requirement, computational power, and qualified human resources are necessary to monitor and predict the availability of water resources.

The best source of hydrologic monitoring is ground-based measurements with sufficient spatial and temporal coverage, which at times can be scarce or absent. Some of the primary reasons for ground-based data unavailability are 1) limited gauge measurements across the world (Alsdorf et al., 2007), 2) dearth of in-situ monitoring networks (Shiklomanov et al., 2002; Vörösmarty et al., 2002), 3) poor quality of measurement, 4) spatial and temporal inconsistency of the measurements (Alsdorf et al., 2007; Yoon et al., 2019), and 5) ineffective transmission of data into information, 6) budgetary constraints for the developing nations (Biswas & Hossain, 2018; Siddique-E-Akbor et al., 2014), 7) data-sharing policy between riparian countries (Gerlak et al., 2011; Marcé et al., 2016; Sikder & Hossain, 2015; Thu & Wehn, 2016; Ward, 2013). Recently, satellite-based observations have addressed some of the limitations of in-situ monitoring by providing a tremendous amount of information (Biswas & Hossain, 2018; Kansakar & Hossain, 2016; Sheffield et al., 2018; Zhang & Gao, 2016).

Remote sensing has proven its application potential in managing water resources in various aspects with the availability of data from different sensors of various wavelengths and a wide range of spatiotemporal, radiometric, and spectral resolutions (Govender et al., 2007; Nijssen & Lettenmaier, 2004; Tucker & Choudhury, 1987). Despite these advancements, the quality of satellite observations may not be accepted due to its indirect method of measurement (Biswas & Hossain, 2018; Huang et al., 2018). One way to minimize the uncertainty is to use the combined observational power of multiple satellites that overlaps spatially and temporally to monitor various aspects of Earth (Hossain et al., 2016). Currently, there are a number of satellites available (figure

1.2) to monitor the earth's water resources, which can be harnessed to produce more durable societal benefits. With such a compound eye view possible from the satellites, different observations across multiple platforms can be used simultaneously to increase monitoring accuracy (Chipman, 2019; Tourian et al., 2015). For example, Landsat satellite provides the water extent, and satellite altimeter provides heights of inland features without knowing its composition and characteristics. By ingesting information from both the sources, river height over the river surface extent can be extracted by minimizing the possibility of non-water pixels inclusion.

Figure 1.2 The current satellite missions available to monitor earth's water resources and it's dynamics (Source: NASA)

Forecasting is another component of operational water management that can capitalize on the potential of multiple satellites along with numerical modeling. Recent advancement has been made in river flood forecasting (Crochemore et al., 2016; Lee et al., 2015; Sharma et al., 2019; Sikder & Hossain, 2019) using multiple satellite observations. Despite the advancement, it is not sufficient in forecasting extreme events (i.e., flash floods) because of its complex characteristics (Borga et al., 2008; Hapuarachchi et al., 2011; Wu et al., 2019). For example, accurate forecasting of flash floods depends on the ability of hydrological and hydrodynamic models and observational data to represent the processes at the small scales of interest (Yatheendradas et al., 2008). Besides the discharge and river flow forecasts, accurate mapping of the spatial extent of inundation forecasts is necessary to trigger location-specific warnings, damage assessment as well as to plan relief and rehabilitation. Till now, there are no published studies where hydraulic processes have been represented along with hydrological models in an operational framework for flash flood forecasting. Possible reasons for the lack of forecasting framework might be due to i) complexity in development, calibration, and validation of multiple models and their integration, ii) dependency on extensive meteorological, hydrological and topographic data, and iii) excessive computation time for the simulation of combined meteorological-hydrological-hydraulic processes. Publicly available weather forecast data from various agencies and improved numerical weather prediction (NWP) models are untapped resources that can be utilized for operational forecasting.

One hurdle that remained in achieving effective water management is the gap between scientific research and the societal application of multisensor platforms in an operational environment. Advanced understanding of remote sensing and modeling is a constraint for stakeholder agencies to use multiple satellites in real-time monitoring and management. Fortunately, there have been technological advancements that can now address computational resource constraints. Advancement in the cloud and distributed computing with big data handling reduced the requirement of high internet bandwidth to process large-scale datasets. As an example, Google Earth Engine (GEE) (Gorelick et al., 2017) combines a multi-petabyte satellite imagery data with planetary-scale analysis facility applied in several water-related studies (Biswas et al., 2019; Bonnema & Hossain, 2017; Zhao and Gao, 2018).

With the availability of an unprecedented amount of satellite data and computational advancements, this proposal aimed to address the existing challenges and builds the proof-of-concept to empower the water management community. This study applied multiple satellite observations to not only address the current limitations in quantifying human impacts but also presented a proof-of-concept to operationalize in computationally-constrained regions of the world.

1.2 Research Objectives

The study's overarching goal was to use multi-mission satellite observations in advancing monitoring and forecasting component water resources management to quantify human intervention. The research question was further subdivided into the following objectives:

a. Establishing a river monitoring system using multi-source satellite data
   Research questions:
   - *How much improvement in river monitoring can be achieved using ancillary satellite platforms?*
   - *Under what geophysical conditions do the use of information from ancillary satellite platforms maximize monitoring accuracy?*

b. Developing a computationally efficient forecasting technique for extreme events
   Research questions:
   - *What are the optimal combination of scale, time-step, and complexity for topographic and hydrometeorological data to produce forecasts?*
   - *What is the baseline accuracy of a forecasting system that is achievable using NWP weather forecasts?*

c. Quantifying the impact of existing and planned reservoirs on natural hydrology
Research objective:
- *Build a global monitoring framework for impact analysis of existing and planned reservoirs*
- *Quantifying the impact of reservoirs in natural river flow at the continental and regional scales*

1.3 Outline of the dissertation

This dissertation is organized as follows:

Chapter 2: Establishing a river monitoring system using multiple satellites

The objective of this chapter was to improve river monitoring from satellite altimeter using ancillary satellite datasets. Here, satellite imagery derived river morphology-based technique was proposed to improve river heights from Jason 3 altimeter. This study addressed a potential limitation in current approaches to altimeter height extraction for dynamically varying rivers (highly braided and meandering rivers with seasonality and complex topography). In the traditional methods, altimeter processing techniques were limited to large rivers that remain relatively stationary in width and course over time. Thus, there was always a possibility of mixing of non-water features of the radar return when the size of the river was smaller than the altimeter radar footprint or when the rivers were highly variable in time. Here, river morphology information from Landsat and Synthetic Aperture Radar (SAR) of Sentinel-1 was applied to filter out non-water radar returns in different methods. More than 150 potential locations in South and South-East Asia were identified where satellite altimeter could provide skillful data on river heights. The proposed methods were checked in locations with unique topographical features and hydrodynamic characteristics. From the findings, the picture that emerges is that river morphology can consistently improve the estimation of heights in morphologically active rivers compared to the conventional methods. Also, the SAR based imagery technique performed consistently better than the Landsat imagery to improve height extraction. This chapter's finding has been published in Remote Sensing of Environment Journal (Biswas et al., 2019).

Chapter 3: Developing a computationally efficient forecasting technique for extreme events

In the second chapter, the applicability of the combination of multiple satellite observations in hydrologic extreme event forecasting was examined. This chapter's objective was to explore the optimal combination of scale, time step, and complexity in topographic and hydro-meteorological observations for developing a flashflood forecasting framework. A mountainous and transboundary river basin in Bangladesh was chosen as the study area which experiences flash floods nearly every year during the pre-monsoon season (March-May). The core component of the framework was based on a globally available real-time numerical weather forecast. The precipitation forecasts were forced into the hydrologic-hydrodynamic framework without any computationally expensive downscaling. Besides the discharge and river flow forecasts, an accurate mapping of the spatial extent of inundation forecasts was also generated to trigger location-specific warnings. Based on the performance of the forecasts in the reference stations, it was found that the framework able to produce a skillful flash flood early warning for up to 5 day lead time. In addition to the computation time and forecast accuracy considerations, some other key features of the framework considered during development were i) economic constraints and ii) scalability of the framework. The framework was built using open-source models and publicly accessible global datasets with near-real-time availability, which is essential in scaling to similar topographic and hydrometeorological conditions and for economically constrained countries. The finding of this chapter has been published in the Journal of Hydroinformatics (Biswas et al., 2020)

Chapter 4: Building of a global monitoring framework for impact analysis of existing and planned reservoirs

After finishing the monitoring and forecasting component of water management, this chapter was focused on the building of a global monitoring framework for impact analysis of existing and planned reservoirs. According to Zarfl et al. (2014), dam construction is on the rise in developing nations. In this study, a multi-satellite based method was proposed to monitor these dams, which is necessary to understand the downstream hydrologic impacts and better planning and management. The framework was developed based on a mass balance approach to monitor reservoir state (i.e., inflow, outflow, storage change). Reservoir inflow was calculated using meteorological observations forced in a globally calibrated hydrological model. The storage change was calculated based on the reservoir area-elevation relationship (from reservoir topography) and satellite imagery analysis. Reservoir outflow was estimated from the inflow and storage change and evaporation component. Initially, 1598 reservoirs from South America, Africa, and South-East Asia were added to the framework. The developed software framework was validated against in-situ data of 77 reservoirs for storage change and 18 stations of large river basins for hydrological model simulated discharge. The developed online software framework for reservoir monitoring called RAT is a tool that is the first of its kind to provide detailed information for existing and planned reservoirs across the world in near real-time. This tool helped the scientific community to obtain a global picture of reservoir monitoring, how they are being operated, and how they are impacting natural river flow and its variability. It also facilitated the feasibility study of proposed/planned dams by providing reservoir capacity and inflow availability. The finding of this chapter has been submitted in the Environmental Modelling and Software Journal.

Chapter 5: A multi-decadal Analysis of Impact on Water availability due to Reservoir Operation in Ungauged Regions

The multi-satellite based reservoir monitoring framework proposed in chapter 4 was used in this chapter to demonstrate its application potential. The research objective of this chapter was to find the pattern of reservoir storage change over the last three decades and to identify the potential drivers of reservoir storage change. The framework was used to generate a multi-decadal record of reservoir storage change. The variability of storage change was studied based on the dam size, age, and hydro-climatic variability. Reservoir variability was compared with trends of four critical hydrologic parameters (precipitation, runoff, evaporation, and Palmer Drought Severity Index) to understand the role of natural drivers. It was found that the reservoirs in Africa were losing storage at a rate of more than 1% per year of the installed capacity. Also, in most cases, the drought index was the predominant driver of change in storage.

Chapter 2 An Altimeter Height Extraction Technique for Dynamically Changing Rivers of South and South-East Asia

Note: This chapter has been published mostly in its current form in *Remote Sensing of Environment* (Biswas et al., 2019).

Abstract

A new approach is proposed in this study to maximize the skill of satellite altimeter-derived heights by utilizing river extent information from additional sensors. We apply this approach for the JASON-3 nadir altimeter. First, locations were identified in the South and South-East Asia region as potential candidates for this approach based on river extent. Information on river extent composed of river width and course (i.e., path) from visible (Landsat) and Synthetic Aperture Radar (SAR) platform (Sentinel-1). The extent-based approach was applied to filter out nonwater radar returns in two methods: 1) River Mask (RM) based K-means (KM) clustering (hence, RM+KM) and 2) K-means clustering embedded with River Mask (RM) (hence, KMRM). Both methods were validated over 12 locations with long records of in-situ height observations and distinct river characteristics. The maximum benefit observed in utilizing dynamic river mask is during low flow season when the probability of non-water radar signal contamination is highest. For highly varying seasonal widths, satellite imagery on river conditions, as an ensemble of techniques, yields heights with higher accuracy. An average RMSE improvement of 40% in 8 out of 12 stations is observed. Overall, at least one of the two dynamic mask-based techniques studied consistently outperformed the conventional altimeter height extraction technique based on a fixed river mask. Information on river mask or extent can play an important role in highly meandering

rivers as the deviation between actual satellite altimeter passes and nominal passes can be considered during the heights extraction. Compared to visible (Landsat) imagery, SAR was much more effective at improving altimeter height extraction because of the all-weather capability during frequently cloudy conditions. The practicality of the river mask-based approach for altimeter height extraction needs to be carefully considered by the operational end-user based on available computational resources and the latency that can be afforded. An ensemble of morphology-based techniques using SAR imagery is likely the future of satellite altimeter-based river height extraction in South and South-East Asia, where rivers are increasingly impacted by human regulation, encroachment, and seasonality.

2.1 Introduction

Satellite altimetry is a technique that uses orbiting spacecraft to make measurements of the height of Earth's surface. The two-way traveling time of a pulse emitted by the antenna onboard a satellite and its reflection from the earth's surface yields the range measurements of surfaces. The surface height of any target is determined by the difference between the satellite orbit and the altimeter range measurement. Although satellite radar altimeters today are primarily designed to monitor the dynamic topography of the ocean, there are several advantages of satellite altimeter over the land. Satellite altimeter measurements of terrestrial water storage provide unique capabilities with consistent and accurate measurements with near real-time availability, which is essential for decision-making purposes in water resources management (Birkett, 1995; Berry et al., 2005; Calmant and Seyler. 2006).

Some examples of the advantages of satellite altimeters on inland water studies are open access of the datasets, near real-time availability, day/night and all-weather conditions, and long-term observations for seasonal and inter-annual variation since 1991. Radar altimeters have demonstrated their value for measuring heights of inland water bodies, such as rivers and lakes (Birkett, 1995; Ponchaut & Cazenave, 1998; Medina et al., 2008; Cretaux et al., 2011). Swenson & Wahr (2009) used satellite-derived storage changes of a small lake downstream of Lake Victoria to estimate outflow. Muala et al. (2014) used altimetry-derived storage changes and in-situ inflow measurements to estimate the discharge from Lake Nasser and Rosaries Reservoir in the Nile Basin. Gao et al. (2012) characterized the potential of satellite altimeter in deriving stage time-series and changes in storage estimation of large lakes. Bonnema et al. (2016) and Bonnema & Hossain (2017) estimated reservoir outflow using a mass balance approach as a function of hydrologic controls, satellite altimeter datasets and, visible imagery products. Altimetry measurements have demonstrated an ability to provide reliable water stages over rivers (Birkett, 1998; Frappart et al., 2006; Biancamaria et al., 2011; Michailovsky et al., 2012) and floodplains (Lee et al., 2009; Santos da Silva et al., 2010). Biancamaria et al. (2011) and Hossain et al. (2014) collectively provided proof of JASON-2 satellite altimetry application for transboundary flood forecasting in the Ganges and the Brahmaputra river basin using river heights.

One of the significant challenges of height extraction using satellite altimetry is the removal of non-water pixels and outliers within altimeter footprints (Sulistioadi et al., 2015). With the advances in satellite altimetry and its diverse applications, a considerable amount of research has been carried out on the continuous improvement of algorithms. Most of the published methods for the detection of water features were developed by studying the waveform of returned power (e.g., Birkett, 1995; Birkett, 1998). Frappart et al. (2006) proposed the Ice-1 retracker to be the most accurate retracker for Envisat altimetry measurements over large rivers. Birkett & Beckley (2010) used land mask flags to detect the outliers in altimeter data using a manual observation of the returned signals. Huang et al. (2013) used the radar return threshold reflectivity and Shuttle Radar Topography derived Digital Elevation Model (DEM) to remove land pixel outliers from ICESat data. Schwatke et al. (2015) used the Kalman filter approach to detect the outlier in altimeter-derived heights. Most recently, Okewo et al. (2017) proposed an automatic water height extraction algorithm based on a combination of K-means clustering, interquartile range (IQR), and statistical error computation for monitoring lakes and reservoirs at the regional and global scales without using any ancillary dataset. This method has been successfully used in estimating water heights of lakes, reservoirs, and large rivers using altimeter data. Tourian et al. (2015) used the Landsat 7 images to extract the narrowest river mask to subset altimeter datasets to avoid contamination from neighboring topography. Hall et al. (2011) extracted ICESat laser altimeter heights over Amazon to determine the datum correction of ground-based measurements. They used Landsat Thematic Mapper (TM) images to identify ICESat satellite passes closest to gauge locations. The currently available altimeter processing techniques are useful for large rivers that remain relatively stationary in width and course over time. To the best of our knowledge, the river's physical characteristics have not been considered for improving altimeter height extraction techniques for rivers that frequently vary in width and flow direction. Almost all the developed algorithms require the assumption of a 'fixed' (or stationary) river extent. Thus, there is always a possibility of mixing of non-water features of the radar return when the size of the river's geophysical features is smaller than the altimeter radar footprint or when the features are highly variable in time.

For example, large variation in river width and river stage due to seasonality can lead to contamination of non-water pixels even in large rivers. Figure 2.1(a) shows the variation in the Ganges River's width at the Bhagalpur station in India. During the wet season (July to September), the river benefits from a 9 km long track from the JASON-3 altimeter, and thus, is more likely to have a significant number of altimeter signals on water. However, during the dry season (see February 2016 and March 2017 images), the track along the river reduces to 3km, and most of the signals within the altimeter footprint tend to be on land if caution is not applied. For such rivers and locations, there remains a significant probability of non-water radar signal contaminating the estimation of river height.

In the case of braided rivers during the dry season, sandbars and river island formations may also lead to incorrect land surface height selection when a predefined river width and shoreline are assumed. Some rivers are very dynamic, and the course of those rivers change throughout the year. Long-term variation in river course and river width makes the fixed river extent approaches less meaningful. In addition to river extent variation, there can also be a deviation between satellite visit and nominal ground track (Lee, 2008). In highly meandering rivers, it is almost impossible to define a river extent based only on the nominal altimeter track. Altimeter signals within the defined bounds can be entirely outside of the river, as shown in figure 2.1(b) for Annapurnaghat station in the Barak River in India. In the figure, selected correct and incorrect water pixels due to static latitude range are shown. It can be seen that a considerable amount of signals were incorrectly selected as water pixels. Even some of the actual JASON-3 altimeter passes are completely outside the actual river course, and they were considered as water features when the static latitude bound is assumed.

In addition to the river's variation in width and course, there are other limitations for river height estimation. For example, high neighboring topography around the river can cause the misinterpretation of heights from the inappropriate returned pulse. Heavy precipitation, intense wind events, surface slope variation, tidal effects in rivers, and ice presence affect satellite altimeter data quality.

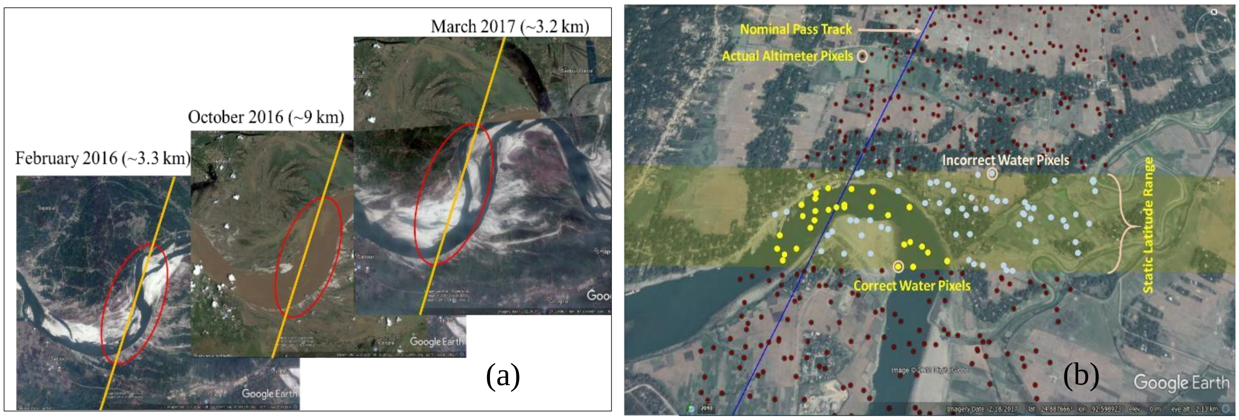

Figure 2.1 (a) JASON-3 Altimeter travel distance variation in Ganges River at Bhagalpur Station (Latitude: 25.2990, Longitude: 87.1210); (b) Deviation of actual signals from nominal pass track of Altimeter at the location of Annapurnaghat station of Barak River (Latitude: 28.880, Longitude: 92.60, Altimeter Pass: 053, Geophysical Data Records used: 2/19/2016 to 10/16/2017).

Thus, additional imagery on river's changing conditions (i.e., river extent in the context of this study) is required to maximize the accuracy of satellite altimeter in rivers that are highly dynamic and driven by seasonal hydrology. Such rivers are common in South and South-East Asia, where the monsoon system drives contrasting changes in physical dimensions within a year. Our proposed solution presented in this study is premised on the notion that an altimeter's observational capability needs a priori delineation of the dynamic river shoreline. Additional observational platforms such as visible/infrared (Landsat/MODIS, Sentinel-2) or SAR (Sentinel1, Radarsat, ALOS-PALSAR) or ground-based arrangements (GPS sensors) can provide this *a priori* dynamic information on the river's morphological state. Because ground-based methods not globally scalable, satellite observations are the only viable method. The visible and SAR platforms may also be complementary with the visible platform that provides long historical records since the 1980s characterizing dynamic rivers' trend. SAR also provides all-weather capability during cloudy situations, unlike visible imagery. We believe that if we dynamically assimilate the information on the river's state into altimeter height estimation, the accuracy can be improved for rivers that experience tremendous variability in shape and direction as a function of time.

The objective of this study is to utilize multiple satellites to improve the accuracy of altimeter-derived river heights. We have developed herein a dynamic river mask-based technique based on a systematic investigation of three potential (candidate) approaches. Our development work has led us to a set of rules and pre-conditions for which such a river extent based height extraction technique is useful. This set of rules, which we also document in this study, informs the user of situations when the more complex approach based on river extent may be warranted in place of the conventional technique of a fixed river mask that is more widely used. Hereafter, we use the term 'mask' or 'extent' interchangeably to refer to the river and its dynamic boundary.

The specific research questions we ask in this study are: How much can the use of river extent information from ancillary satellite platforms improve nadir altimeter based height estimation for dynamically changing rivers? Under what geophysical conditions do river extent information on river width and shoreline maximize height accuracy and why? Answers to our questions can potentially help the remote sensing community for water management with two dual goals: 1) to maximize the skill of altimeter heights for dynamically changing rivers in an automated and operational setting, and 2) to automatically minimize the misuse of altimeter data in situations where it is unlikely to have any skill for surface water applications. Currently, the second goal is achieved by manually exploring each virtual station (i.e., where an altimeter crosses a river) and observing the response of heights over a long period to infer the accuracy for water height estimation. While this is the most accurate method by the book, it is not a feasible method if our goal is to maximize the application of altimeter data over land globally. For example, for JASON-3, there are more than 3500 such river locations worldwide, and thus it is impossible to apply a manual approach to identify where and when altimeter data will yield skillful data on river heights and where/when it will not. Our proposed methodology can accelerate the identification of locations where altimeter is likely or unlikely to be useful.

2.2. Data and Methods

2.2.1 Datasets

In this study, we used 20-Hz Geophysical Data Records of the JASON-3 along-track satellite. Datasets used from cycle 0 to cycle 61 and dated from 12th February 2016 to 20th October 2017 were downloaded from ftp://ftp.nodc.noaa.gov/pub/data.nodc/JASON3/gdr/gdr/. A global river bankfull width and depth database developed by Andreadis et al. (2013) was downloaded from http://gaia.geosci.unc.edu/rivers/ and used to develop a reach specific bankfull width database. This dataset comprised reach-based width (5 percentile, 50 percentile, and 95 percentile), and 95-percentile width is used as the river's bankfull width. A continuous global large river network dataset was downloaded from Natural Earth Server (http://www.naturalearthdata.com/downloads/10m-physical-vectors/10m-rivers-lakecenterlines/). The methodology for developing a bankfull width database using the above river datasets (bankfull width database from Andreadis et al. (2013) and continuous river network dataset from Natural Earth) is described in more detail in section 2.2.2.1.

Dynamic river extent datasets (Landsat and SAR) were processed using Google Earth Engine (GEE). Landsat 8, Collection 1, Tier 1 datasets were cropped according to the Region of Interest (named ROI and explained in section 2.2.2.1). Normalized difference water index (NDWI) and cloud score were calculated using the GEE simple cloud scoring algorithm (SCR). River extent was also derived from Sentinel-1 datasets using GEE. During the processing of 10 m resolution Sentinel-1 imagery, “VV” polarization was used, and the backscatter coefficient's monthly median values were calculated for extracting a monthly average river extent. The backscatter coefficient of an extremely low value (-15dB to -20 dB) is assumed waterbody (Liu, 2016).

In this study, we validated the proposed technique in the South and South-East Asia region. This is a region populated with transboundary rivers where satellite altimetry is likely to be more useful than in other regions. Some of the issues pertaining to Indus, Ganges-Brahmaputra, Mekong, and other transboundary basins are the absence of hydrological data sharing mechanisms (Maswood & Hossain, 2016), hydro-political issues (Hossain et al., 2014), and lack of sufficient observation network (Shiklomanov et al., 2002). For comparison and performance assessment of the proposed methods, we needed in-situ datasets at the locations of potential virtual stations. Because in-situ data from different national agencies are difficult to access, we resorted to an innovative technique of creating our own in-situ river height database via web analytic tools. This method is based on using information technology and web crawling to scour the website and pull river height information posted by an agency every day to build a historical record. We have successfully applied such a technique in the past for real-time precipitation correction of satellite data or for calibration or validation of hydrologic models as outlined in Biswas & Hossain (2017). Several public domain websites of South Asian government agencies were used to crawl in-situ water level datasets. A list of websites and stations is provided in table A1, Appendix 1.

2.2.2 Methodology

The methodology of this study can be divided into two major parts. These are, 1) Bankfull width database development, and 2) Operational height extraction procedure. In the first part, a bankfull river width database was prepared. This dataset was used to identify potential virtual stations and prepare a region of interest (ROI) to define the maximum river extent and process ancillary datasets. Utilizing the Bankfull Width database and Nominal Pass, potential virtual stations are identified. In the second part, the river mask was derived based on the ROI (from the first part), and filtered signals were processed using different approaches to estimate the average height. Both of the parts are explained in section 2.2.2.1.

2.2.2.1 Bankfull River Width Database Development

We developed an approach to identify the potential virtual station location based on the topographical attributes of the rivers. We used river networks and river width/extent information during the development of the database. The reach based river width database and global river network datasets (the datasets are explained in section 2.2.1) are blended to prepare this dataset. JASON-3 altimeter data is measured at 20 Hz, which means that the signal interval is approximately 300 m along the track. To optimize the virtual location number and reduce erroneous height return, rivers with 50^{th} percentile width of more than 500m are selected from the river width database. The reach-based river dataset consists of discontinuous river networks, and it was difficult to estimate the actual river course based on the single data source. To fill the river network gap and make it a continuous river bankfull database, a global large river network was used. We used google earth-based visible imagery to verify the network and made necessary corrections in network abnormalities. The procedure for bankfull width database development is shown in Figure 2.2. The corrected and validated river network database was used to identify potential locations of virtual stations.

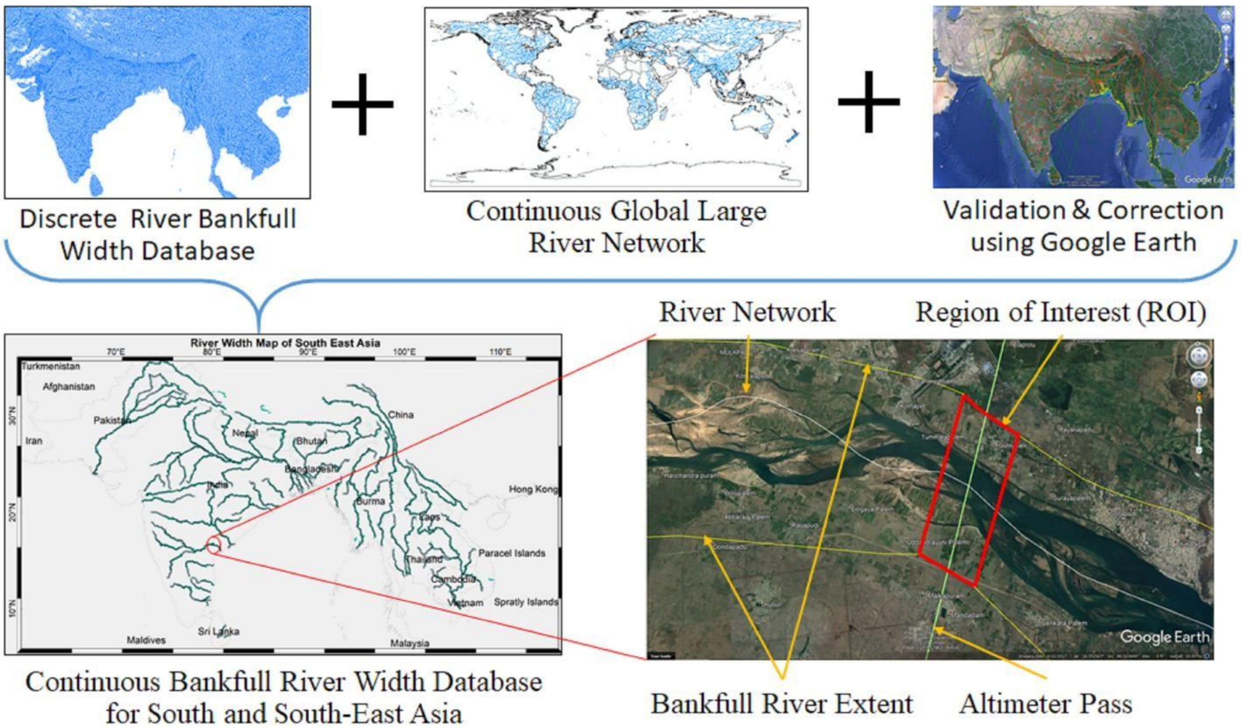

Figure 2.2 Bankfull River Width Database Development Procedure

This river network is also used to define a region of interest (ROI) for each virtual station. An example is shown in the lower-right corner of figure 2. This ROI was used to calculate cloud cover percentage and dynamic river extent from satellite imagery. The extent of ROI polygon was defined using maximum river extent from bankfull width database and the bound of 1.2 km between actual satellite pass and nominal pass. This ROI was used to subset granule data and extract dynamic river mask from Landsat imagery and SAR via GEE.

2.2.2.2 Potential Virtual Station Identification

Each intersection of the nominal altimeter pass and river network of the bankfull river width database is identified as a potential virtual station. Using this criterion, we were able to identify more than 150 potential virtual stations along several large and small rivers in the South and Southeast Asia region. In figure 2.3, the locations of potential virtual stations are shown.

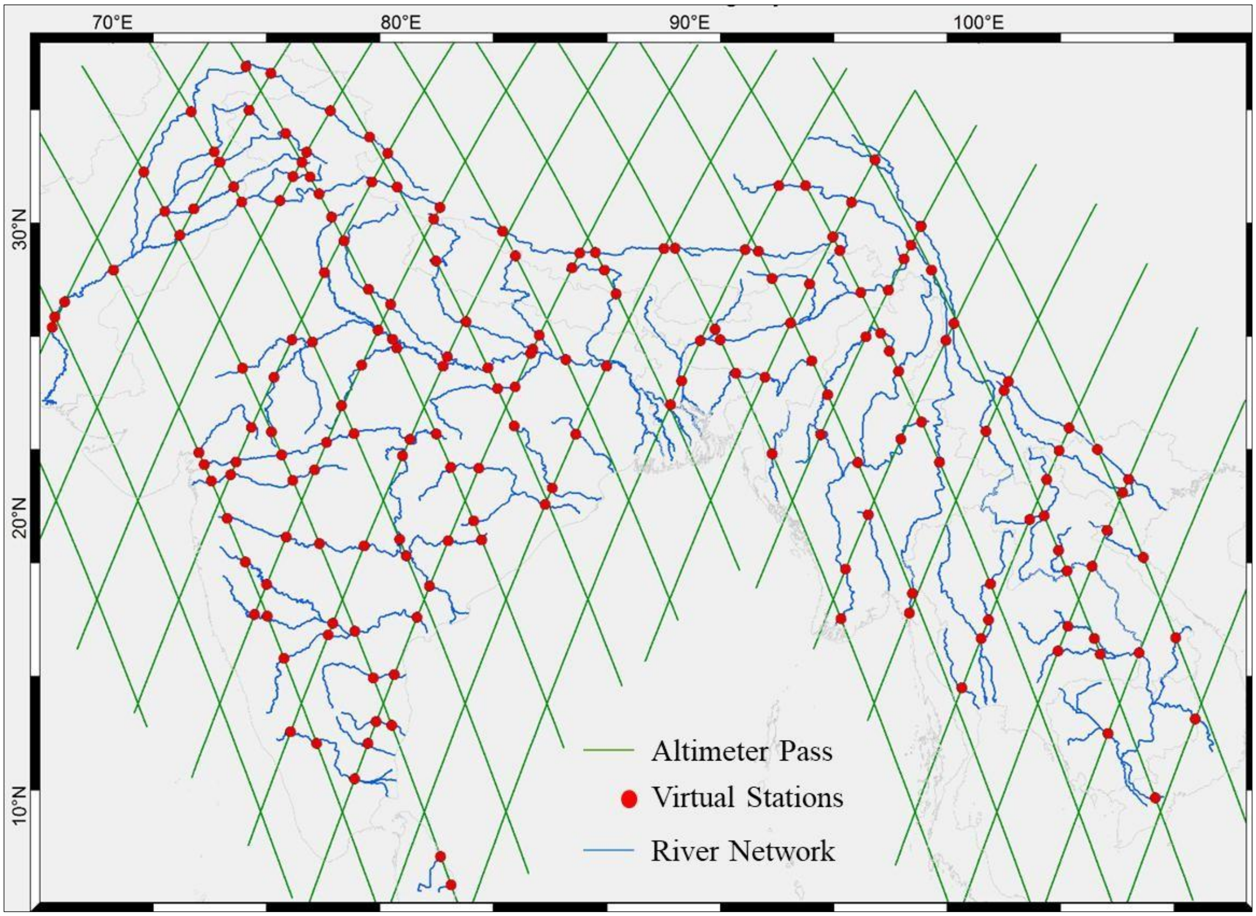

Figure 2.3 Potential Virtual Stations in South and South-East Asia Region.

2.2.2.3 Height Extraction Procedure

In this study, we tested three different height extraction methods based on river masks (from additional satellite imagery) to check the improvement in height estimation from the Kmeans clustering algorithm developed by Okeowo et al. (2017). The methods are a) River Mask (RM) based K-means (KM) clustering method (RM + KM) and b) K-means clustering embedded with River Mask method (KM_{RM}). Both of the methods are described in section 2.2.2.4 and 2.2.2.5 in details and shown in figure 2.4. During extracting height data from the JASON-3 altimeter, Ice retracked range was used to compute the elevation above the datum using the following equation:

$$H_{corr} = H_{sat} - \left[R - \Delta R + C_{wet} + C_{dry} + C_{iono} + T_P + T_E + T_L\right] - - - - - - - - - (2.1)$$

Where H_{corr} is the corrected elevation, H_{sat} is the satellite altitude, R is the measured range to the water surface, C_{wet}, C_{dry} *and* C_{iono} are the correction for the wet troposphere, dry troposphere, and ionosphere, T_P, T_E *and* T_L are pole, earth, and tide corrections, and ΔR is the retracked range correction. The datum is then converted into WGS-84 ellipsoidal height, and then using EGM 2008 (Earth Gravitational Model, 2008), ellipsoidal height is converted to orthometric height.

2.2.2.4 River Mask with K-means clustering method (RM+KM)

We applied the K-means clustering technique of Okeowo et al. (2017) along with dynamic river mask information in this method. Here, the altimeter datasets for the pass over the potential virtual station were spatially cropped using Region of Interest (ROI) polygon. The latest Landsat imagery processed in GEE was checked with the Simple Cloud Score (SCR). If SCR was less than 10%, dynamic river extent was extracted from the Landsat imagery. Otherwise, the next most recent Landsat imagery was checked in the same manner to infer the state of the dynamic river extent. If the ROI area of both of the most recent Landsat images contained more than 10% cloud cover, the maximum river extent from the ROI was used. After getting river extent (dynamic or maximum, decided based on the cloud cover), the altimeter signals were spatially subset to get the altimeter signals over the river extent.

The selected signals were appended to the historical signals of all the cycles of the particular station and filtered based on the Interquartile Range (IQR). Signals with the height lower than 75% of the lower quartile and higher than 125% of the upper quartile of heights were discarded from the current cycle record. Statistical Range (SR) was calculated from the IQR filtered heights of the current cycle. If the SR value was more than 5m, then K-means clustering was applied to divide the datasets into two clusters of heights (water and non-water pixels). An assumption was made regarding the SR value of 5m that at any location of a river at any particular time, height variation of water surface across the river should not be more than 5m. A smaller threshold could be used to obtain better height estimation, but a considerable amount of return signals were discarded, which is undesirable. K-means was applied until the SR of the maximum likelihood class is less than 5m. The sample standard deviation (SD) of the maximum likelihood water pixel class selected by the K-means was calculated. If the SD value was greater than 0.3m, the height pixel with maximum Absolute Deviation (AD) was discarded from the datasets, and the process was repeated until SD was less than 0.3m. If the SD value was less than 0.3m, the mean elevation was considered the height for the particular cycle.

For operational purposes, we marked flags on the extracted heights. If the height was extracted based on the latest Landsat imagery, it was marked with “A Grade” which means quality controlled with the latest river mask information. If the second recent Landsat imagery was used, the extracted height was marked as “B Grade” data, which was used to define quality controlled with the second recent imagery product. If no river mask information assisted in extracting the height, the height was marked as “C Grade” which means that no quality control was performed during height extraction. The whole procedure of height extraction using the River Mask with K-means clustering is explained in figure 2.4.

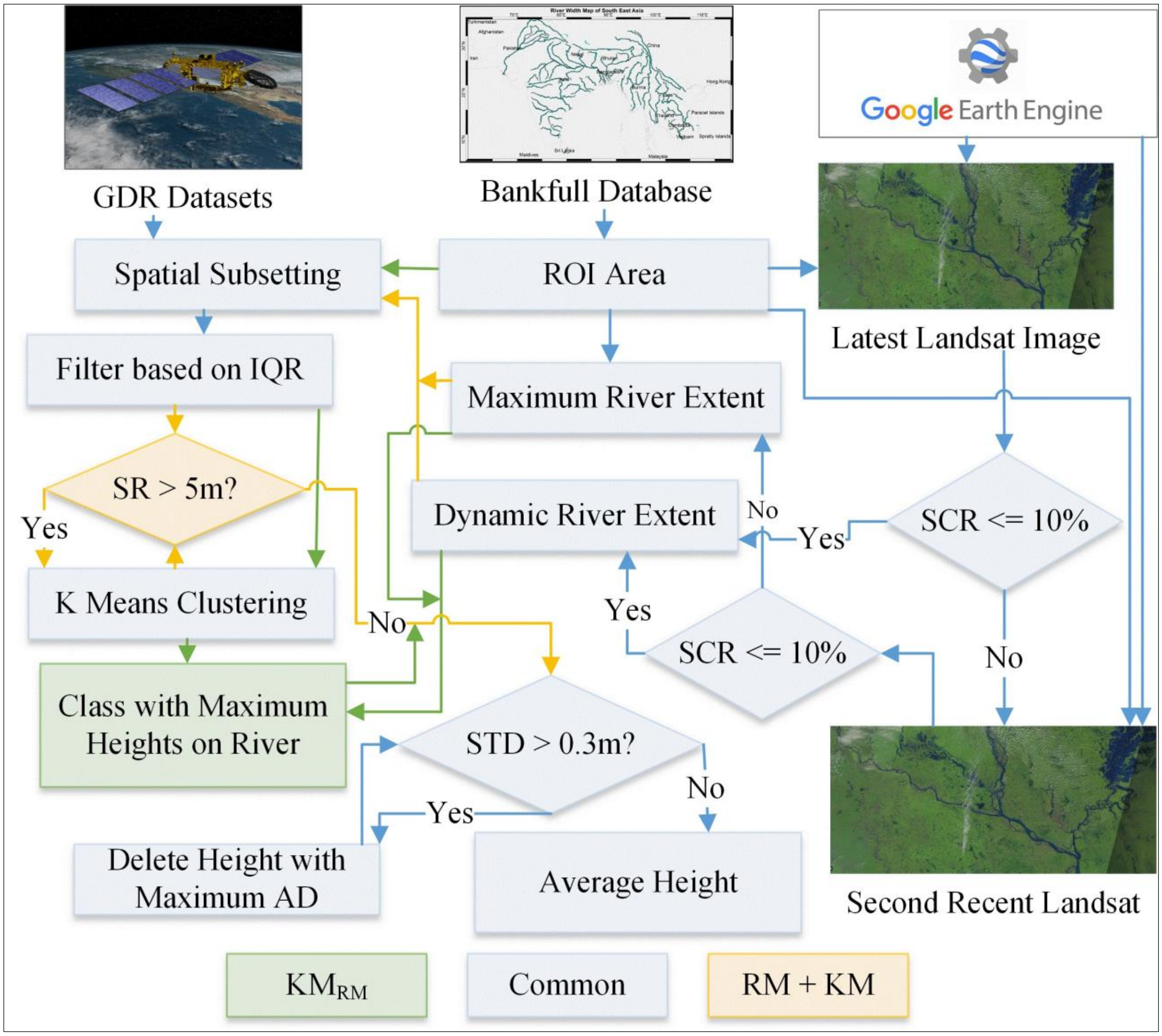

Figure 2.4 Algorithm to extract heights based on the proposed River Mask included K-means clustering method (RM+KM; shown in light orange arrows and boxes) and K-means embedded with River Mask Method (KMRM; shown in light green arrows and boxes). Here, GDR = Geographic Data Record, ROI = Region of Interest, IQR = Interquartile Range, SR = Statistical Range, SCR = Simple Cloud Score, STD = Sample standard deviation and AD = Absolute Deviation.

2.2.2.5 K-means clustering embedded with River Mask method (KM_{RM})

The second method of height extraction from the JASON-3 altimeter was tested using Kmeans (KM) clustering embedded with River Mask (RM) and labeled as KM_{RM}. The idea behind applying this method was to reduce error during applying K-means clustering. K-means clustering was applied to divide the datasets into the water and non-water pixels. To prevent the selection of non-water features of the radar signal, the water pixels class was selected based on dynamic water extent. In this method, after applying K-means clustering, all the signals were checked with river extent information. The class containing the larger number of the height data point on the waterbody was identified as water pixels rather than arbitrarily picking the most likelihood events.

During the application of the KM embedded with the RM method (KM_{RM}), IQR was applied similarly to the RM + KM method. K-means clustering was applied to IQR filtered signals to divide the altimeter signals into two categories (water and non-water pixels). Landsat derived dynamic river extent used to define the water pixel class among the classes generated by the K-means application. Standard deviation was checked to filter out data points with maximum absolute deviation. When the standard deviation was less than 0.3 m, the mean of obtained heights was considered the mean height.

2.2.2.6 SAR with K-means Method (RM_{SAR} + KM)

The above methods (RM + KM and KM_{RM}) were tested using the Landsat imagery as the source of the water mask. To reduce the error associated with the detection of water using visible imagery during high cloud cover situations, we tested SAR imagery as the source of river mask to determine the dynamic river extent in the ROI (region of interest). Monthly median backscatter coefficients of SAR imagery from Sentinel-1 were used during the classification of water pixels.

The monthly average river extent was extracted and applied in the same way as the Landsat imagery to calculate the average height using the River Mask included K-means clustering (RM+KM) method.

During validation of the above algorithms, in-situ heights were used from web crawled height datasets. To reduce the error related to the location shifting (upstream or downstream of the actual virtual station) or local datum difference between potential virtual stations and in-situ stations, the height changes were used instead of absolute heights. Root Mean Square Error (RMSE), Mean Absolute Error (MAE), and Correlation Coefficient formula are shown in equations (2.2), (2.3), and (2.4), respectively. In these equations, O_i is the in-situ height difference from average, P_i is the calculated height difference from the mean of calculated heights, $\bar{O}$ is the average of in-situ height difference, $\bar{P}$ is extracted height difference, and n is the sample size. Normalized Root Means Square (NRMSE), Normalized MAE (NMAE) were calculated using formulas (2.5) and (2.6), where $O_{max}$is the maximum of in-situ height difference and O_{min} is the minimum of in-situ height difference. For cross-comparison of stations and relative performance assessment of the methods, NRMSE, NMAE, and Correlation Coefficient metrics were rescaled from (0-1) using a unified score calculated for every method and station. The unified score derivation formula is shown in equation (2.7).

$$Root\ Mean\ Square\ Error\ (RMSE) = \sqrt{\frac{\sum_{i=0}^{n}(P_i - O_i)^2}{n}} \text{---------------} (2.2)$$

$$Mean\ Absolute\ Error\ (MAE) = \frac{1}{n}\sum_{i=1}^{n}|P_i - O_i| \text{-----------------} (2.3)$$

$$Correlation\ Coefficient = \frac{\sum_{i=0}^{n}(O_i - \bar{O})(P_i - \bar{P})}{\sqrt{\sum_{i=0}^{n}(P_i - \bar{P})^2 \sum_{i=0}^{n}(O_i - \bar{O})^2}} ------------ (2.4)$$

$$Normalized\ RMSE\ (NRMSE) = \frac{RMSE}{O_{max} - O_{min}} ------------------- (2.5)$$

$$Normalized\ MAE\ (NMAE) = \frac{MAE}{O_{max} - O_{min}} -------------------- (2.6)$$

$$Unified\ Score = \frac{\left(1-\frac{NRMSE}{Maximum\ NRMSE}\right)+\left(1-\frac{NMAE}{Maximum\ NMAE}\right)+Corr.\ Coeff.}{3} ----------- (2.7)$$

The maximum NRMSE was taken as the maximum value of NRMSE of all stations, and maximum NMAE was taken as the maximum of NMAE of all the stations. The maximum of NRMSE was found 19.58 in this study, and the maximum of Normalized MAE was 19.24.

2.3 Results and Discussion

2.3.1 Validation of Algorithm over South and South East Asia

To test the above-mentioned algorithm, we selected a region of South and South-East Asia, which is composed of extreme hydrometeorological variability and morphodynamic rivers with strong seasonal and inter-annual variation. Twelve stations are selected based on the in-situ data availability for the validation purposes of the proposed methods. Topographic properties and morphological attributes of the selected virtual stations are shown in table 2.1 and figure 2.5. For instance, Annapurnaghat station is located on the Barak River of India, which is extremely sinuous. Sariakandi and Goalpara stations are located along very braided reaches of Brahmaputra River with relatively flat topography. There are snow and ice in Kibithu station, which lies in the high terrain of the Himalayas. Kampong Cham station has tidal effects. Khong Chiam station of Mekong River is in a sinuous reach covered with a dense canopy layer.

Table 2.1 List of stations used for validation of the proposed algorithm

Name	River	Longitude (degree)	Latitude (degree)	J3 Pass	Average Width (m)	95th percentile Width (m)
Kampong Cham	Mekong	105.48	12.01	140	1322	4570
Khong Chiam	Mekong	105.56	15.33	001	1193	4106
Srisailam	Krishna	78.39	16.07	218	1514	5264
Bhadrachalam	Godavari	80.98	17.65	079	860	2924
Sariakandi	Brahmaputra	89.69	24.72	231	1413	4961
Annapurnaghat	Barak	92.59	24.88	053	506	1594
Bhagalpur	Ganges	87.12	25.30	155	1466	5086
Goalpara	Brahmaputra	90.36	26.17	231	1431	4961
Delhi Bridge	Yamuna	77.34	28.52	105	512	1359
Haridwar	Ganges	78.05	29.52	116	504	1089
Kibithu	Luhit	97.03	28.22	129	500	1113
Tuting	Brahmaputra	95.20	29.26	064	584	1955

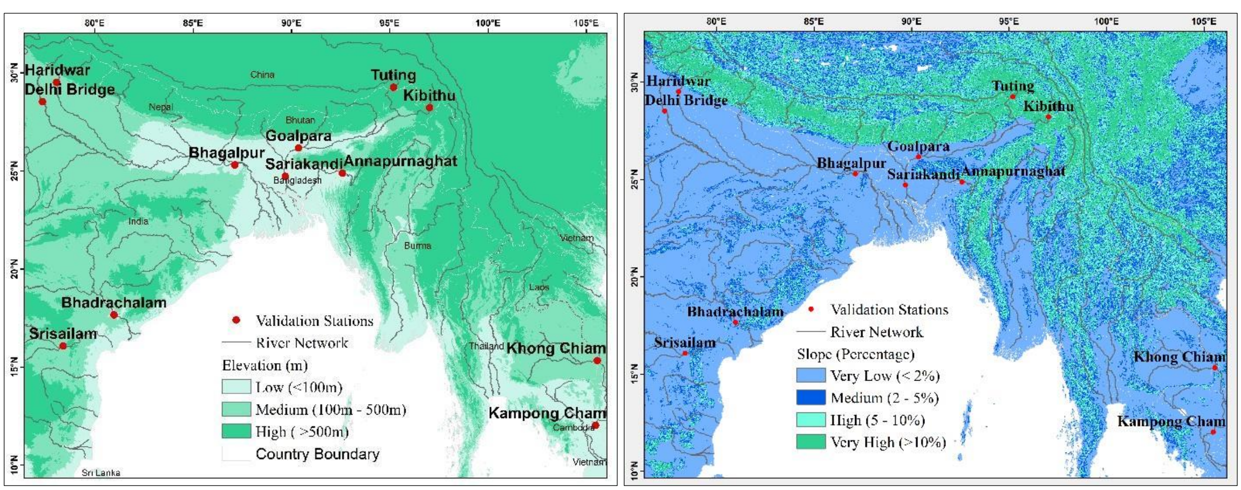

Figure 2.5 Variation in topographic properties of the stations, (a) Elevation (SRTM 30m) and (b) Slope Variation (calculated using SRTM 30m DEM).

2.3.1.1 Performance using GDR Datasets and Landsat Imagery

During performance assessment of the methods, height changes (from the mean) were compared instead of absolute heights to eliminate the uncertainties about the datum difference between the extracted heights and in-situ heights. Based on the calculated unified score of 12 stations in South and South-East Asia, it can be seen that using river mask information (the combination of KM_{RM} and RM+KM), extracted height quality improved in 8 stations (Figure 8).

The error in estimated heights during the monsoon season is less than the amount during the dry season for all of the stations. In most cases, improvements occur in the rivers varying highly in width due to the use of satellite imagery on river conditions. An example of IQR application, conventional K Means, and proposed methods filtered altimeter pixels are summarized next for Sariakandi Station along Brahmaputra River. The range of points returned from altimeter signals was 56-58 throughout the study period of February 2016 to October 2017. Upon application of IQR, the average number of points filtered out are 12.28. After filtering using conventional K Means clustering, an average number of pixels selected as water feature was 24.2. Using the RM+KM method, the average number of pixels reduced to 18.134, and for the KM_{RM} method, it was 19.154.

As examples of performance of the approaches, time-series, and scatterplots of four specific stations are provided in figure 6. All methods proved useful in the case of the Sariakandi station, which is on the very large and braided reach of the Brahmaputra River (Figure 2.6a and 2.6b). Similarly, all approaches captured the in-situ height difference during the high flow season with few uncertainties in the dry period. Errors were observed in the case of the Tuting station (Figure 2.6c and 2.6d). This station lies in the Himalayan region's high mountainous area, with a high topographic slope of 13.5% in the neighborhood. The higher slope leads to a very high river velocity at that location, while depth likely remains supercritical (low depth). Thus, the RM+KM method was not able to detect the frequent change in river extent. In contrast, the KM_{RM} approach easily filtered out the non-water pixels due to considerable variation in elevation between banks and rivers. Application of RM embedded with KM reduced the uncertainty during the selection of the class containing water-pixels. Therefore, bias estimated by the KM_{RM} method is comparatively less compared to the other methods in both dry and wet seasons in that station. A similar scenario is observed in figures 2.6e and 2.6f in the Haridwar station of the Ganges River. At that location, RM+KM was not able to filter out non-water pixels, and thus KM_{RM} performed better compared to RM+KM and KM methods.

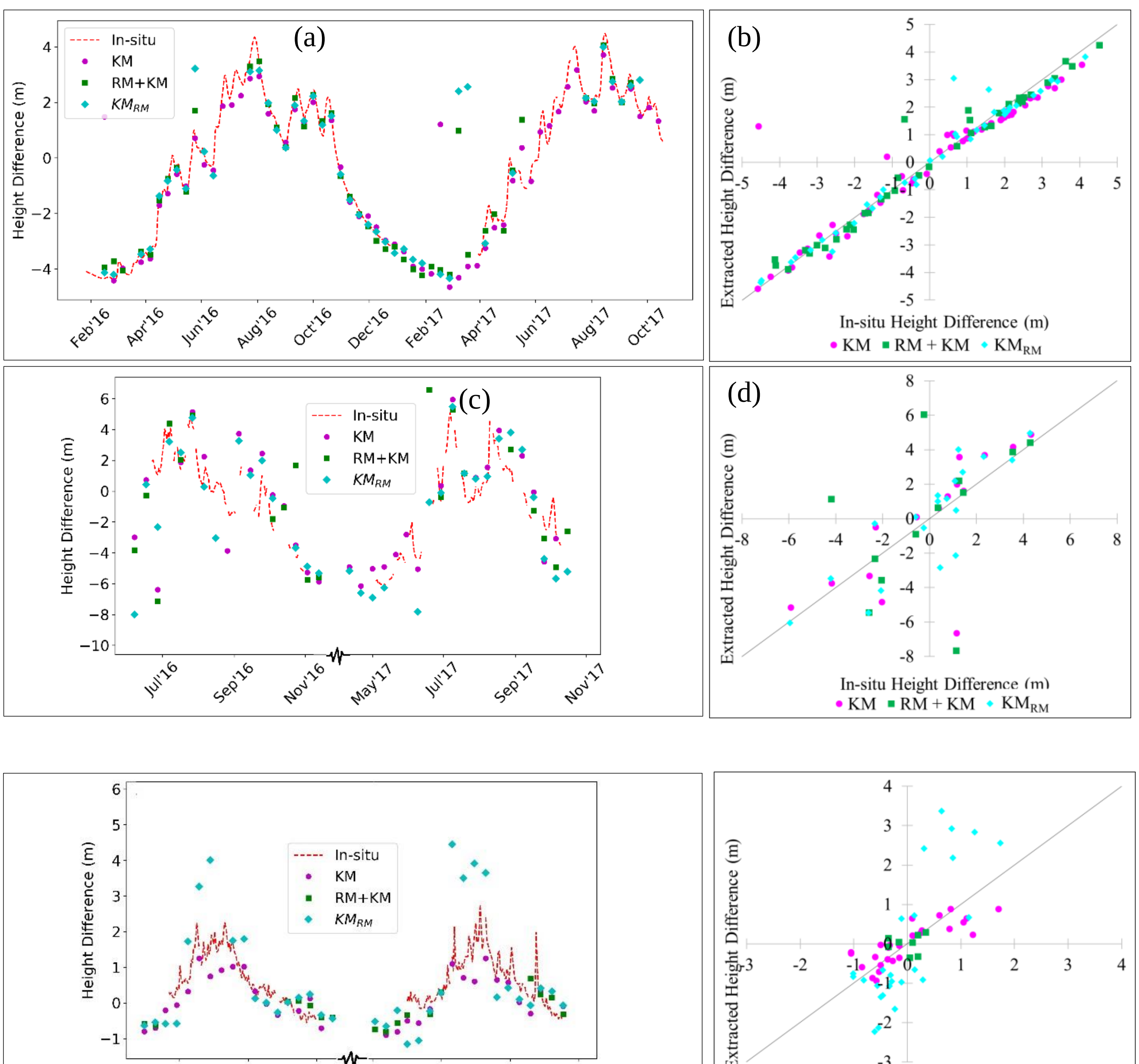

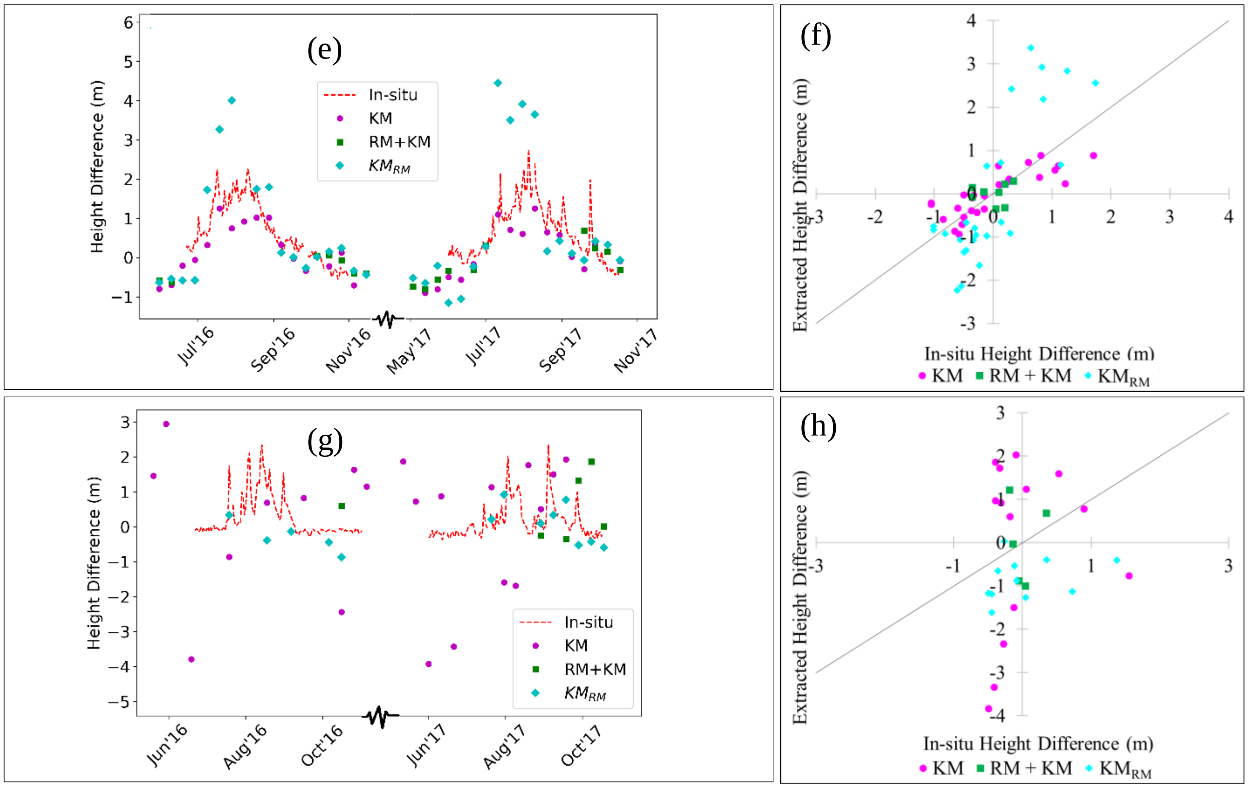

Figure 2.6 Timeseries comparison and the scatterplot of height extraction methods, (a) and (b)Sariakandi station of Bangladesh on Brahmaputra River, (c) and (d) Tuting Station of India on Brahmaputra River, (e) and (f) Haridwar Station of India on Ganges River and (g) and (h) Delhi Bridge Station of India on Yamuna River

Srisailam station showed the opposite scenario compared to the Haridwar and Tuting station. The elevation difference between river banks and water surface in Srisailam station was minimal (less than 10 m in the dry period, which usually decreases during flood season). K-means was performed to classify the extracted datasets into clusters based on only statistical characteristics. When there is a small difference in heights of water and neighboring features, K-means cannot perform well. In this case, when KM_{RM} is applied, KM was not able to classify water and land pixels correctly due to its poor classification performance with a smaller statistical range. Then, the RM identified the mixed pixels as water class. In contrast, when RM+KM was applied, RM first filtered out the land pixels from returned signals. K-means application over the RM filtered pixels then returned a more accurate estimation of heights. In that way, RM+KM outperformed the KM_{RM} in that particular station.

Figures 2.6g and 2.6h of Delhi Bridge station show that no methods were able to represent the actual water height trend. It was due to the Okhla Barrage, which is located approximately 3.5 km upstream of the virtual station. This barrage heavily regulates the river, which frequently results in very narrow width, and therefore is difficult to capture by the satellite-based methods. The location of the Delhi Bridge Virtual station and Okhla Barrage is shown in figure 2.7.

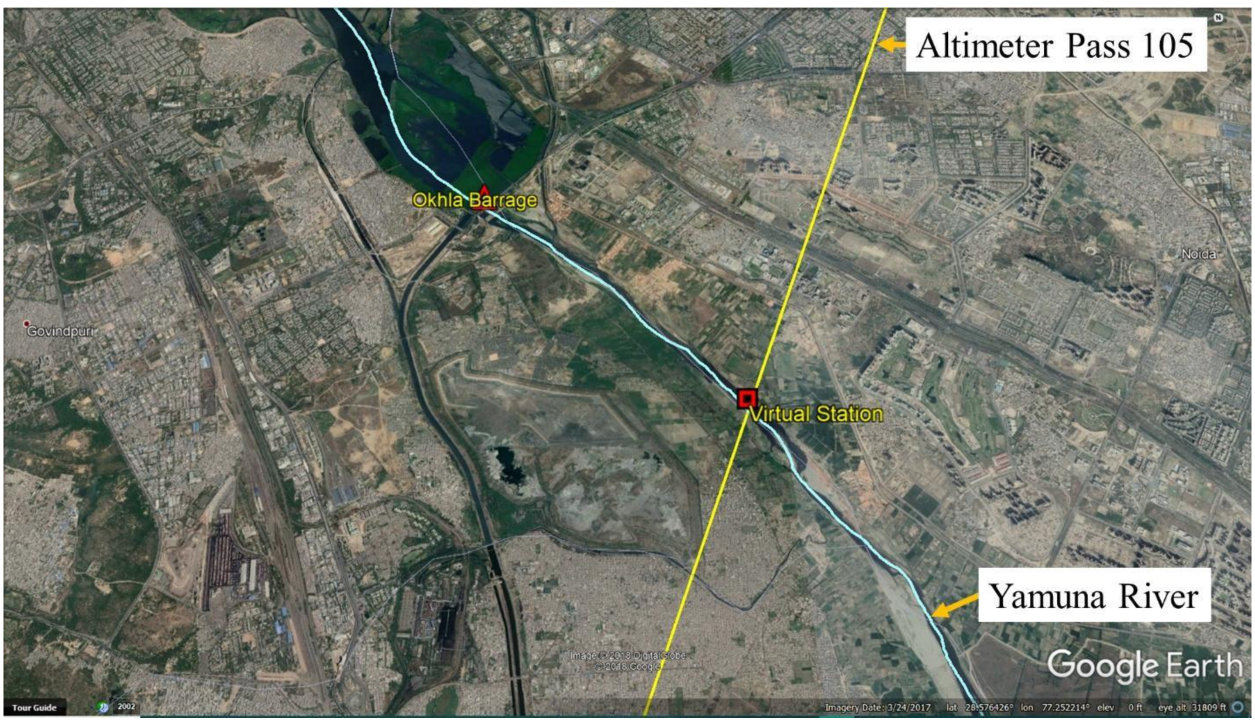

Figure 2.7 Delhi Bridge Station along with Okhla Barrage along with Altimeter Pass and Virtual Station

All approaches for the selected validation stations were compared using correlation coefficient, normalized RMSE, normalized MAE, and derived Unified Score by using equation (7). The comparison plots are shown in figure 8. From the metrics comparison, it can be seen that all methods were able to capture the trend in very large rivers along with low topography (i.e., Bhagalpur, Sariakandi). Stations located in the low topography and highly varying river width (i.e., Kampong Cham, Bhadrachalam, Goalpara) show improvement due to the use of the river extent information. When elevation variation between banks and the river level is high (i.e., Bhadrachalam, Tuting), KM_{RM} performed best among the three methods. Barak River at Annapurnaghat station is highly sinuous (i.e., exhibits cyclical pattern), and GEE was failed to derive dynamic river extent from 10 scenes among 31 Landsat scenes due to cloud cover, which leads to the poor performance of all the methods. Khong Chiam station of Mekong River is also sinuous along with dense canopy cover with high neighboring topography causes poor performance. Due to the frequent cloud cover occurrence and dense canopy layer, Landsat imagery derived water extent could not filter out the contaminated pixels from returned heights, which leads to unrealistic heights. The highest error is observed at Kibithu station, where the elevation was more than 2500 m, and the slope was 18% with the influence of snow. Although the error is too high at that location, the KM method performed modestly better than RM based method. Since the station lies in the Himalayas, the river's seasonal variability at that location is negligible.

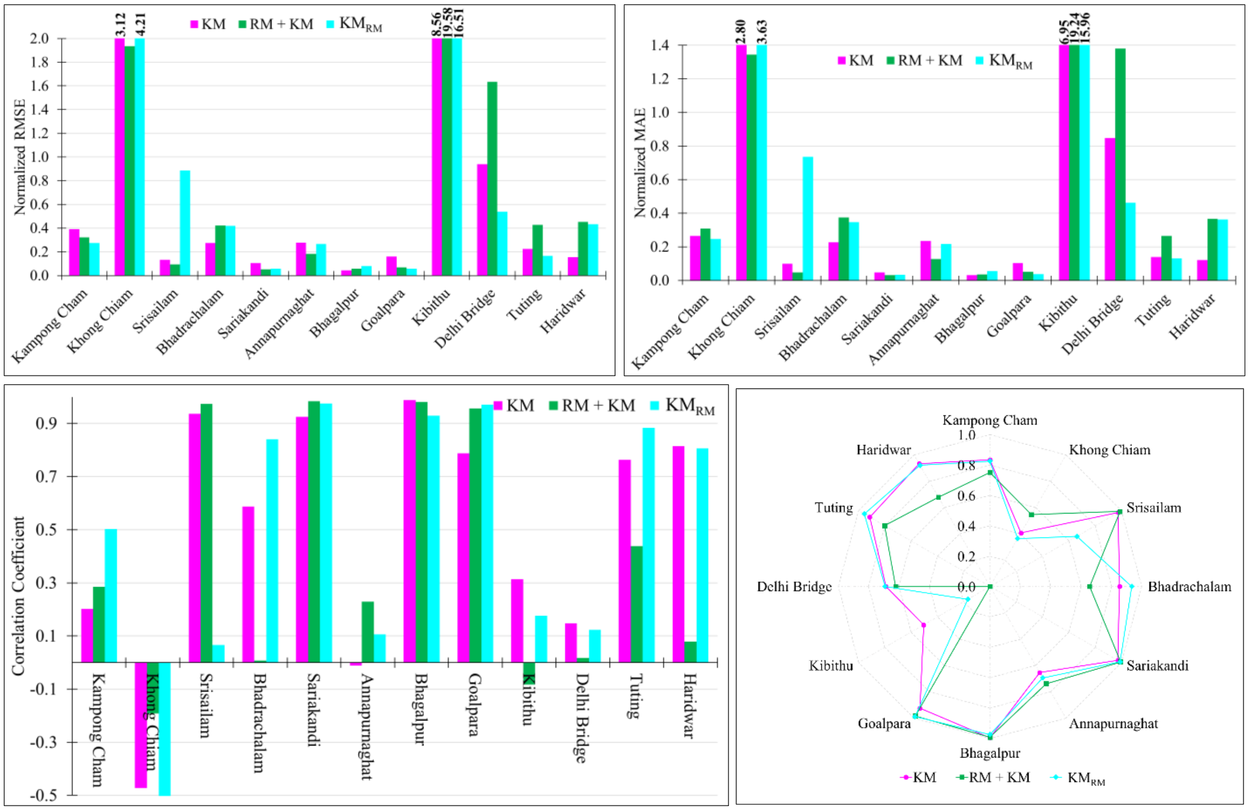

Figure 2.8 Comparison of error metrics for various approaches for the stations, (a) Normalized RMSE, (b) Normalized MAE, (c) Correlation Coefficient, and (d) Unified Score.

Landsat imagery has some limitations over the region with cloud cover detection and very dense canopy cover (i.e., Annapurnaghat and Khong Chiam). Also, Landsat revisit period is longer than the JASON-3 cycle. Consequently, it was not able to detect the exact river extent during the satellite revisit time. For the same reason, the onset and offset of flood events (for example, flash floods), rapid changes in river course introduced an additional source of uncertainties. Visible imagery products also have limitations in shallow water detection, which remains a challenge with river extent derivation using this data as a source. The percentage improvements (RMSE and MAE) in each station by using river mask based methods compared to the conventional method using K-Means is shown below in Table 2.2. The rows of the table where at least one river mask based methods from the ensemble showed improvements from the conventional method are shown with gray color.

Table 2.2 RMSE and MAE improvements by using river mask based methods relative to the conventional KM method

Station	KM		Improvements in RM + KM		Improvements in KM_{RM}	
	RMSE (m)	MAE (m)	RMSE	MAE	RMSE	MAE
Kampong Cham	0.39	0.26	31%	4%	18%	-19%
Khong Chiam	3.12	2.80	-35%	-30%	38%	52%
Srisailam	0.13	0.10	-585%	-640%	31%	50%
Bhadrachalam	0.27	0.23	-56%	-52%	-56%	-61%
Sariakandi	0.10	0.05	40%	40%	50%	40%
Annapurnaghat	0.28	0.23	4%	4%	36%	43%
Bhagalpur	0.04	0.03	-100%	-100%	-50%	0%
Goalpara	0.16	0.10	63%	60%	56%	50%
Kibithu	8.56	6.95	-93%	-130%	-129%	-177%
Delhi Bridge	0.94	0.85	43%	46%	-73%	-62%
Tuting	0.22	0.14	23%	7%	-95%	-86%
Haridwar	0.16	0.12	-169%	-200%	-181%	-208%

2.3.1.2 Performance using SAR Imagery

To overcome the limitations in detecting river extent using visible imagery, we applied SAR imagery in place of Landsat to derive dynamic river mask information. SAR based RM derived heights (RM_{SAR}+KM) were compared with other methods in four selected stations and presented in figure 2.9. From the time-series plot of Kampong Cham station (shown in figure 9a), it can be seen that this method was able to capture the trend of water level variation more accurately. In the case of Annapurnaghat station showed in figure 2.8b, all the methods except RM_{SAR} + KM were impacted by non-water heights (no variation in seasonal scale). The methods of KM, RM+KM, and KM_{RM} at Khong Chiam station showed a height range of 80 m (which is unrealistic), whereas RM_{SAR}+KM showed a height range of 13 m and fitted very well with the in-situ height difference.

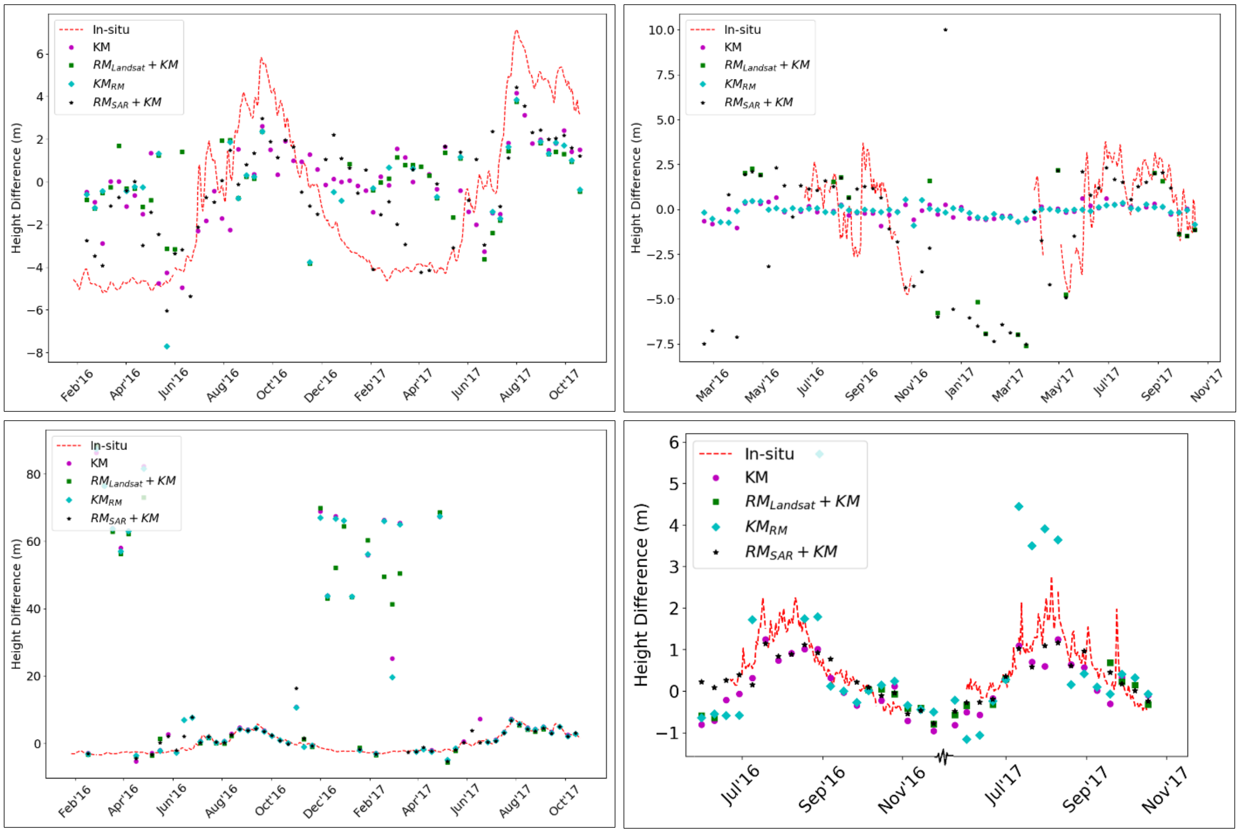

Figure 2.9 Timeseries comparison of KM, RMLandsat + KM, KMRM (Landsat) and RMSAR + KM methods in 4 different stations, (a) Kampong Cham Station (Mekong River, Cambodia); (b) Annapurnaghat Station (Barak River, India); (c) Khong Chiam Station (Mekong River, Vietnam)

The improvements due to the use of SAR based RM are universal for the stations investigated here and can be seen in figure 2.10. RM_{SAR} +KM was compared with three earlier methods where significant improvements in all stations are observed. For Annapurnaghat station, as the SAR based imagery overcame the Landsat limitation in detecting water under clouds, the improvements are evident. Heights at the Khong Chiam station also improved due to the use of the SAR imagery, which is reflected in the unified score plot of figure 2.10.

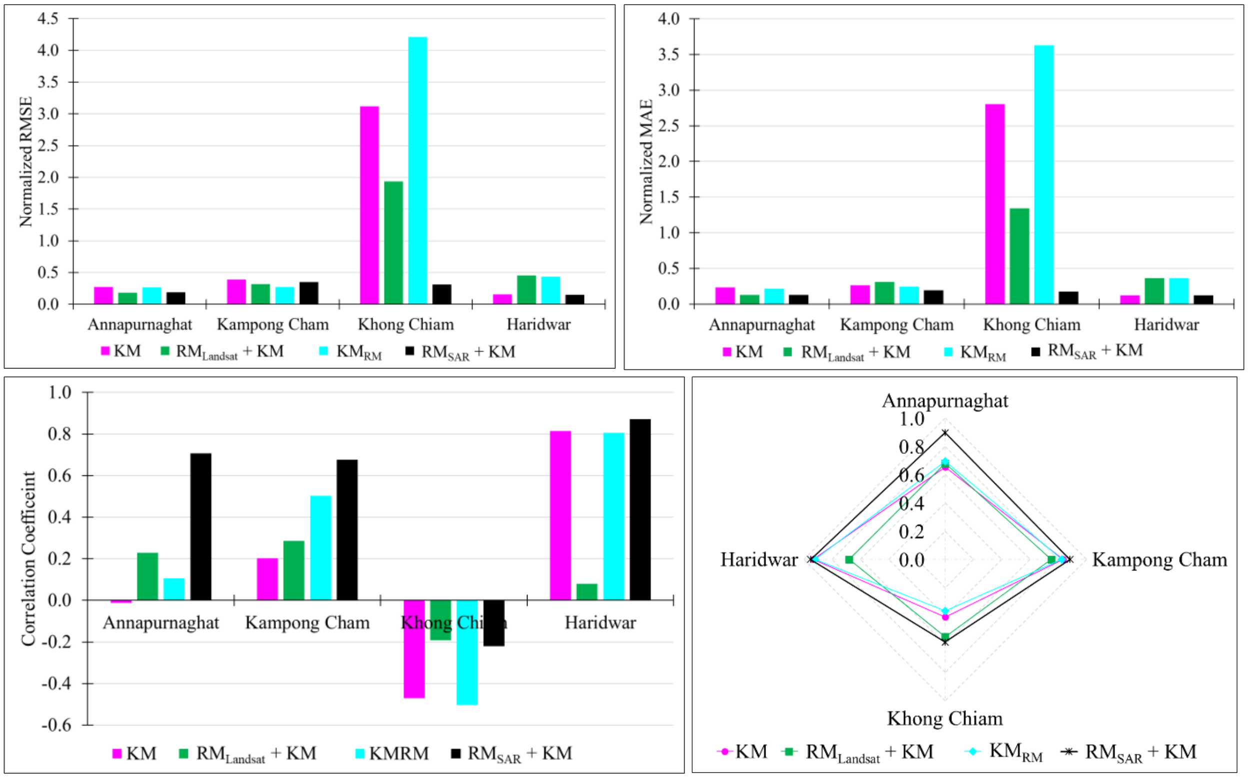

Figure 2.10 Comparison of height extraction methods in 4 different stations (a) Normalized Root Means Square Error (RMSE), (b) Normalized Mean Absolute Error (NMAE), (c) Correlation Coefficient, and (d) Unified Score (close to circumference is better). Note the KMRM

The percentage improvements (RMSE and MAE) in each station using the SAR imagery-based RM_{SAR}+KM method compared to the conventional method using K-Means are shown below in Table 2.3. From the table, it can be seen that every station improved due to the use of SAR imagery.

Table 2.3 RMSE and MAE improvements by using SAR Imagery relative to the KM methods.

Station	KM		Improvements in RM_{SAR} + KM	
	RMSE (m)	MAE (m)	RMSE	MAE
Kampong Cham	0.39	0.26	31%	46%
Khong Chiam	3.12	2.80	11%	28%
Srisailam	0.13	0.10	90%	94%
Annapurnaghat	0.28	0.23	5%	-1%

One assumption is made regarding the time difference between altimeter acquisition and the latest Landsat imagery acquisition. Although the situation is unique for each station and temporal period, negligible change in hydrological regime was assumed due to the lag time. During the occurrence of fast-evolving extreme hydrological events (especially during the flood recession period), the assumption may not hold a comparatively larger extent that may be returned by the satellite imagery. To verify the assumption, the Khong Chiam station is chosen that poses the highest time difference of 25 days between altimeter and Landsat acquisition. Neighboring elevation contours, elevation versus width change of river along the altimeter pass, and in-situ WL hydrograph of Khong Chiam Station are shown in Figure 2.11. Two altimeter data acquisition and Landsat acquisition date during rising and recession limb of hydrograph are also shown in figure 2.11c. From figure 2.11c, the difference in heights between altimeter and Landsat date is less than 3m. From figure 2.11b, it is seen that a 3m height difference may cause less than 200m river width difference along the altimeter pass.

The altimeter radar signal interval for JASON-3 is approximately 300m (at a frequency of 20Hz). Thus, for a 200m width variation during the sharp rise/fall in the hydrograph, the use of time-synched cloud-free (hypothetical) Landsat imagery would have yielded similar results as the time-lagged imagery we have had to use in this study for reasons of practicality. We have also confirmed the same for the Annapurnaghat station, where there was a significant time mismatch between the JASON-3 overpass and the Landsat data.

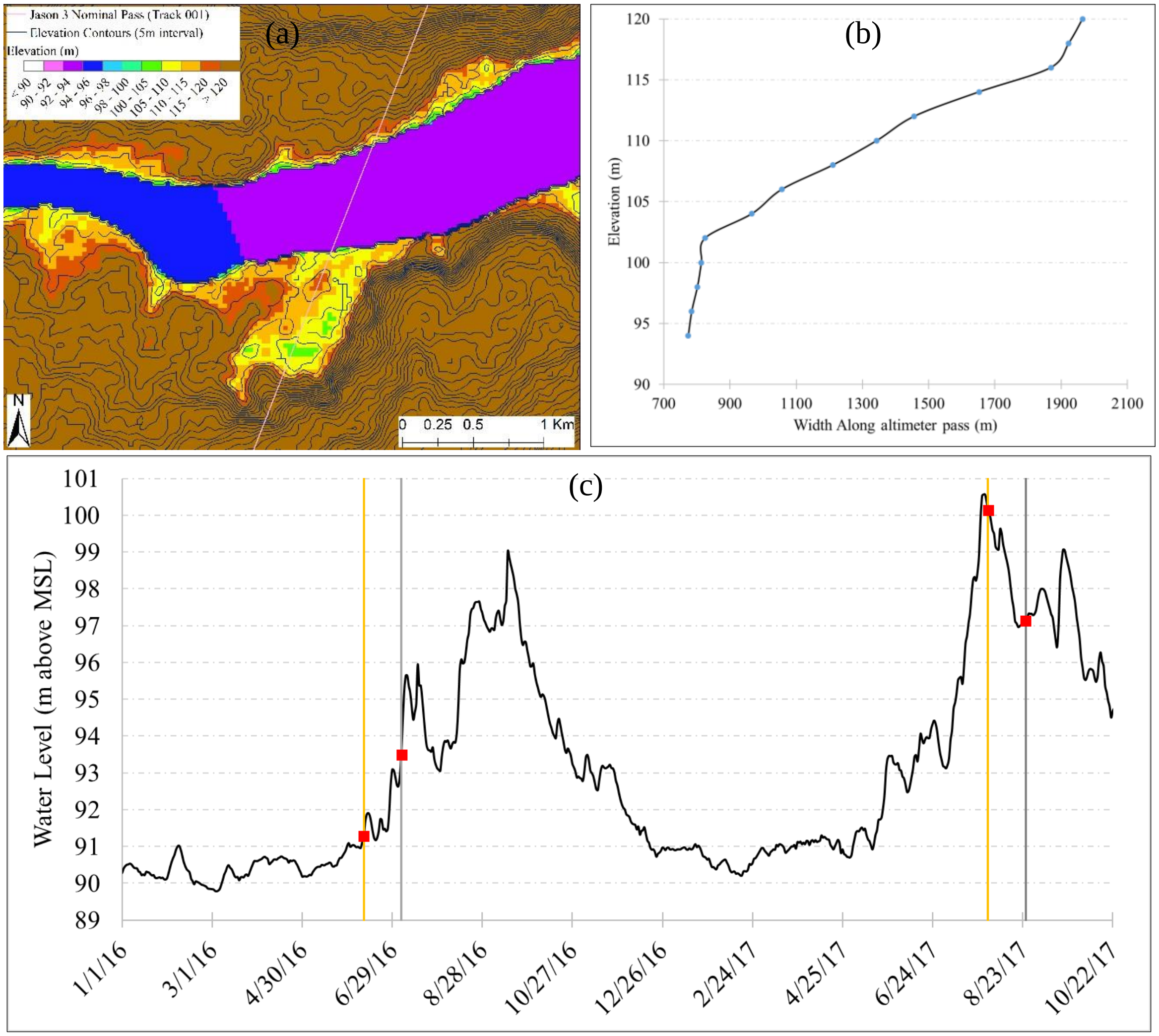

Figure 2.11 (a) Elevation contours of neighboring topography at Khong Chiam Station, (b) Elevation versus River Width along the nominal pass and (c) In-situ WL along with altimeter pass date (gray color) and considered Landsat imagery acquisition date (orange color)

2.4 Conclusion

The objective of this study was to develop a river mask informed technique to extract altimeter heights over dynamically changing rivers and maximize altimeter application for water management. This study addressed a potential limitation in current approaches to altimeter height extraction for dynamically varying rivers, such as braided and meandering rivers with seasonality and complex topography. In the proposed approach, we introduced the idea of using additional satellite imagery on river mask to improve the extraction of altimeter water surface heights. The proposed methods were checked in locations with unique topographical features and hydrodynamic characteristics. From the analysis and findings, the picture that emerges is that river mask can consistently improve height estimates although the improvement at times is modest and not unique to a specific technique (RM+KM or KM_{RM}). A key reason for the increase in performance is that one of the significant application limitations of the conventional Kmeans is minimized by using a river mask. We also found that in most of the cases, using the KM_{RM} method, the temporal resolution of returned heights improved compared to simply using the Kmeans method. The K-means method divides datasets between two classes without any prior information of the river mask. Although the use of river mask does not worsen height estimation compared to current baseline approaches, the practicality of using massive amounts of visible or SAR data has to be weighed in by the end-user with the quantitative improvements achieved.

From this study, we have also seen that the SAR based imagery technique performed consistently better than the Landsat based imagery technique to improve height extraction. We have also observed that in some cases, the K-means conventional application returned very unrealistic heights. For example, in Bhadrachalam station of India and Khong Chiam station, the average of returned heights considering the dynamic river mask performed better than applying the non-morphology based K-means technique. Overall, from the study, we can summarize that the river mask incorporation improves the estimation of heights in the case of dynamically changing rivers compared to the conventional methods based on fixed width.

Based on the study, we can confidently provide the following rules of thumb for users of data from satellite altimetry such as JASON-3 river height extraction in South and Southeast Asia:

- The maximum benefit of utilizing additional satellite imagery-based river mask is during low flow season when the probability of non-water radar signal contamination is highest.
- For dynamically varying rivers (i.e., highly varying seasonal widths), river mask incorporation, as an ensemble of techniques, yields heights with more accuracy than the existing methods used today. Among the two river mask based methods, we found that when the difference between the river bank and water surface is considerably high, Kmeans embedded with the river mask method worked better than the river mask-based K-means method. In cases of smaller differences between bank and water surface, the river mask based K-means method worked better.
- The imagery on river extent can play an important role in highly meandering rivers as it considers the deviation between actual satellite altimeter pass and nominal pass.
- For braided rivers, river extent information is useful in filtering out the heights returned from river islands.
- In the case of very large rivers (median width > 1 km), there is expectedly minimal improvement in derived heights when using additional satellite imagery on river extent.

Perhaps the main take-home message our study provides is that while there is value in the use of massive datasets from ancillary sensors from visible and SAR platforms, the practicality of the river mask-based approach for JASON-3 height extraction needs to be carefully considered by the operational end-user based on available computational resources and the latency that can be afforded. For example, the large data size of visible or SAR imagery can frequently pose problems in downloading and processing the data in the operational environments of South Asian agencies.

We have observed in our interactions with Vietnamese agencies that performing as much of the computations in the cloud (GEE) and downloading only subset data pertaining to relevant bands is a better strategy when internet and CPU bandwidths are limited. As computational resources become more affordable and latency of satellite mission data shortens, an ensemble of many morphology based techniques dynamically using SAR imagery is perhaps the future of river height extraction in river systems of South and South-East Asia that are currently undergoing rapid change due to natural and anthropogenic factors.

Given the findings of the application of multimission satellite observations in river monitoring, the next logical step was to investigate the application potential of satellite observations along with the numerical modeling in the forecasting component of the operational water management. In chapter 3, a computationally efficient flash flood forecasting framework was explored using the satellite observations and numerical weather forecasting (NWP) outputs.

Chapter 3 A computationally efficient flash flood early warning system for a mountainous and transboundary river basin in Bangladesh

Note: This chapter has been published mostly in its current form in the *Journal of Hydroinformatics* (Biswas et al., 2020). ©IWA Publishing, allowed to use in a thesis or dissertation.

Abstract

A computationally efficient early warning technique was developed for forecasting flash floods during the pre-monsoon season that are associated with a complex topography and transboundary runoff in Northeastern Bangladesh. Locally conditioned topographic and hydrometeorological observations were the key forcing to the modeling system that simulate the hydrology and hydraulic processes. The hydrologic model was calibrated and validated using satellite-based observations to estimate the correct amount of transboundary and mountainous inflow into the flash flood-prone plains. Inflow was then forecasted using precipitation forecast from a global numerical weather prediction (NWP) system called the Global Forecasting System (GFS). The forecasted inflows served as the upstream boundary conditions for the hydrodynamic model to forecast the water stage and inundation downstream in the floodplains. A real-time in-situ data-based error correction methodology was applied to maintain the skill of the system. The simulation grid size and time-step of the hydrodynamic model are also optimized for computational efficiency. The framework's historical performance revealed that at least 60% accuracy at 5-day lead-time in delineating flood inundation when it was compared against Sentinel-1 Synthetic Aperture Radar (SAR) imagery. The study suggested that higher resolution

topographic information and dynamically downscaled meteorological observations can lead to significant improvement in flash-flood forecasting skills.

3.1. Introduction

Flash floods are one of the most dangerous natural hazards due to their sudden nature of the occurrence. They are generally caused by heavy or excessive rainfall over a very short period of time, where runoff generation is accelerated due to saturated or poorly infiltrating soil or steep terrain. The time difference between the rainfall event and flood peak is often less than 12 hours, making forecasting extremely challenging (Lee & Singh, 1999). Flash floods are the number-one cause of death among all storm-related hazards in the USA, with approximately 100 lives lost each year (Ashley & Ashley, 2008).

Over the past few decades, flash floods have drawn attention in many parts of the world, including the United States, European Union, Australia, and Egypt (Hapuarachchi at al., 2011; Abuzied & Mansour, 2019). Flash floods are of particular concern in the Northeastern region of Bangladesh (shown in Figure 1a), which experiences flash floods nearly every year during the pre-monsoon season (March-May). This area is the home to extensive agriculture and aquaculture activities that support the country's economy and food security. During the dry season, the region contributes 16% of the whole country's total rice production (Quddus, 2009). However, the pre-monsoon sudden peak discharge as a flash flood from the adjacent upstream areas often cause immense damage to the harvest-ready crops. The March 2017 flash flood affected nearly 1 million people and caused a potential loss of approximately 1 million metric tons of crops accounting for 3.7% of the country's agriculture sector GDP. This event compromised the overall food security of the country (ReliefWeb Flood Situation Report, 2017). The Northeastern region has been experiencing the same type of flash flood every year with varying degrees of damages and consequences. An operational flash flood forecasting and early warning system is critical for ensuring the local population's safety and protecting Bangladesh's food security.

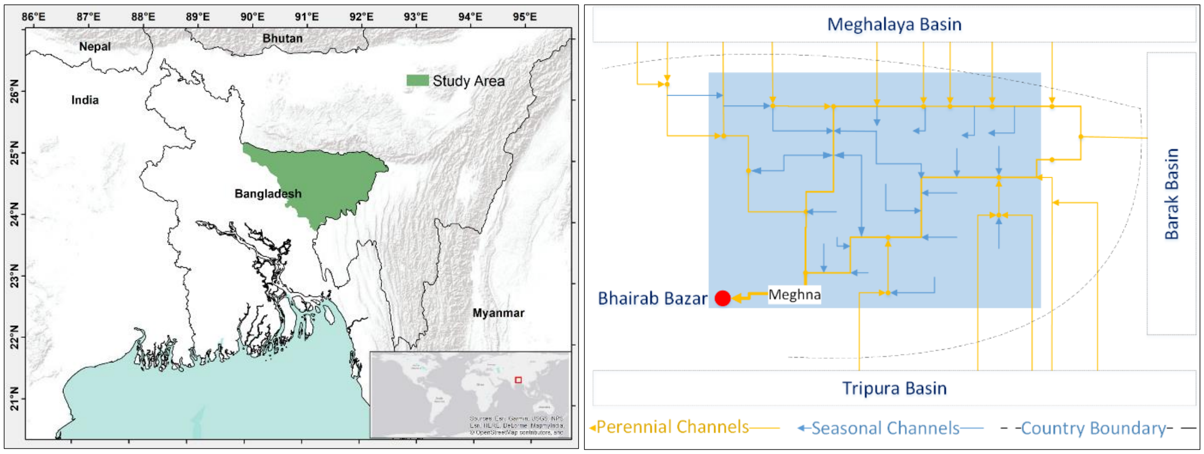

(a) (b)

Figure 3.1 (a) North-east region of Bangladesh. (b) Schematic Diagram of river network along with floodplain (shaded area)

One challenge in developing a skillful forecasting framework in the Northeastern region of Bangladesh is the complex nature of the flash flood generation mechanism. The region consists of interconnected stream networks, perennial and seasonal channels, lowland regions, and internal depressions locally known as *Haors*. In figure 3.1b, a schematic diagram of the area is shown to illustrate the hydraulic connectivity of channels and floodplains. The flashflood region is located in the downstream portion of the transboundary Meghna River basin. The upstream region consists of the mountainous Meghalaya, Tripura, and Barak river basins of India. In figure 2, the topography of the basin shows the rapid transition from hilly areas in the northern upstream region to floodplains in the southern and southwestern parts of Bangladesh. Tributaries in the north originate from Khasi and Jaintia Hills, which receive an average of 12000 mm of rainfall annually and are some of the wettest places in the world (Parry, 2013). In upstream channels where precipitation is orographically enhanced by mountainous terrain, hydrologic processes dominate the flood generation mechanism. This shifts in the downstream floodplain, where the hydrodynamic process control flood propagation. Thus, the forecasting of flashflood inducing flow depends on the ability of hydrological and hydrodynamic models to represent the processes at the small scales of interest as well the availability and accuracy of rainfall, soil moisture, and topographical data used to drive the models (Yatheendradas et al., 2008; Simons et al., 2014). This also means that conventional techniques used in river-based flood forecasting are not suitable for flash floods in floodplains where two-dimensional hydrodynamic processes dominate the hydrological or channel flow processes (Sangati, 2009). The characteristics of the rain (intensity, duration, amount, and time-space distribution) and the physical and hydrological characteristics of the watershed (area, length, slopes, shape, type of soil and land cover, and antecedent conditions) need to be accurately captured for any framework to forecast flash floods.

Another critical ingredient for flash flood forecasting is forecasted precipitation. Forecasted precipitation is a key parameter in forecasting flows for a lead time longer than the time of concentration of a river basin (which is short for mountainous basins). Recent advancements in satellite earth observations and enhanced capabilities of computer models now enable Quantitative Precipitation Forecasts (QPF) (Liguori et al., 2012; Liu et al., 2015). Forecasted precipitation produced by Numerical Weather Prediction (NWP) models, with global scale coverage, and near real-time availability, are already being applied in river flow forecasting and monsoon flood forecasting (Verbunt et al., 2006; Roberts et al., 2009; Liguori et al., 2012). Some recent studies also dynamically downscaled the NWP forecasts using the high-resolution Weather Research and Forecasts (WRF) model and terrain and land-use features (Rao et al., 2007; Hsiao et al., 2013; Sikder & Hossain, 2016). Although WRF based downscaling methods improve the accuracy of the forecasts, computational resources, and limited internet accessibility are a concern in developing countries like Bangladesh (Sikder & Hossain, 2017). Thus, it is also crucial for flash flood forecasting methods to be computationally efficient for use in an operational setting without compromising accuracy.

Among the available methods, the most widely used operational method for flash flood forecasting is Flash Flood Guidance (FFG) method (Georgakakos, 1986). Estimation of threshold runoff volume of various durations and soil moisture accounting (Sweeney et al., 1992) was required in this method. It is usually lumped over the basin; spatial and temporal distribution of threshold runoff within the basin and influence of soil and land cover characteristics are not considered. Other approaches have used multi-sensor data and Neural Networks (NN) for the purpose of flash flood forecasting (Kim & Barros, 2001; Piotrowski et al., 2006; Chiang et al., 2007). Kim & Barros (2001) used NWP forecasts, wind, and pressure data along with rain gauge data in an artificial neural network to produce streamflow forecasts with up to 24h lead-time. Chiang et al. (2007) developed a data-based approach using Recurrent Neural Network using gauge observations and satellite-derived PERSIANN-CCS (Precipitation Estimation from Remotely Sensed Information using Artificial Neural Networks-Cloud Classification System) precipitation (Hong et al., 2004). Chen & Yu (2007) proposed a probabilistic approach for flood stage forecasts based on hourly water stage and rainfall data using support vector regression and the probability distribution of forecast error based on fuzzy inference. In most methods published in the literature, hydrological and topographical characteristics of the catchments do not appear to be explicitly represented, except for rainfall and discharge. Also, all of the statistical and probability-based approaches (i.e., Kratzert et al., 2018; Sajikumar & Thandaveswara, 1999; Wang et al., 2015) require a long time-series for training the model, which is not available in the case of ungauged and transboundary basins, like Northeastern Bangladesh.

The most recent computing advancements have made modeling approaches to flash flood forecasting more feasible (Liang & Smith, 2018). Jasper et al. (2002) first used numerical weather prediction models to produce meteorological observations and then used them as forcing data in a distributed hydrological model to forecast flash floods in an alpine watershed. England et al. (2007) applied a physically-based distributed Two dimensional, Runoff, Erosion, and Export (TREX) Model to simulate (hourly) extreme floods in semi-arid regions in the western United States. There are also atmosphere-hydrological coupled models, such as the National Center for Atmospheric Research (NCAR) developed WRF-Hydro modeling system (Gochis et al., 2015). For flash floods, WRF-Hydro can be applied to simulate high-resolution hydrometeorological processes such as surface overland flow, saturated subsurface flow, channel routing, and baseflow processes. The lack of representation of interconnection between stream networks is a common limitation in all hydrological models, which makes WRF-Hydro unsuitable for Northeastern Bangladesh. It is necessary to include hydrodynamic/hydraulic models in conjunction with hydrologic models to properly represent the hydraulic processes in the river channels and floodplains.

Besides the discharge and river flow forecasts, it is also necessary to produce an accurate mapping of the spatial extent of inundation forecasts to trigger location-specific warnings, damage assessment as well as to plan relief and rehabilitation. A minimal number of studies used the hydrodynamic modeling approach, and those that did were limited to one-dimensional (1D) flow simulation (Fread, 1993, Ghoneim & Foody, 2013) to produce station-based forecasts. There are no such published studies where two-dimensional hydraulic processes have been represented along with hydrological models in an operational framework for flash flood/flood forecasting to the best of our knowledge. Possible reasons for this might be due to i) complexity in modeling development, calibration, and validation of multiple models that depend extensively on meteorological, hydrological, and topographic data and ii) computation time of simulation of a complex framework consisting of meteorological-hydrological-hydraulic processes.

In this study, the objective is to explore the optimal combination of scale, time step, and complexity in topographic and hydro-meteorological observations for developing a flashflood forecasting system. The core component of the framework is based on making use of globally available weather forecast data in real-time from NWP models. These precipitation forecasts can drive the hydrologic-hydrodynamic framework without any computationally expensive downscaling. As a first step, the approach here is to investigate how publicly available forecasts on precipitation from the global NWP model like GFS perform and whether skill remains acceptable without any regional NWP based downscaling using WRF. The specific research questions that this study answered are 1) *What is the optimal combination of scale, timestep, and complexity for topographic and hydrometeorological data to produce skill flashflood forecasts?* And 2) *What is the baseline accuracy of a flashflood forecasting system that is achievable without the dynamic downscaling of NWP weather forecasts?* In the paper, datasets used and detailed methodology is described in section 3.2 (Data and Methods) followed by section 3.3 (Results and Findings). Significant findings, conclusions, and recommendations are presented in section 3.4.

3.2 Data and Methods

3.2.1 Datasets

3.2.1.1 Hydro-meteorological data

We used Climate Hazards Group InfraRed Precipitation with Station data (CHIRPS, link: http://legacy.chg.ucsb.edu/data/chirps/index.html) (Funk et al., 2015) as the reference precipitation product during the model calibration-validation phase. The temporal accumulation is of daily scale, and the spatial resolution of the dataset is 0.05 degree by 0.05 degree. As a nowcast source of precipitation for the operational framework, we explored two near-real-time precipitation products, namely GSMaP-NRT (link: https://sharaku.eorc.jaxa.jp/GSMaP_NOW/index.htm) (Okamoto et al., 2005; Kubota et al., 2007; Aonashi et al., 2009; Ushio et al., 2009) and Global Precipitation Measurement (GPM) Integrated Multi-satellitE Retrievals for GPM (IMERG, link: https://pmm.nasa.gov/data-access/downloads/gpm) Early Run Version 05B. GSMaP and IMERG precipitation's spatial resolution is 0.1^0 by 0.1^0, and temporal resolution is half an hour (IMERG) and 1 hour (GSMaP). Both of the products are available with a latency of 6 hours.

Solar radiation, average wind speed, maximum and minimum temperature, relative humidity datasets are also collected from various sources. Gridded monthly solar radiation data collected from NASA Prediction of Worldwide Energy Resources (link: https://power.larc.nasa.gov/data-access-viewer/). Average wind speed, maximum and minimum temperature, and relative humidity data are retrieved from the National Climatic Data Center of NOAA (https://www7.ncdc.noaa.gov/CDO/cdoselect.cmd?datasetabbv=GSOD). In situ observed WL are provided by Bangladesh Water Development Board (www.bwdb.gov.bd). Rated discharge is generated using the rating curve provided by the same institution.

3.2.1.2 Numerical Weather Prediction (NWP) Outputs

NWP products are the key parameter used in this study. The Global Forecasting System (GFS) developed by the National Oceanic and Atmospheric Administration (NOAA) was used as the source of forecast precipitation from a global NWP model. Historical dataset of GFS forecast precipitation was downloaded from https://www.ncdc.noaa.gov/data-access/model-data/model-datasets/global-forcast-system-gfs. In the nowcast system we developed, the datasets are downloaded from https://nomads.ncep.noaa.gov/cgi-bin/filter_gfs_0p25.pl utilizing the online spatial and parameter-based subsetting facility. The GFS weather forecast products are updated every 6 hours up to 16 days lead-time at a spatial resolution of 0.25^0 by 0.25^0. The temporal accumulation of precipitation products used in this study was 3 hours.

3.2.1.3 DEM, soil, and land cover data

The Shuttle Radar Topography Mission (SRTM) developed void filled Version 3.0 SRTM Global 1 arc second product was used as the DEM, downloaded from https://earthexplorer.usgs.gov/. Land cover data for the hydrologic and hydrodynamic models were derived from Climate Change Initiative developed Land Cover Maps of 2015 by using MERIS of Envisat along with SPOT-Vegetation, AVHRR, and PROBA-Vegetation mission datasets, which is available at http://maps.elie.ucl.ac.be/CCI/viewer. Soil data and information related to soil properties were retrieved from http://www.fao.org/soils-portal/soil-survey/soil-maps-and-databases/en/.

3.2.1.4 Sentinel-1 (SAR) Datasets

Sentinel 1 (SAR) imagery products were used to compare the framework generated flood inundation maps. Synthetic Aperture Radar (SAR) is an all-weather satellite with the advantage of operating at wavelengths not impeded by cloud cover and day-night image acquisition. The images are at 10m spatial resolution with an average temporal resolution of 10 days. All of the sentinel images were processed using Google Earth Engine (GEE) (Gorelick et al., 2017). A backscatter coefficient of -14db (Ahmad et al., 2019) was used to differentiate between water and non-water features. Finally, the extracted maps were used to assess the accuracy of the generated forecasts.

3.2.2 Methodology

The critical steps of our flash flood forecasting framework development are DEM correction and recondition, base hydrological and hydrodynamic model calibration-validation, and operationalization of the system. Each of these steps is discussed in the following sub-sections.

3.2.2.1 DEM correction and reconditioning

Generally, rivers in a high terrain region can easily be delineated using any hydrological analysis tool (e.g., Automatic Watershed Delineation of SWAT, ArcHydro tool of ArcGIS). However, in the floodplain, it is quite difficult to distinguish between the floodplain and the river channels using automated tools. For accurate representation, the river network in the floodplain was manually derived first using google earth. The automatic watershed delineation tool of the ArcSWAT model was also used to delineate the river network in the basin. The delineated network and manually digitized networks were then merged to create a more accurate river network map. Using this river network, the SRTM DEM was reconditioned, and the watersheds were delineated for further processing. The DEM was reconditioned using a sharp drop of 10m (burning) and a smooth drop of 5m along the channels. This reconditioned DEM was finally used as the topography input into the hydrological model. During the development of the base hydrodynamic model, a sensitivity analysis was performed using different amounts of systematic errors in SRTM DEM tested (i.e., 2.0m, 2.5m, 3.0m, 3.5m, and 4.0m). Finally, it was found that an assumption of 3.5m of error in SRTM Dem produced the best estimation of flood inundation when compared with independent and in-situ observations.

3.2.2.2 Base Hydrological Model Development and Calibration

The Soil and Water Assessment Tool (SWAT) was used here to develop the hydrological model. SWAT (Soil & Water Assessment Tool) is a river basin scale hydrological model used to simulate the quantity of surface and groundwater. The hydrologic cycle simulated by SWAT is based on the water balance equation. It is a semi-distributed physically-based model that divides the basin into a number of Hydrologic Response Units (HRU). An HRU is a unit of area with uniform land use, soil type, elevation, and slope. We used the SWAT Model at daily timestep to simulate streamflow at the floodplain boundary locations. The model was developed using the reconditioned DEM, land use, and soil data. For the SWAT model, the following parameters were computed: monthly climatology of precipitation; the average number of days of precipitation; the standard deviation of precipitation; skew coefficient of daily precipitation; the probability of wet day following a dry day; the probability of wet day following a wet day; maximum 0.5 h rainfall; maximum and minimum air temperature; average wind speed; daily dew point temperature and daily solar radiation. Most of these parameters (monthly climatology of precipitation; the average number of days of precipitation; the standard deviation of precipitation; skew coefficient of daily precipitation; the probability of wet day following a dry day; the probability of wet day following a wet day; maximum 0.5 h rainfall;) were calculated using CHIRPS precipitation for the period of 1980-2017 or climatology datasets from National Climatic Data Center (NCDC). Except for precipitation, the climatology of all other datasets is used during the simulation of the SWAT model. During the calibration phase, the CHIRPS precipitation dataset was used in this model.

The model was calibrated using the observed data from 2004-2012. The optimized parameters were used to validate the model from 2013-2017. In figure 3.2, the model domain is shown along with basin boundary and modified stream network. Inflow calibration locations of the hydrological model are also shown in the same figure.

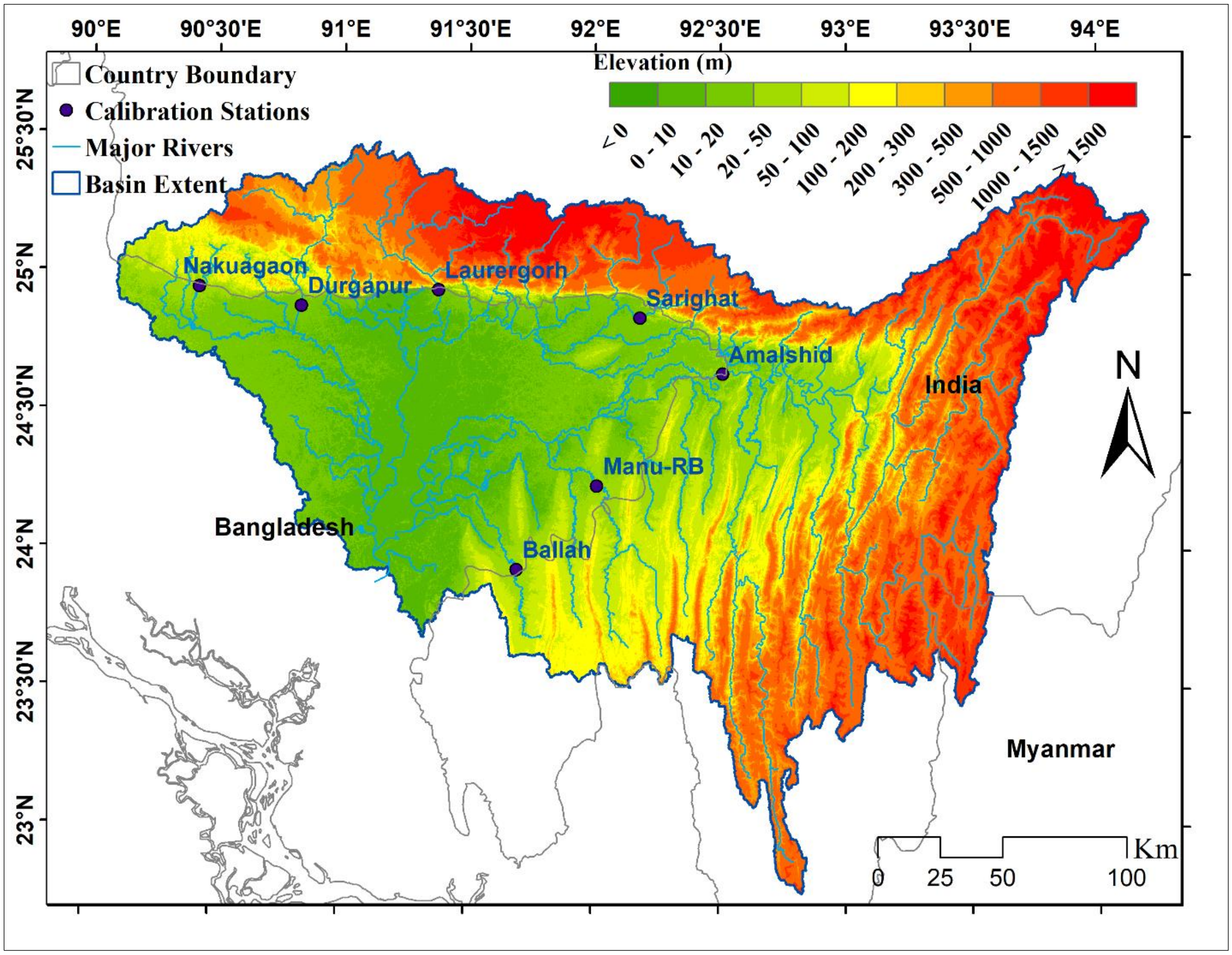

Figure 3.2 Hydrological Model Domain and calibration-validation stations (elevation is based on corrected and reconditioned SRTM DEM and shown as above mean sea level).

3.2.2.3 Hydrodynamic Model Development and Optimization

Using the Climate Change Initiative (CCI) developed land cover data, Manning's n values were defined for overland flow in the floodplain. Hydraulic Engineering Center developed HecRAS version 5.0.5 was used to develop the hydrodynamic model. The main advantage of this model is improved stability due to the use of an implicit finite volume approach, which is more robust than the finite element or finite difference method (used by the earlier versions of HecRAS). It allows larger simulation timestep compared to explicit methods allowing a higher value of Courant–Friedrichs–Lewy (CFL) condition. Diffusion wave or full momentum 2D equations are being used in this model. The simulation grid cells have stage-storage relationships derived from terrain or DEM dataset, allows larger computational cells without loss of terrain details. The hydraulic geometry was created as a 2D flow area of the floodplain. Manning's n was assigned according to the Landcover type following the suggestions from HEC-RAS River Analysis System 2D Modeling User's Manual. The hydrological model generated calibrated inflow into the floodplains was defined as the upstream boundary condition. The downstream boundary condition of the model was the observed water level during calibration-validation of the framework. Average precipitation over the floodplain was also included as a boundary condition in the model. The domain of the hydrodynamic model and unsteady boundary locations are shown in figure 3.3.

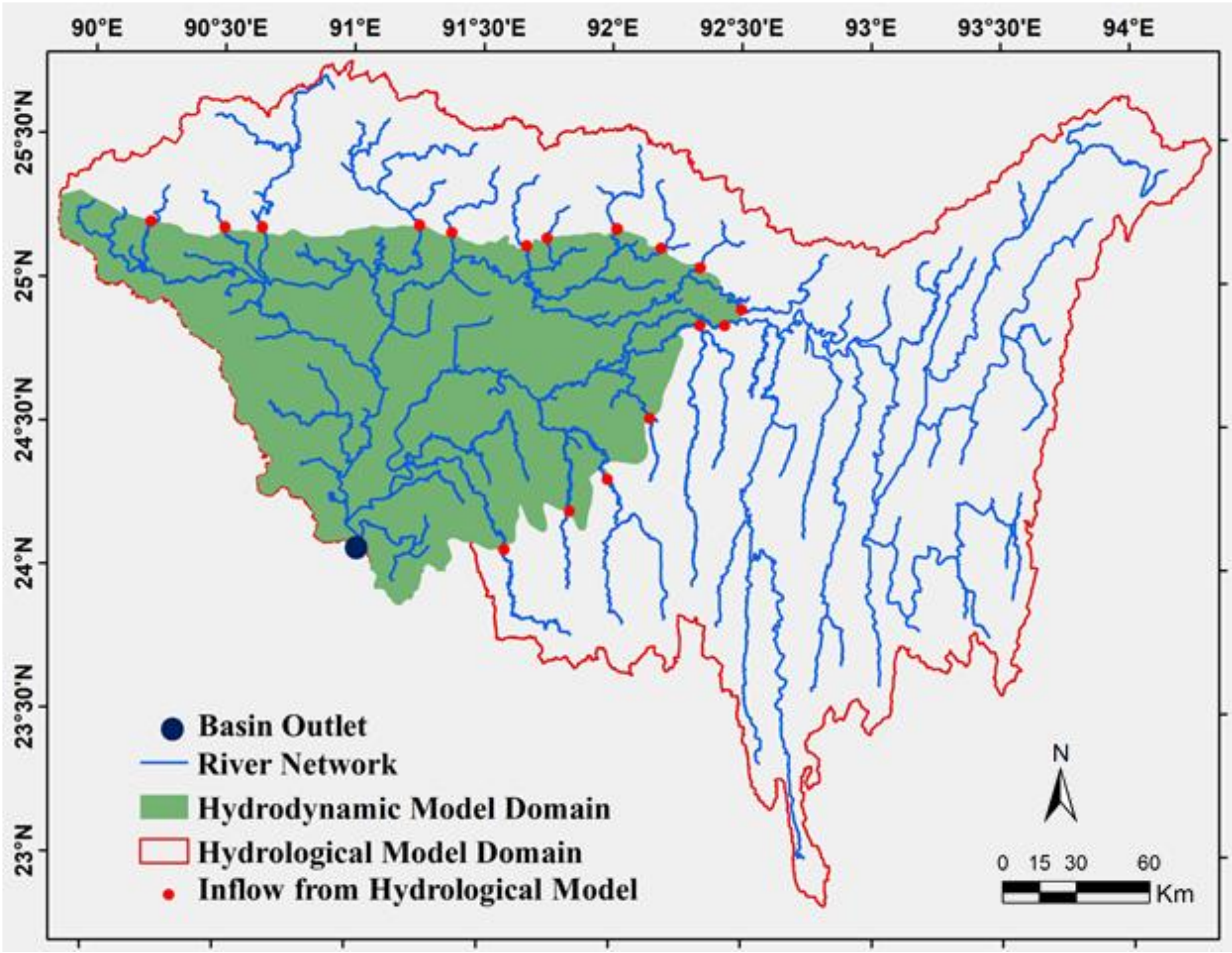

Figure 3.3 Hydrodynamic Model Domain along with unsteady boundary locations

3.2.2.4 Bias Correction of simulated results

To increase the accuracy of the modeling framework, an error correction strategy was used as follows. In-situ measurements available on the day of making a forecast were utilized to improve the accuracy of forecasts. The error in simulated (nowcast) results was calculated by comparing with observed water heights for that day (time t=0 or nowcast). This systematic error amount was subtracted from the forecast water heights. The error correction is explained in equations 3.1 and 3.2. Finally, an average of the bias of all of the observed stations was subtracted from the model generated inundation depth to generate actual forecast inundation.

$$\text{error} = \text{WL}_{\text{simulated}}[\text{x}] - \text{WL}_{\text{observed}}[\text{x}] \quad (3.1)$$

$$WL_{forecast}[i] = WL_{simulated}[i] - error \quad (3.2)$$

$Where, x =$ forecast date, $i =$ forecast lead time

3.2.2.5 Operational Framework Development

Using the optimized selection of model configurations and the error correction strategy, the framework was made functional for real-time operations. In the operational setting, the latest GPM-IMERG nowcast and GFS forecast precipitation data were downloaded at every model timestep. GFS forecast precipitation was resampled to 0.1^0 by 0.1^0 to match the resolution of GPM-IMERG precipitation. The SWAT hydrological model was simulated, and the inflow at different locations was calculated. These inflows were then used in the HecRAS model as boundary flow conditions. For the forecast period, different downstream boundary conditions were tested (for example, model-simulated discharge, rating curve, normal depth), and it was found that the hydrodynamic model performed best when hydrological model simulated discharge was used as the downstream boundary condition.

The HecRAS model was then simulated for every forecast time-step using a restart option to conserve computational time. The computed water heights and inundation maps were then corrected using the error correction technique mentioned in section 3.2.2.3 and equations 3.1-3.2. Finally, all the simulated maps and time-series forecasts were pushed to the web-based user-interface at http://depts.washington.edu/saswe/flashflood. On this web-interface, users can view the real-time forecast precipitation, discharge, water heights, and inundation for up to 5 days lead-time. In figure 3.4, the methodology for the operational system is summarized as a flowchart.

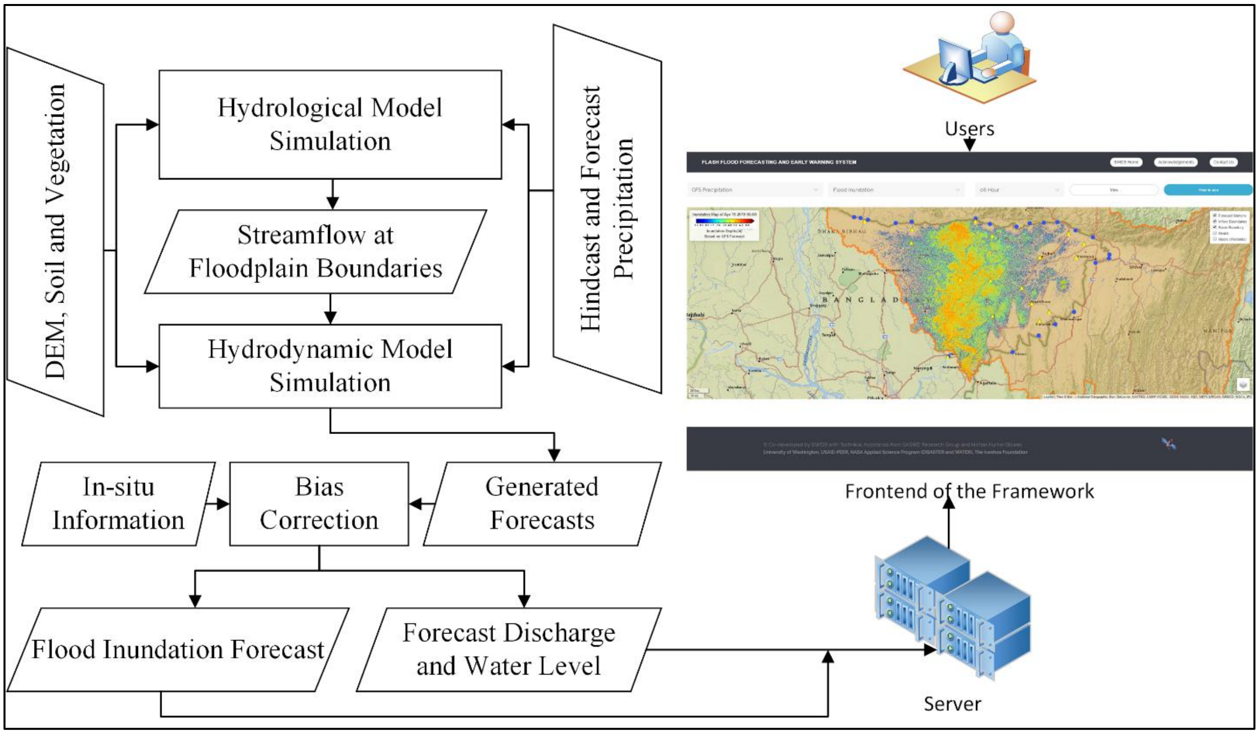

Figure 3.4 Operational flow-chart and the frontend of the framework.

3.3 Results and Discussion

In this section, all the findings during calibration-validation and operationalization are discussed. The stations used during performance assessment of hydrological and hydrodynamic models, including calibration and validation were shown in figure 3.5.

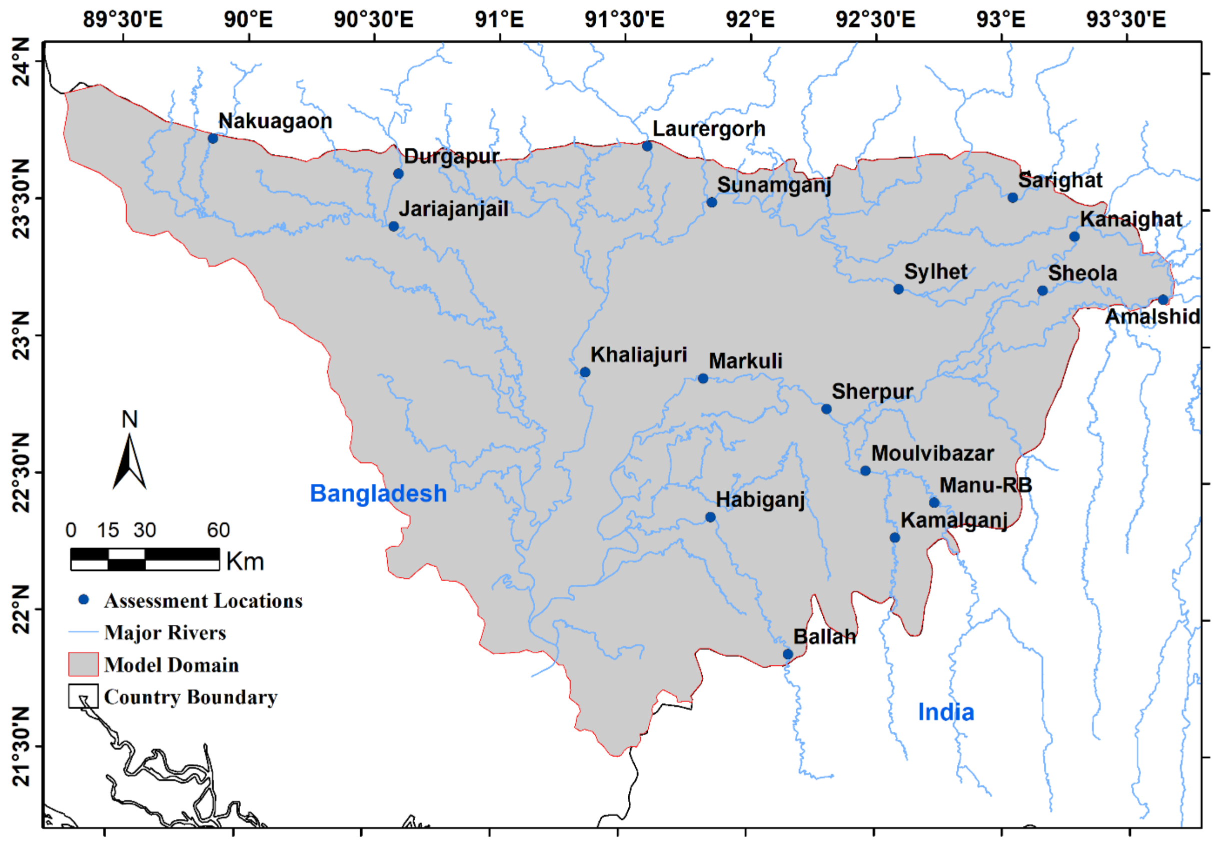

Figure 3.5 Floodplain river stations for performance assessment

3.3.1 Hydrological Model calibration

The SWAT model was calibrated manually using rated discharge at six inflow boundary stations. These were the locations within the basin and on the boundary of the floodplain, which contributes almost all of the inflows into the floodplain (shown in figure 3.2). Calibrated parameters were selected from Neitsch et al. (2001), and their optimized values are reported in Table 3.1. These parameters are i) 3 surface water components (Curve number and Plant Uptake and Soil Evaporation Factor); ii) 2 soil water factor (Available soil water capacity and Soil Saturated Hydraulic Conductivity) and iii) 4 groundwater parameters (Groundwater delay, groundwater revap constant and Re-evaporation threshold). Among these parameters, Curve numbers were optimized by a multiplication factor of 1.231 from the original values, and others were replaced with the mentioned values.

Table 3.1 Calibrated parameters of SWAT hydrological model of Meghna Basin

Parameter	Description	Type	Range	Optimized Value
CN2	Curve Number for Moisture Condition	Surface Runoff	35 – 98	Variable
EPCO	Plant Uptake Compensation Factor	Surface Runoff	0.75 – 1	1
ESCO	Soil Evaporation Compensation Factor	Surface Runoff	0.75 – 1	0.95
SOL_AWC	Available Soil Water Capacity	Soil Water	0.0 - 1.0	0.2625
SOL_K	Soil Saturated Hydraulic Conductivity	Soil Water	0 – 2000	8.45
ALPHA_BF	Baseflow Recession Constant (Days)	Groundwater	0.01 – 1	0.5
GW_Delay	Groundwater Delay	Groundwater	1 – 500	25
GW_Revap	Groundwater “revap” Constant	Groundwater	0.01 - 0.2	0.2
RevapMN	Re-evaporation Threshold	Groundwater	0.01 - 500	375

Calibration-Validation summary and statistics of the base hydrologic model were presented in table 3.2. As an example, the Amalshid station’s calibration and validation comparison and scatterplots are shown in Figure 3.6. It was observed that the model matches well with observations for all stations, except for a few unusual peaks. The unusual peaks and deviations from observations occurred mainly during the monsoonal flood season rather than the pre-monsoon flash flood season. The independent validation period yielded similar or improved results than the calibration period because of fewer extreme peaks in the flows. The Naukaugaon station (shown in figure 3.2) showed a very unrealistic mismatch with the simulated results. We believe this is an issue related to the rating curve used, which represents low to moderate flow, but is inappropriate for high flow. Using this calibrated model, the hydrodynamic model was simulated and validated in different locations within the floodplain.

Table 3.2 Calibration and Validation results of base hydrological model

Station	Calibration (2004-2012)			Validation (2013-2018)		
	Correlation Coefficient	Root Mean Square Error (m^3/s)	Nash-Sutcliffe Efficiency	Correlation Coefficient	Root Mean Square Error (m^3/s)	Nash-Sutcliffe Efficiency
Amalshid	0.84	758.83	0.78	0.81	795.9	0.75
Laurergarh	0.76	466.36	0.65	0.78	489.87	0.63
Manu-RB	0.68	111.1	0.56	0.71	102.32	0.54
Sarighat	0.82	182.5	0.74	0.78	205.43	0.71
Nakuagaon	0.59	105.25	0.58	0.58	77.58	0.59
Durgapur	0.81	81.24	0.65	0.84	75.19	0.64

3.3.2 Hydrodynamic Model Calibration and Validation Summary

3.3.2.1 Effect of DEM correction and reconditioning

Using the output of the calibrated hydrological model, the hydrodynamic model (HecRAS) was simulated over the corrected and reconditioned DEM for the floodplain region inside Bangladesh. Calibration of the hydrodynamic model was completed manually at different locations by optimizing Manning’s n values. Optimized Manning’s n values are shown in table 3.3. In figure 3.7, the comparison plot of simulated and observed water levels of Sunamganj and Sylhet stations are shown. Overall, the hydrodynamic model results are slightly more accurate in the calibration period compared to the validation period except at the Sarighat station. We also observed that the simulated water level hydrographs at the stations lying within the floodplains (e.g., Sunamganj, Sheola, Sylhet, Sherpur) performed better than the stations located at the edge of the hydrodynamic model boundary (Amalshid, Manu-RB). Flows at the upstream boundary locations of the floodplains were more hydrologically dominated, which might explain the reason for lower hydrodynamic prediction accuracy downstream.

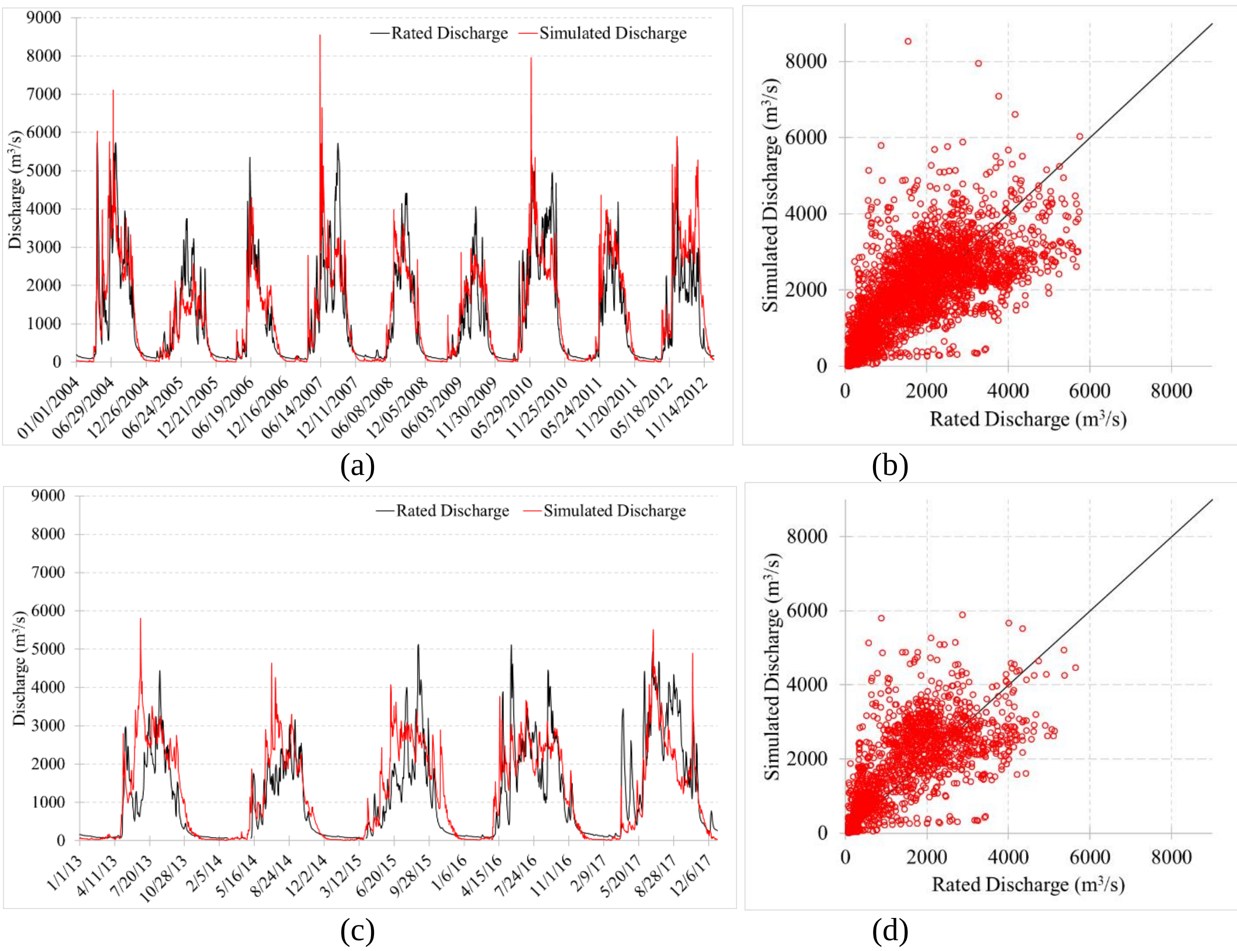

Figure 3.6 Hydrological Model Calibration (2004-2012) and Validation (2013-2017) plot of Amalshid station. (a) Calibration period timeseries comparison, (b) Calibration period scatter plot, (c) Validation period timeseries comparison, and (d) Validation period scatter plot.

Table 3.3 Optimized Manning's n for different land cover types

Land cover type	Calibrated Manning's n
Mixed Broadleaf	0.16
Bare	0.025
Vegetation	0.035
Semi-deciduous	0.16
Broadleaf	0.16
Needleleaf	0.16
Water	0.04
Mosaic Forest	0.16
Mosaic Grassland	0.035
Shrubland	0.1
Croplands	0.035
Grassland	0.035

Urban	0.15
Cropland	0.035

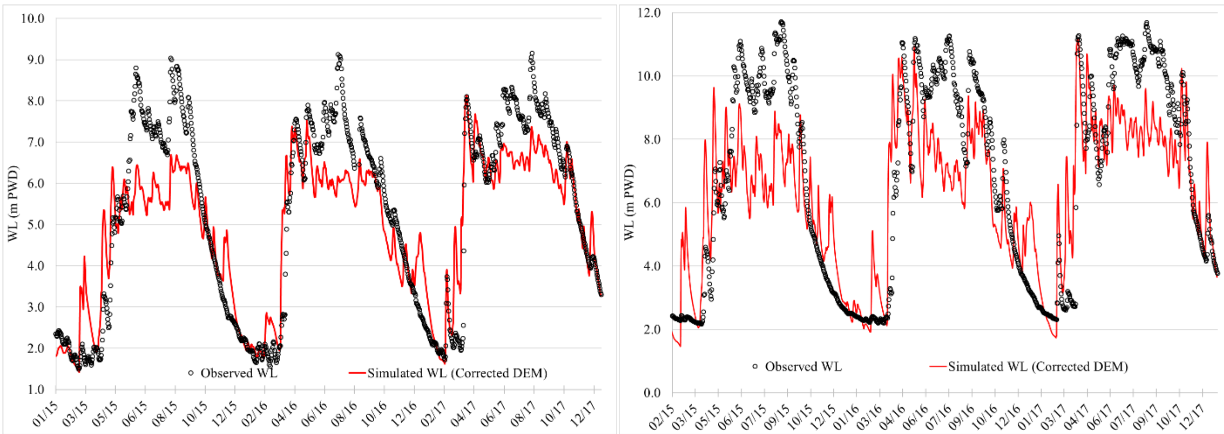

(a) (b)

Figure 3.7 Comparison of observed and HecRAS model calibrated water level at different stations, (a) Sunamganj and (b) Sylhet station.

Table 3.4 Calibration and Validation summary of the HecRAS Model

Station	Calibration (2015-2017)		Validation (2018)	
	Correlation Coefficient	Root Mean Square Error (m)	Correlation Coefficient	Root Mean Square Error (m)
Amalshid	0.68	2.82	0.61	3.29
Laurergarh	0.80	1.89	0.67	2.60
Manu-RB	0.54	3.23	0.71	0.84
Sarighat	0.80	1.93	0.72	1.47
Sheola	0.78	2.15	0.73	2.29
Sherpur	0.86	1.24	0.84	1.31
Sunamganj	0.91	1.12	0.79	1.85
Sylhet	0.83	1.88	0.72	2.59

Using the calibrated and validated modeling framework, GPM IMERG and GSMaP NRT precipitation were used to simulate water heights at four different locations reported in table 3.5. We found that GSMaP simulated water heights underestimated the measured WL in all stations. We selected GPM IMERG precipitation as the nowcast precipitation product. For further improvements of the results of the base modeling framework simulation, we proposed an error correction method described in equations (3.1) and (3.2) and then simulated the framework in forecast mode. In this case, GFS forecast precipitation along with nowcast GPM-IMERG precipitation was used to simulate SWAT and HecRAS models and generated forecasted inundation maps.

Table 3.5 Comparison of accuracy of different precipitation products-based simulated water heights

	IMERG Early Run		CHIRPS		GSMaP NRT	
Metrics	R^2	RMSE (m)	R^2	RMSE (m)	R^2	RMSE (m)
Sunamganj	0.91	1.12	0.92	1.07	0.92	1.26
Sylhet	0.83	1.88	0.88	1.73	0.86	2.15
Sheola	0.78	2.31	0.79	2.27	0.83	2.06
Sherpur	0.86	1.24	0.88	1.17	0.92	1.15

3.3.2.2 Selection of grid resolution and simulation time-step

The HecRAS model was optimized using different spatiotemporal combinations. Various simulation time-steps (5 minutes, 10 minutes, 15 minutes, and 30 minutes) were used along with different spatial grid resolution (250m, 500m, and 1000m) to perform the unsteady simulation of the model for the pre-monsoon season of 2017. The comparison of simulation time for different combinations are shown in figure 3.8. From figure 3.8, we observed the unnoticeable sensitivity of the framework to simulation timesteps. A likely reason is that final results are accumulated over the hourly and daily scale, which minimizes the error associated with simulation time-step at the minute scale. On the contrary, the simulation grid size greatly influenced the computational time of the model. It took less than 5 minutes to simulate the model at 1000m grid resolution (for any time step), whereas computation time was more than 1 hour for 250m resolution. Root mean square error (RMSE) and correlation coefficient comparison of different simulation grid sizes are also shown in figures 3.9 and 3.10, respectively. In the case of the finest spatial grid size (e.g., 250 m), the hydrodynamic model was found to be unstable, and there was a large variation in the simulated water stage in some stations. The sensitivity of simulated results was also dependent on the location of the grid cells. Some of the stations are located on river banks that lie on the boundary between two adjacent cells, which can have highly varying modeled water stage (e.g., Nakuagaon, Amalshid station for 250m spatial resolution). The 1000m grid resolution, on the other hand, yielded very unrealistic results at most of the stations. The river channels in the floodplain area are not large enough to be covered by a single coarser simulation grid cell. Sudden elevation drops from neighboring grids at 1000 m resolution gives rise to uncertainty. Based on the required simulation time and obtained accuracy for different grid sizes, the 250m simulation grid size was chosen as the optimal grid resolution. Using optimized simulation time-step and spatial grid resolution based on the 2017 simulation, historical simulation of the framework was also performed for the pre-monsoon period of years 2016 and 2018.

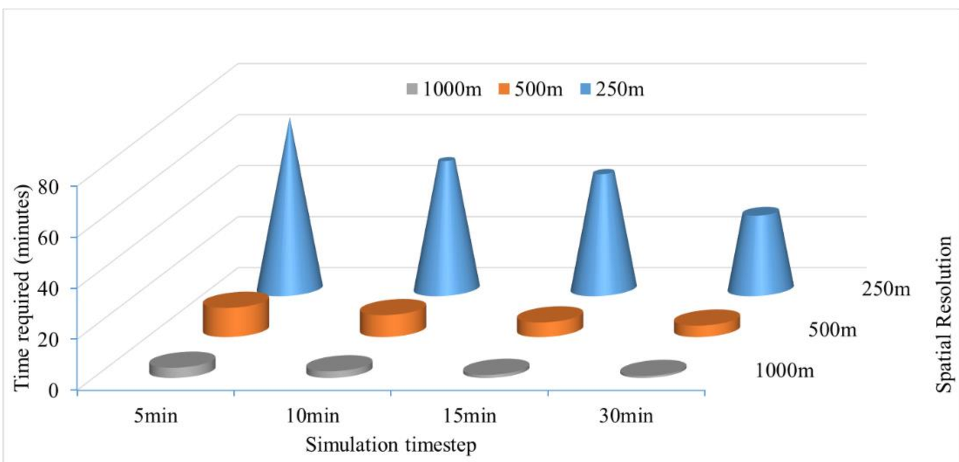

Figure 3.8 Comparison of simulation time of HecRAS model for the different combination of time-step and simulation grid resolution

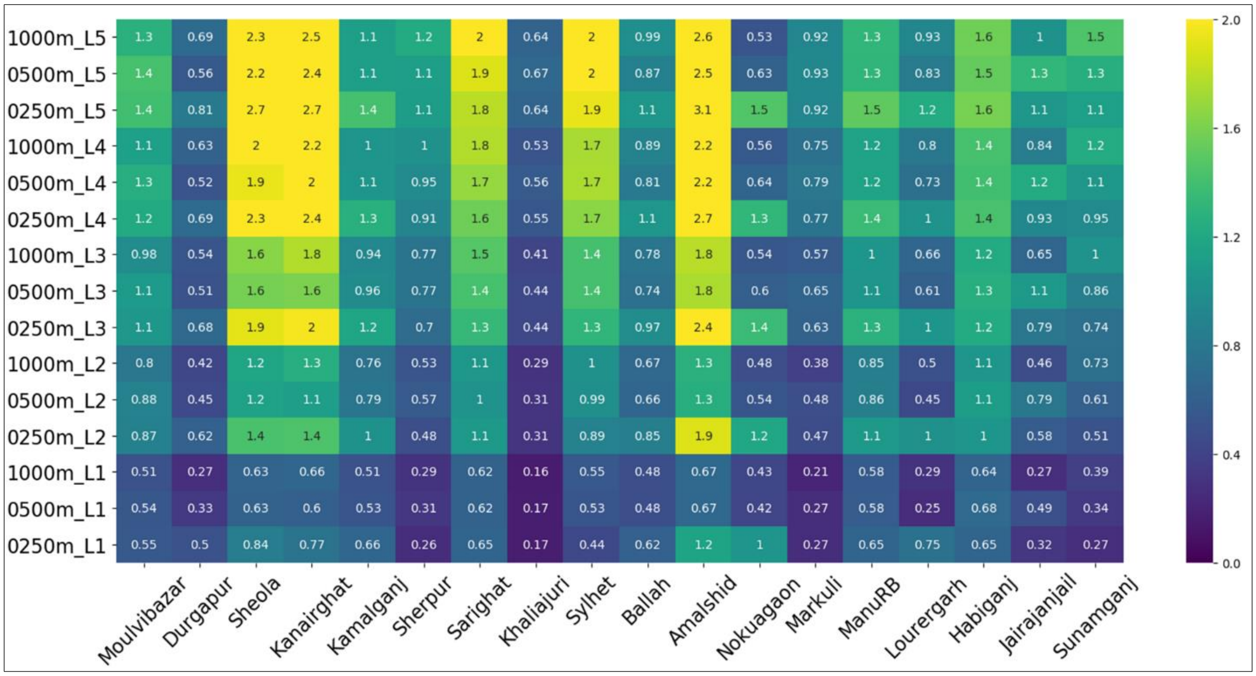

Figure 3.9 RMSE (m) comparison of the stations for different spatial resolution and lead-time for March 2017- May 2017 period, y-axis labels indicate grid resolution and forecasting lead time (i.e., 1000m_L1 means grid resolution is 1000m and L2 means two days forecasting lead time)

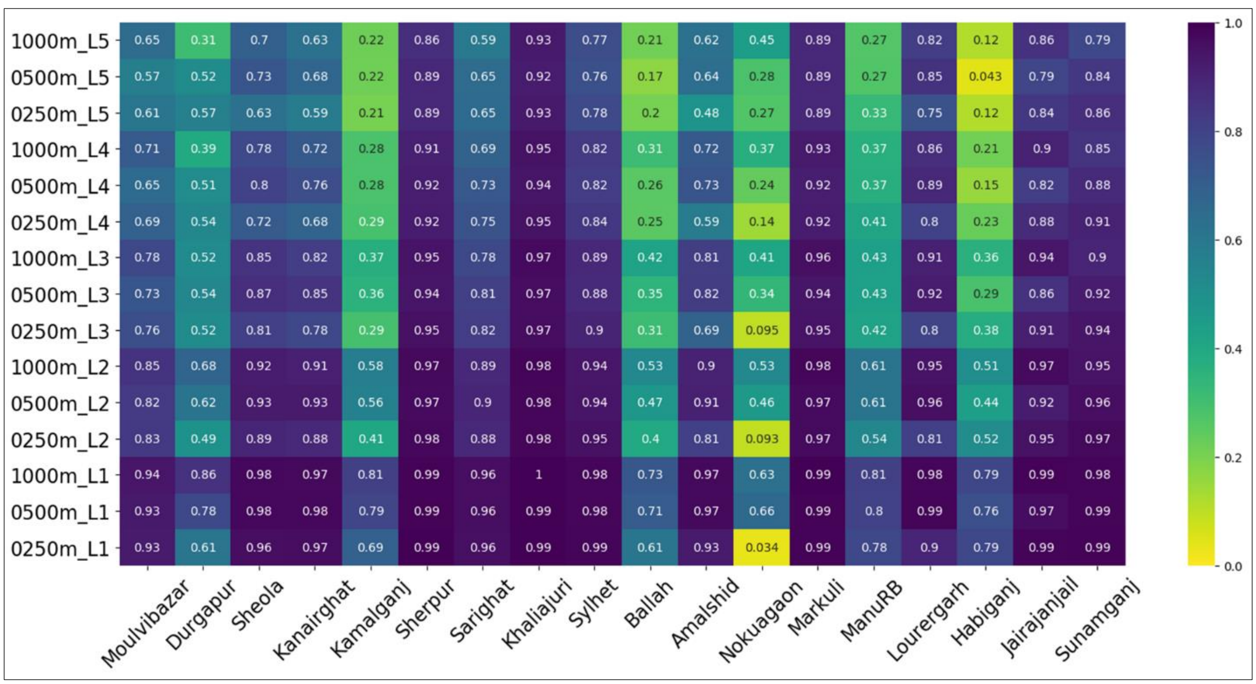

Figure 3.10 Correlation coefficient comparison of the stations for different spatial resolution and lead-time for March 2017- May 2017 period; y-axis labels indicate grid resolution and forecasting lead time (i.e., 1000m_L1 means grid resolution is 1000m and L2 means two days forecasting lead time)

3.3.3 Historical performance of the framework

In both years of validation (2016 and 2018) of the HecRAS model, all stations yielded better results than the year 2017. In figure 3.11a and 3.11b, simulated forecasts for different lead times with the observed data are shown. The Root Mean Square Error (RMSE) and Correlation Coefficient for March-May are shown in figures 3.11c and 3.11d.

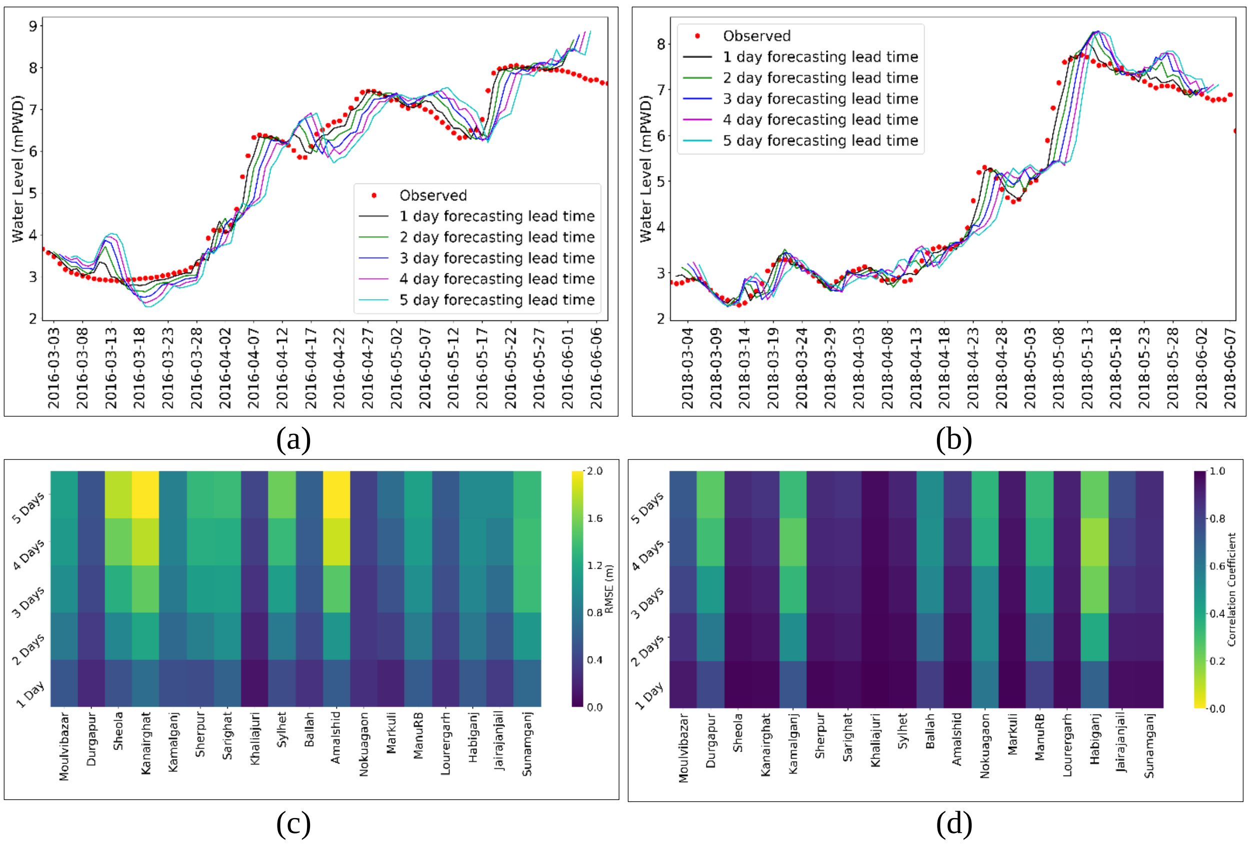

Figure 3.11 (a) and (b) Timeseries comparison for different forecasting lead-time of Markuli station for the pre-monsoon season of 2016 and 2018, (c) RMSE (m) comparison of the stations for the year of 2016, and (d) Correlation Coefficient comparison of the stations for the year of 2016

Another plot is shown in figure 3.12 for the average of model performance vs. lead time to illustrate the framework's predictive skill. Here the average RMSE and correlation coefficient of the stations are taken for different lead times and plotted against the lead time. From the figure, it can be seen that the average RMSE of the stations is less than 0.5m for three days lead time with a correlation coefficient of more than 0.75.

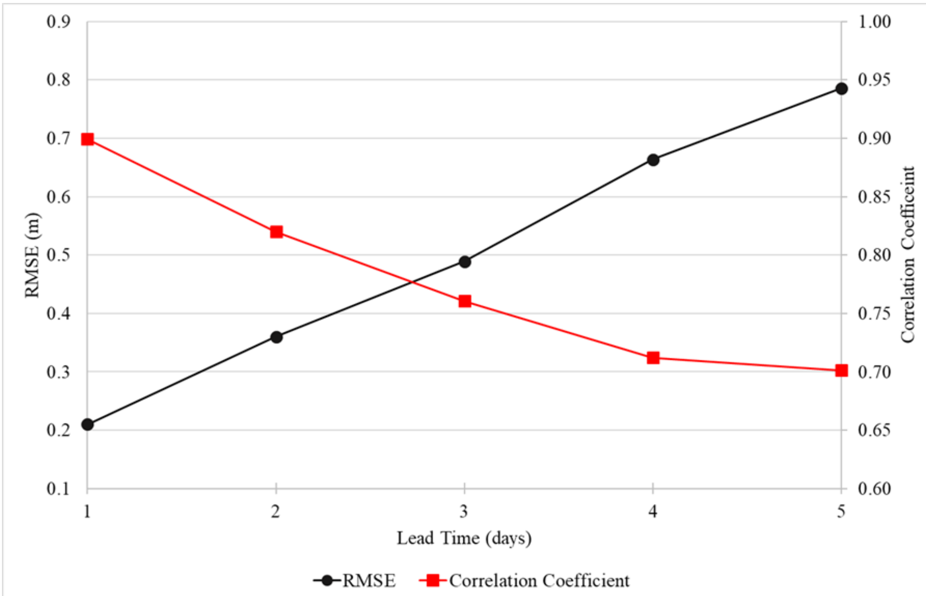

Figure 3.12 Average performance of the framework vs. Lead time graph

3.3.4 Spatial Accuracy of forecast inundation

The proposed framework was designed to produce discharge/water level forecasts as well as inundation forecasts. Sentinel 1 (SAR) based imagery product used to assess the model generated forecasts. The assessment was performed in three modes: 1) Historical analysis of the framework for the years 2016-2018, 2) Single extreme episode-based analysis for March 2017 flood, and 3) Performance in an operational setting. In the following sections, these modes of assessment are described.

3.3.4.1 Historical performance

The model generated inundation forecasts of the pre-monsoon season of 2016, 2017, and 2018 were compared with Sentinel 1 Synthetic Aperture Radar (SAR) imagery derived inundation. Google Earth Engine (GEE) was used to extract inundation from Sentinel 1 gridded SAR data. A total of 69 Sentinel 1 images during the model simulation were considered. From the analysis, we found the probability of detection (POD) of non-water and POD of water to be more than 60% for up to 5-day lead-time. Here, POD was expressed as a percentage that the model correctly identified water and non-water features compared to the selected Sentinel imageries. In figure 3.13, the POD comparison of water and non-water features for different lead times were shown. In figure 14, the spatial POD map of water and non-water for 1-day lead time and 5-day lead time was shown. Some issues were observed during the water detection and non-water feature detection by the model. For example, in some locations identified as non-water by Sentinel 1 SAR data, the model was erroneously identified as inundated. A possible reason for these errors is due to the age of the DEM used. SRTM was created more than 18 years ago and is not up to date with recent human developments and modifications of the region's floodplain.

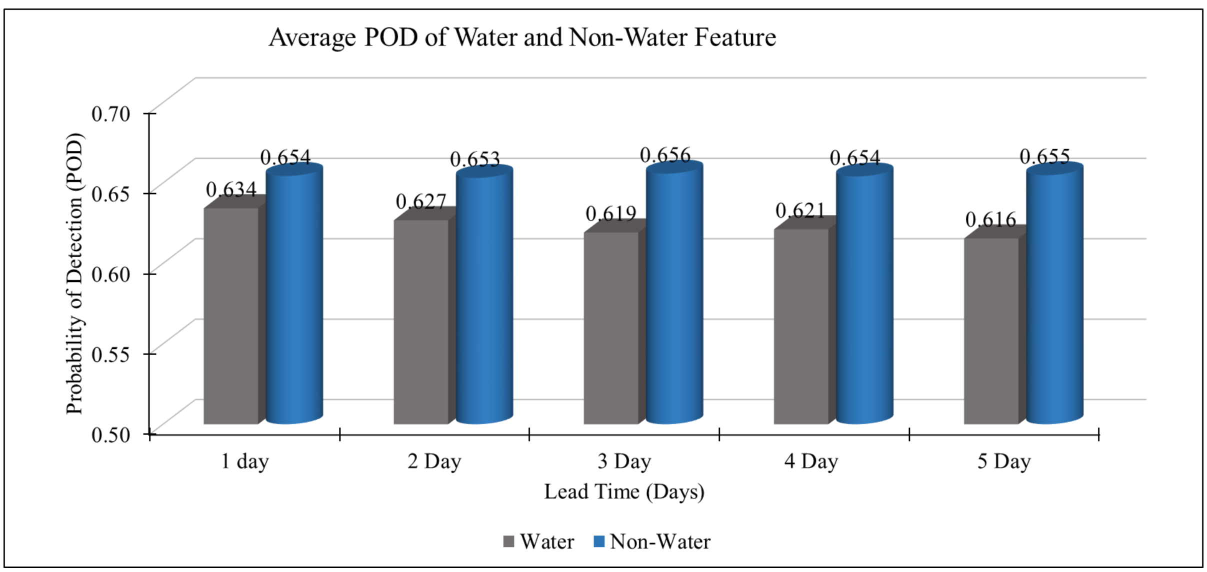

Figure 3.13 Probability of Detection of water and non-water features during the period of March-May of 2016, 2017 and 2018

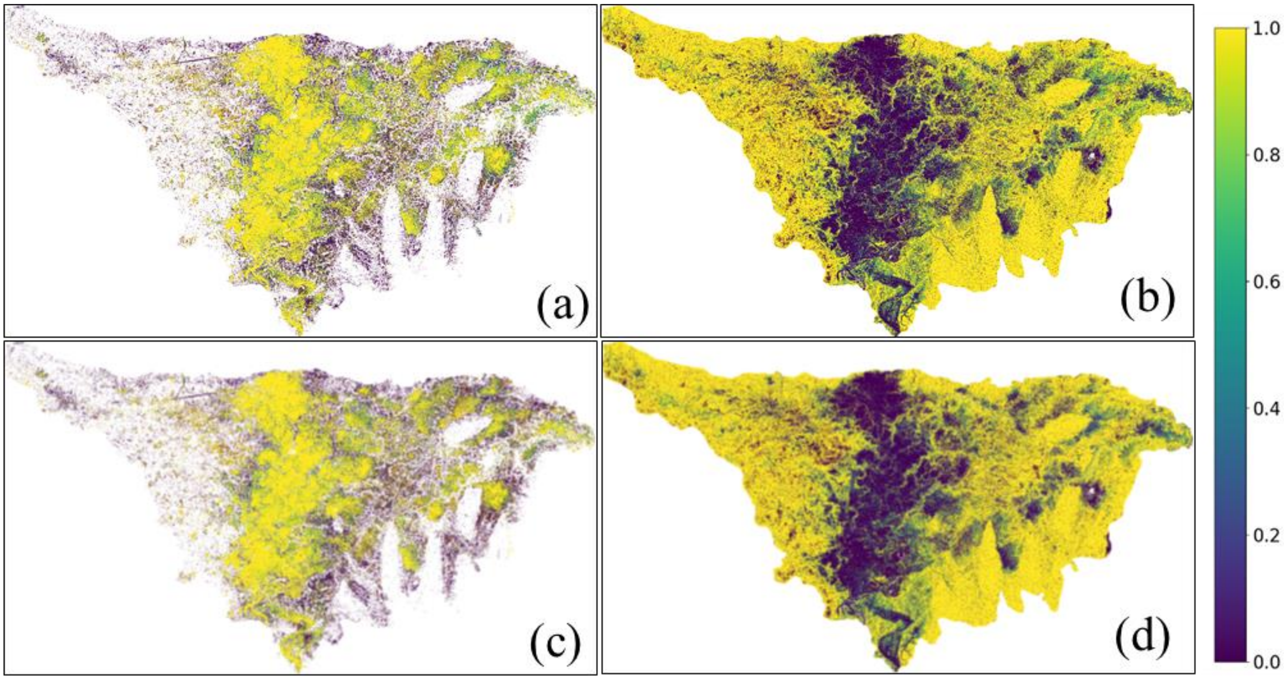

Figure 3.14 POD Map of water and non-water for different lead times. (a) Water for 1-day lead time. (b) Non-water for 1-day lead time. (c) Water for 5-day lead time. (d) Non-water for 5-day lead time

3.3.4.2 Event-based Performance

The proposed framework was also tested for a single event when a major flash flood occurred in the region. For the event of the March 2017 flood, five Sentinel-1 images were considered separately to illustrate the performance during a single extreme event. Two images from before the flood event (21st March 2017 and 26th March 2017), one image during the flood event (31st March 2017), and two images from after the flood event (2nd April 2017 and 7th April 2017) were considered.

We observed that model simulated inundation overestimated the Sentinel 1 based water area. During the dry period, the model overestimated the SAR based inundation. It is possible that Sentinel-1, which employs a C-band radar, may not be the best choice for inundation mapping in the Haor area where flooded vegetation is widespread. Also, the difference between the actual acquisition time of the imagery and the simulated inundation maps could be another potential reason. In figure 3.15, the POD of water and non-water comparison is shown for different imagery dates and lead-times.

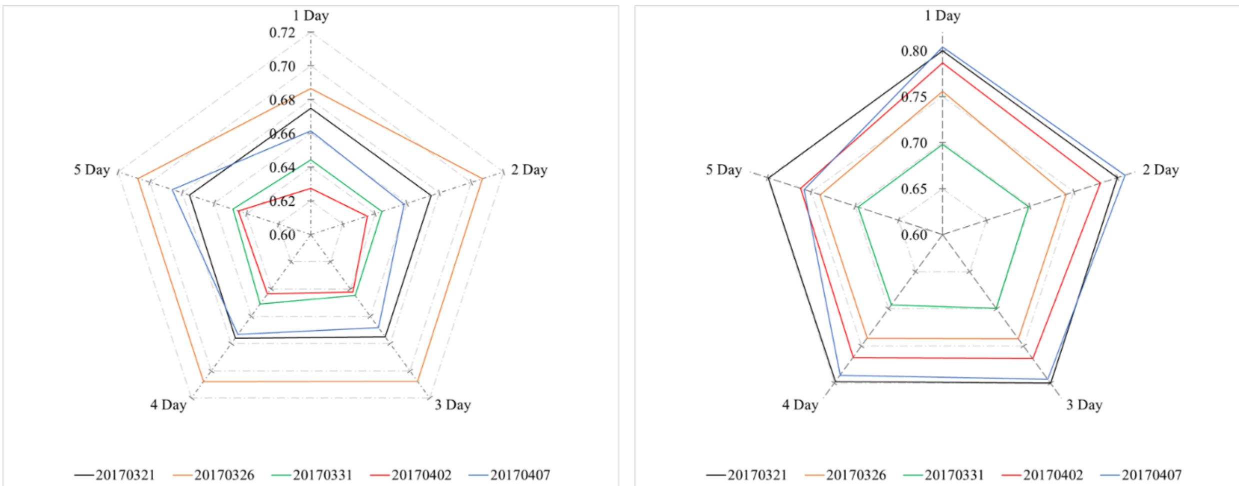

(a) (b)

Figure 3.15 Probability of Detection (POD) comparison of Sentinel 1 imagery and model-simulated inundation. (a) POD of non-water and (b) POD of water.

3.3.4.3 Performance in the operational setting

Upon making the framework operational, there was one flood peak observed on March 4th of 2019 that was assessed via the user interface at http://depts.washington.edu/saswe/flashflood. To quantify the system's accuracy in an operational setting, the inundation forecast was compared with Sentinel 1 SAR derived inundation. The SAR imagery acquisition date was 4th March 2019, 11:47 AM UTC. For comparison, simulated forecast inundation of 4th March 2019 12:00:00 PM UTC used. The overall accuracy showed a 60% probability of detection compared with reference even after four days lead-time. In figure 3.16, the derived SAR imagery based water inundation is shown along with the model simulated inundation for comparison. For locations close to Khaliajuri and Markuli stations, SAR imagery indicated inundation, which was accurately detected by the forecasting system. The recent structural measures are taken to improve flood management through submersible embankments in that region that are not reflected in the SRTM DEM. This limitation in the DEM propagates to the modeling framework at those locations.

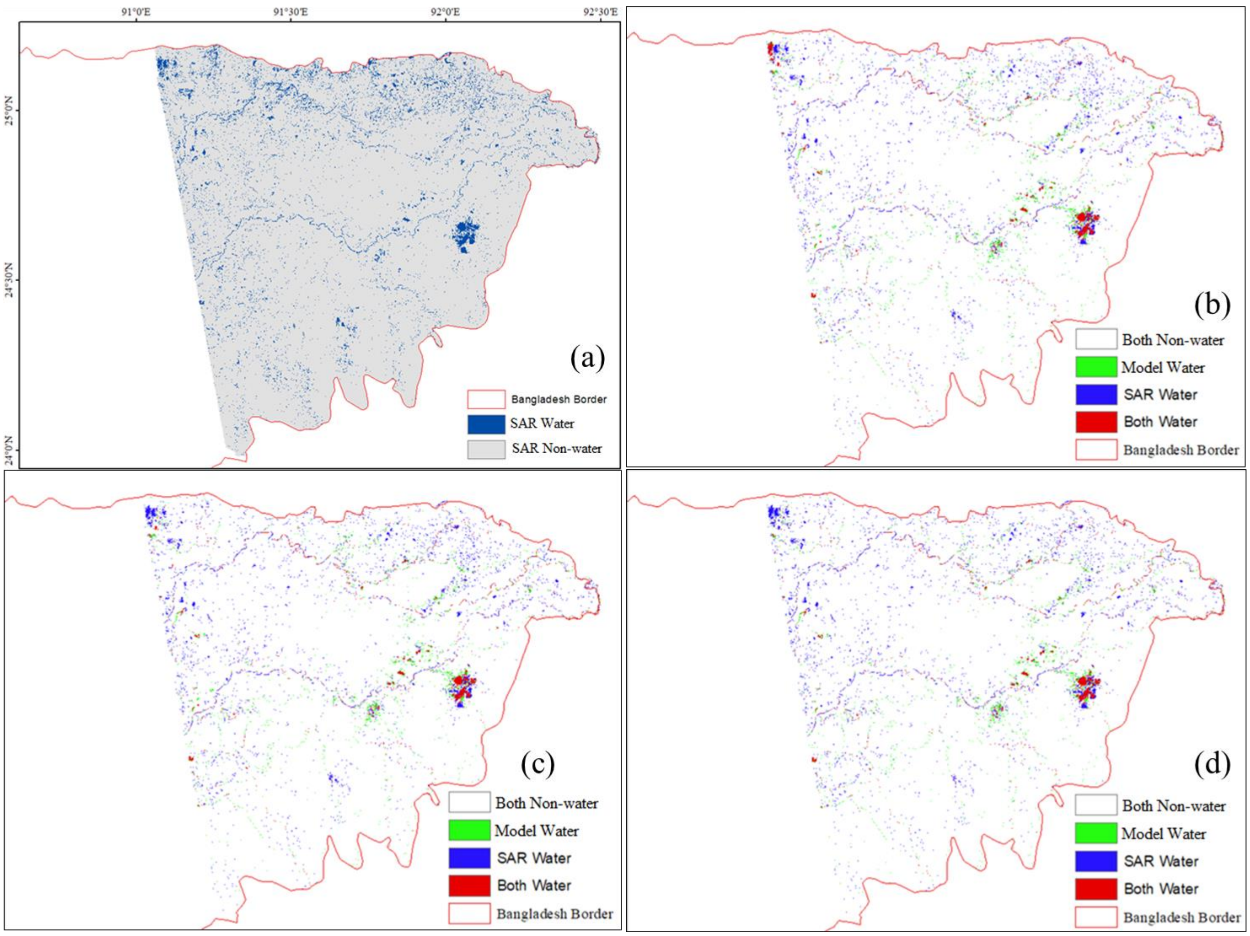

Figure 3.16 Spatial comparison of inundation forecasts with SAR imagery derived inundation. (a) SAR Imagery derived. (b) 12 hour lead time comparison (both non-water = Model and SAR detected non-water, Model water = Model simulated water but SAR detected non-water, SAR Water = SAR derived water but model simulated non-water, both water = Model and SAR agree on water), (c) 60 hour lead time and (d) 108 hour lead time forecasts

The performance of the framework was also examined against available fine resolution satellite imagery. Two planet imageries (May 15, 2019, and August 26, 2019) with 10m spatial resolution were downloaded and classified using the maximum likelihood method. They were compared with the framework generated forecast inundation and the results are shown in figure

3.17. On the left panel of figure 3.17, a comparison map of the model simulated inundation forecast of 3 days lead time and planet imagery of May 15, 2019 is shown. From the left panel, it can be seen that the modeling framework was able to identify most of the water and non-water features. It is true that in some regions, the framework failed to identify actual features. It happened because of the recent (post-2017) human-made topographical alterations after the SRTM DEM acquisition time in 2000. Framework forecasted inundation at different lead-time was compared with the two planet imageries, and the result presented on the right panel of the figure. From the classification accuracy metrics (i.e., overall accuracy, omission error of water, and commission error of water) comparison, it can be seen that overall the accuracy of the framework was more than 70% for up to 5-day lead time. Overall, the framework was able to identify water and non-water features with more than 70% overall accuracy having less than 25% omission error and less than 30% commission error of water features.

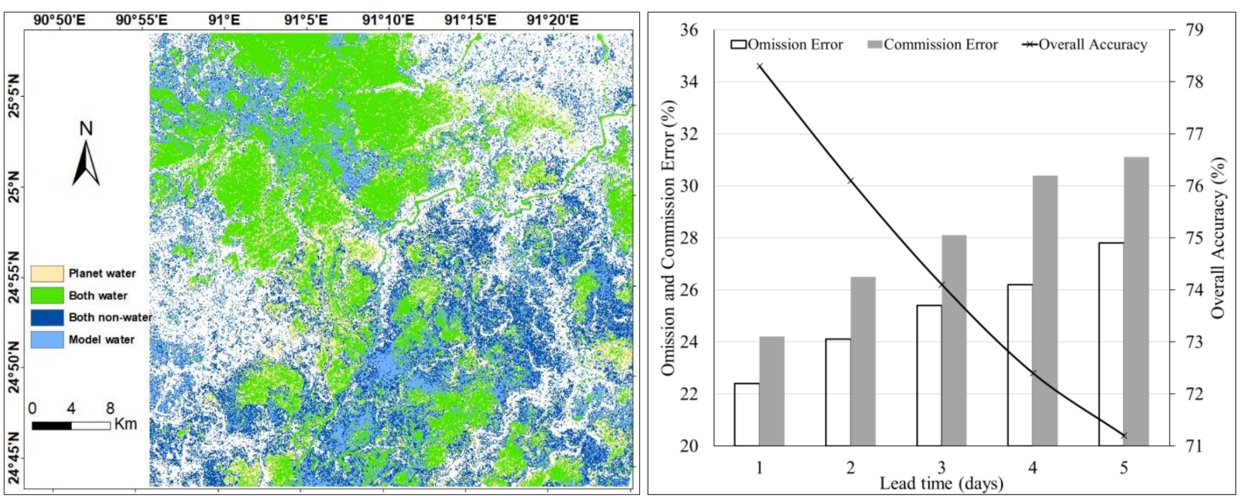

Figure 3.17 Accuracy assessment of the forecasted inundation with planet imageries, left) Comparison of model-simulated inundation of 3-day lead time with planet imagery of May 15, 2020 (both non-water = Model and planet detected non-water, Model water = Model simulated water but planet detected non-water, Planet water = Planet derived water but model simulated non-water, both water = Model and planet agree on water); right) Omission error, commission

error of water, and overall accuracy of the model forecasted inundation compared with planet imageries.

The modeling framework was implemented in the 2019 pre-monsoon season for experimental prototyping and then made fully operational in the Bangladesh Water Development Board (BWDB) stakeholder environment during the pre-monsoon season of 2020. The accuracy of the framework was analyzed and reported in figure 3.18. It can be seen that the framework performance significantly improved during the year 2020. This happened due to the implementation of the Weather Research and Forecast (WRF) downscaling, which downscaled the GFS forecast precipitation to a higher spatial resolution. The framework's live test demonstrated an accuracy of average RMSE of less than 0.5m and correlation coefficient of more than 0.80 for up to 3-day lead-time. Based on feedback shared by BWDB (co-authors to this paper), such accuracy resulted in real-world decision making and uptake of our forecasts for societal dissemination.

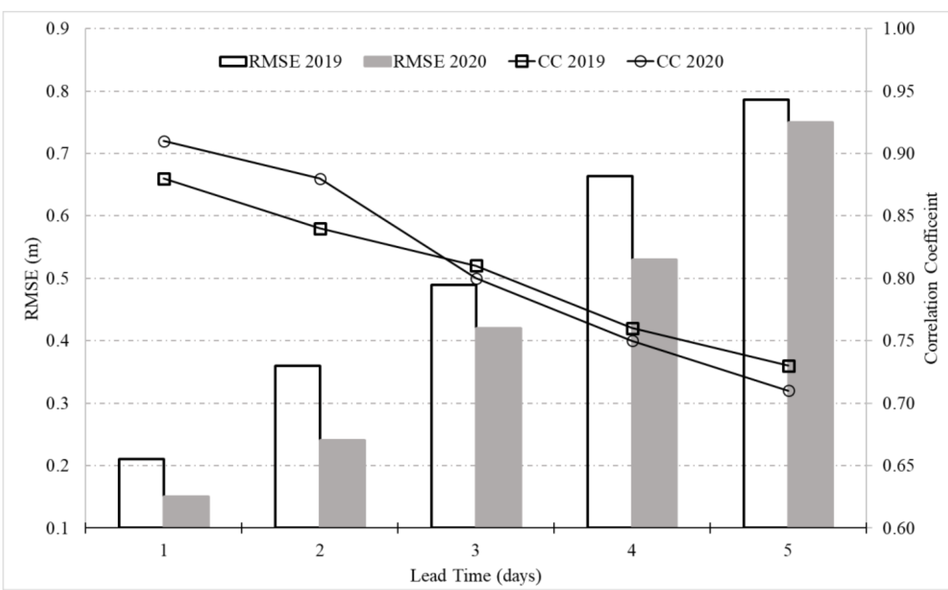

Figure 3.18 Comparison of average Root Mean Square Error (RMSE) and Correlation coefficient (CC) of stations for the year 2019 and 2020.

3.4 Conclusion

In this study, a flash flood early warning framework for Northeastern Bangladesh was developed using both hydrologic and hydrodynamic components of the flash flood generation mechanism. First, the most appropriate combination of topographic and hydrometeorological observations was selected for the base modeling framework. Global numerical weather prediction model forecasts were directly forced into the framework without any spatial downscaling to reduce the computation time. Finally, we analyzed the historical performance to illustrate the applicability of the framework in an operational environment. Based on the performance of the forecasts in the reference stations, we found that the framework could produce a skillful flash flood early warning for up to 5 day lead time.

In addition to the computation time and forecast accuracy considerations, some other key features of the framework considered during development were i) economic constraints and ii) scalability of the framework. The framework was built using open-source models and publicly available datasets, essential for economically constrained countries. In this approach, ground-based monitoring was not required, thus the method can be easily applied in ungauged or transboundary basins with inaccessible areas. The concept can be implemented with minimized computational resources and limited internet bandwidth, resulting in greater applicability in developing regions. Finally, all of the datasets used in this study are of global coverage with near-real-time availability. This implies that the same concept can be implemented anywhere in the world with similar topographic and hydrometeorological conditions. Even in regions where other more expensive methods are feasible, the system introduced here can be used to quickly trigger decisions when resources are limited and time is of the essence.

This study represents a critical step towards more accurate and more accessible flash flood forecasting systems. Potential future improvements to the framework are as follows:

- Improvement of quality of NWP forecasts. This will lead to better results from hydrological and hydrodynamic modeling. WRF Downscaling can be tested to illustrate the relative improvements from the existing methods.
- Explore different correction methods of QPF (i.e., climatology based QPF correction by Sikder & Hossain, 2018). This can also be implemented to improve the quality without compromising the computation time.
- Develop a more representative and recent topographically surveyed DEM. A more recent elevation dataset that better captures up to date human developments and modifications of the floodplain could significantly improve the performance of the Hydrodynamic model and lead to more accurate inundation forecasts.
- Ensemble forecasts in place of QPF can also be tested in this framework to produce a forecast probability range instead of single time series.

With the findings of a computationally efficient flash flood forecasting system development using satellite observations and numerical weather forecasting (NWP) outputs, the third component (human impact quantification) of the operational water management was addressed in the next Chapter. In chapter 4, a global framework was developed to monitor the reservoirs across the globe using only satellite-based observations.

Chapter 4 Towards a Global Reservoir Assessment Tool for Predicting Hydrologic Impact and Operating Pattern of Existing and Planned Reservoirs

Note: This chapter has been adapted from an article submitted to Environmental Modelling and Software. At the time of writing, this article is under review.

Abstract

Dam construction in developing nations is on the rise. Monitoring these dams is essential to understanding downstream hydrologic impacts and for better planning and management of water resources. Satellite observations and advancements in information technology now present a unique opportunity to overcome the traditional limitations of reservoir monitoring. In this study, a global reservoir monitoring framework was developed as an online tool for near real-time monitoring and impact analysis of existing and planned reservoirs based on publicly available and global satellite observations. The framework used a mass balance approach to monitor 1,598 reservoirs in South America, Africa, and Southeast Asia. Simulated streamflow of the developed tool was validated in 25 river basins against a multi-decadal record of in-situ discharge. The simulated storage change was validated against in-situ data from 77 reservoirs. The framework was able to capture reservoir state realistically for more than 75% of these reservoirs. At most in-situ gaging locations, the reservoir tool was able to capture streamflow with a correlation of more than 0.9 and a normalized root mean square error of 50% or less. The tool can now be used to study existing or planned reservoirs for short and long-term decision making and policy analysis.

4.1 Introduction

By the end of the 20th century, approximately 58,000 large dams higher than 15 meters, with a total reservoir surface area of about 300,000 km^2 (Lehner et al., 2011) had been built for hydroelectricity, irrigation, and water supply needs. With rapid growth in human population and energy demand, dam construction in the developing world is currently rising (Zarfl et al., 2014). The majority of dams either planned or already under construction are concentrated in South America, Asia, and Africa, mainly in developing countries with Human Development Index values ranging from “low to medium,” as defined by the United Nations Development Program (Figure 4.1). Many of these new or upcoming dams are designed to harness the hydropower potential of rivers and to supply water for drinking and irrigation.

Dams and reservoirs have long been treated as cheap and clean energy sources with low carbon emissions and benefits related to flood control, food security, irrigation, and socio-economic development. Hereafter, dams and reservoirs will be used interchangeably in this paper. For example, dams built for irrigation purposes provide water to 30–40% of the world’s agricultural lands and produce about 40% of the world’s food (World Bank, 2020). Dams also have long-term downstream consequences due to disruptions they pose to the natural flow regime. Flow regulation and river fragmentation (Bunn & Arthington, 2002), narrowing of river beds and downstream erosion (Khan et al., 2014), seawater intrusion (Sikder, 2013), and thermal stratification (Lugg & Copeland, 2014) are among the many ways dams negatively impact river systems. Grill et al. (2015) studied existing and future large dams, showed a 48% alteration of rivers, and predicted that the number could rise to 93% if all planned dams are built. Unplanned and uncoordinated dam management also affects downstream flooding (Mishra & Shah, 2018), disrupts pre-existing agriculture production (Strobl & Strobl, 2011), and weakens the ecosystem

(Poff & Zimmerman, 2010). Due to significant impacts of dams on the environment, it is necessary for all basin inhabitants, particularly those living downstream, to understand the operating pattern and state of upstream reservoirs.

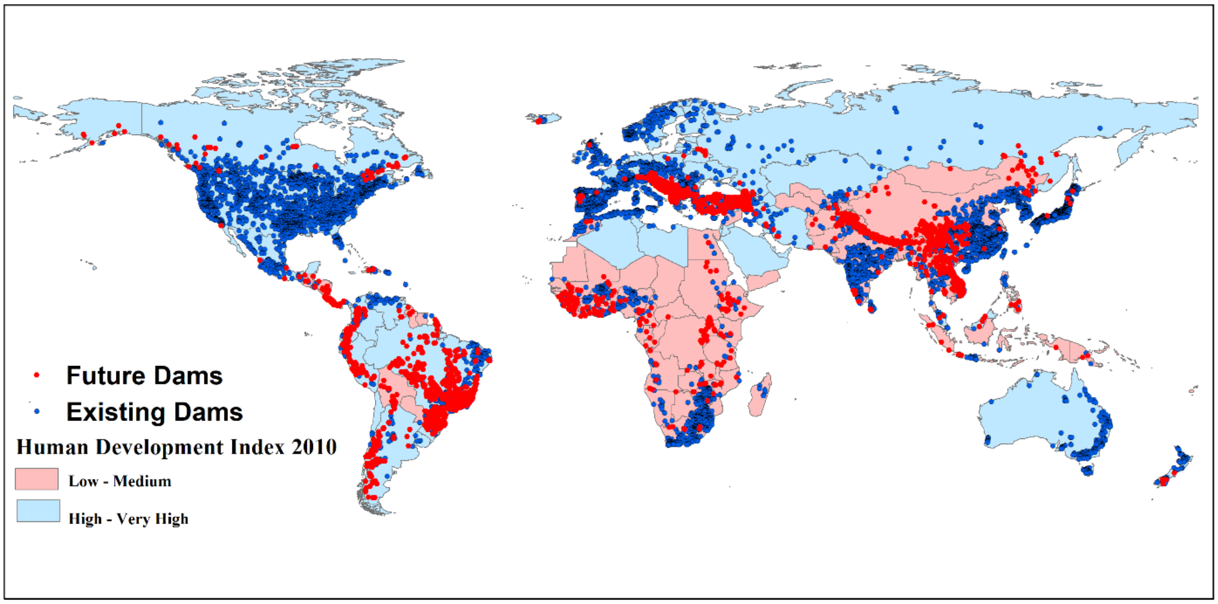

Figure 4.1 Overview of 6,862 large dams (Lehner et al., 2011) and about 3,700 planned and under-construction hydropower dams with an installed capacity >1 MW (Zarfl et al., 2014). The map: United Nations' Development Program's Human Development Index for 2010

Downstream nations, as well as all riparian nations, can make both immediate and long-term decisions for water management and maximize stakeholder benefits, through the unhindered exchange of hydrologic data and reservoir-operating information. Understanding the role dams play in flow regimes is also necessary to manage water-related hazards such as floods and droughts, public safety and infrastructure resilience (Woldemichael et al., 2012), effects of human alterations to the land hydrologic cycle (Gao et al., 2012), and impacts of multi-reservoir systems on downstream river discharge (Döll & Zhang, 2009). It is also critical to know how reservoir operating patterns will need to be revised to address climate change, especially in climate-vulnerable regions such as the Amazon (Pokhrel et al., 2014) and the Mekong basin (Lauri et al., 2012). Despite clear need and urgent calls for the unhindered exchange of hydrologic information (Khattar & Ames, 2020), global and freely accessible reservoir monitoring information is currently unavailable for inhabitants of regulated basins around the world. This is due to insufficient ground observations, particularly in developing regions, limited data sharing protocols (Alsdorf et al., 2007; Hossain et al., 2007) and lack of financial resources (Solander et al., 2016). Such hurdles make it challenging to study and routinely monitor the impact of reservoirs around the world (Gao et al., 2012).

Due to the absence of direct measurements, models have been used to monitor reservoirs at the continental and global scale, as well as to assess future climate projections (Döll et al., 2009; Döll et al., 2003; Hanasaki et al., 2006; Meigh et al., 1999). However, large-scale modeling approaches do not accurately resolve individual dams, making them less relevant for local decision-makers. When global reservoir modeling systems were still in the early stages of development, it was often assumed that a rectangular or inverse pyramid-shaped bathymetry would represent the storage capacity of reservoirs (Döll et al., 2003; Meigh et al., 1999). The first grid-based, explicit representation of a reservoir used in global hydrological models was reported by Hanasaki et al. (2006) and subsequently improved by several other studies (Pokhrel et al., 2014; Voisin et al., 2013). Solander et al. (2016) proposed a very idealized reservoir model by using temperature as the primary factor to simulate seasonal changes in reservoir management. Despite the above-mentioned modeling studies used to simulate the effect of dams on river discharge, several issues remain unsolved relating to spatiotemporal dynamics of the individual reservoir (Bierkens et al., 2015). For example, most schemes were developed for macroscale hydrologic models with typical grid sizes of more than 50 km (Fatichi et al., 2016), which is unsuitable for representing small to medium-sized reservoirs. Also, none of the studies considered reservoir surface area dynamics and bathymetry, which is critical to capturing reservoir evaporation and impacts on the weather (Degu et al., 2011).

The calibration and validation of most global models were completed using in-situ observations from developed regions. Thus, the skill of such modeling systems remained untested for operational decision-making and policy analysis in developing regions (Gao et al., 2012). Most recently, Yigzaw et al. (2018) proposed a method to define a characteristic shape of the reservoir for an area-elevation relationship that facilitates easier software representation of reservoir bathymetry in earth system models that also works well for reservoir related studies. However, every reservoir is unique in its bathymetry, and defining an idealized shape may not be suitable for deriving skillful storage change or detecting reservoir operating patterns for the individual dam. Thus, to reduce uncertainties related to the actual representation of reservoir topography along with surface area dynamics in global monitoring, satellite remote sensing is needed that can measure or estimate a wide range of variables and provide data to determine a reservoir's state.

Over the last few decades, satellite remote sensing has played an important role in providing spatio-temporal observations of surface water and hydrologic processes at global-scale coverage with near real-time availability (Khaki et al. 2020; Biswas & Hossain, 2017; Avisse et al., 2017; Kansakar & Hossain, 2016; Gebregiorgis & Hossain, 2011). The application potential of remote sensing observations for deriving reservoir state and operating patterns has been well established in previous studies (Bonnema et al., 2016; Gao et al., 2012). The same approach used in Bonnema et al. (2016) was later applied to over 20 reservoirs of the Mekong Basin to infer the operating pattern of reservoirs and residence time (Bonnema & Hossain, 2017; Hossain et al., 2019). However, such approaches have so far been limited to individual regions or reservoirs. With the availability of remotely sensed observations and computationally robust and versatile online software tools (such as cloud and distributed computing), it is now possible to have a global scale and freely accessible monitoring framework for existing and planned reservoirs (Wood et al., 2011).

In order to build an online, global-scale reservoir framework for information monitoring, several priority issues must be addressed. These issues include the following: (1) automatic delineation of spatial extent around the reservoir shoreline to derive the dynamic surface area, commonly known as the region of interest (ROI); (2) construction of the area-elevation relationship to define reservoir bathymetry; (3) selection of a universally applicable method to estimate the time series of the reservoir's water surface area; (4) setup and calibration of the upstream hydrological model to derive reservoir inflow; (5) advanced understanding of remote sensing, models and data for the users; and (6) availability of computational resources. With the availability of the GranD Dam Database (Lehner et al., 2011), a georeferenced reservoir database is now available for global-scale studies. This database, however, does not provide all necessary information on reservoirs, such as the maximum areal extent of reservoir or ROI. In previous studies (Gao et al., 2012; Bonnema et al., 2016), the ROI had been manually identified using the visible/Infrared imageries. Some studies (i.e., Zhao and Gao, 2018) used a fixed buffering distance around a reservoir polygon for defining ROI for global-scale studies, which may not yield accurate results for reservoirs that are highly irregular in shape.

The extraction of reservoir surface area poses the most difficult challenge in obtaining a globally scalable method. There are numerous studies (Bonnema & Hossain, 2017; Gao, 2015; Pekel et al., 2016; Zhao & Gao, 2018) related to water area extraction of lakes and reservoirs using different passive and active satellite sensors (i.e., Landsat 5,7, 8, Sentinel 1 and 2). The calculation of reservoir inflow on a global scale is another critical issue. There is no global parameterization for any of the hydrological models that can be applied universally. Nijssen et al. (2001) optimized the Variable Infiltration Capacity (VIC) model parameters at the global scale to estimate global river discharge and sensitivity to climate change. However, the spatial resolution is too coarse for most reservoirs, and the approach lacks a streamflow routing model. There are a number of other streamflow datasets and global hydrological modeling frameworks (Lin et al., 2019; Barbarossa et al., 2018) that exist based on global hydrological model setups. Two major limitations with any dataset are the lack of publicly accessible operational modeling at a daily or weekly timescale and datasets with spatial resolution that is too coarse to capture the dynamics of reservoirs of all sizes. Thus, routine monitoring of reservoirs in near real-time that is also publicly accessible cannot be achieved with existing hydrological models and frameworks. Even if all the above constraints were addressed, an advanced understanding of remote sensing and modeling would still be required for stakeholders from developing countries wishing to manage their river basins under increasing transboundary regulation. Fortunately, there have been recent technological advancements, including the publicly available cloud, which can now eliminate many of the limitations faced by inhabitants of developing nations. Another advancement is distributed computing that reduces the requirement of high internet bandwidth for downloading and processing of large-scale datasets. For example, Google Earth Engine (GEE) (Gorelick et al., 2017) combines a multi-petabyte catalog of satellite imagery and geospatial datasets with the planetary-scale analysis that has been applied in several studies of reservoirs (Biswas et al., 2019; Bonnema & Hossain, 2017; Zhao & Gao, 2018).

This study describes an operational framework for developing the software needed for a global, freely available monitoring system of reservoirs in developing regions. This modeling framework, known as Reservoir Assessment Tool (RAT), is motivated by the need to democratize access to information on reservoir operations and study reservoir impacts on hydrology so that inhabitants and water managers can devise 21st-century solutions. Those end users who lack advanced knowledge of remote sensing, access to in-situ or transboundary data, or the capacity to operate complex hydrological models will find such a software tool useful in their efforts to monitor and manage their reservoirs.

The study describing the development of RAT is organized as follows. First, the reservoir mass balance approach used in RAT is shown in Section 4.2.1, with datasets described in Section 4.2.2. Using these datasets, the specific methods used to estimate different parameters of reservoir states are described in Section 4.2.3. The user interface and overview of the proposed operational framework are briefly described in Section 4.3. Validation results for the RAT framework are presented in Section 4.4, where accuracy of the simulated storage change, surface area estimation, and reservoir inflow is assessed against reference data. The conclusion and scope for further development of the RAT framework are described in Section 4.5.

4.2 Framework Description

4.2.1 Overview and reservoir mass balance approach

In this study, satellite-based remote sensing data were used to estimate reservoir outflow by employing a reservoir mass balance equation (4.1). For monitoring reservoir dynamics (fill, release and storage change), this mass balance is the core component of the RAT framework. A schematic diagram of the mass balance concept is shown in Figure 4.2.

$$O = I - E - \Delta S ------------------------------ (4.1)$$

Here, the terms represent the following: O = Outflow, I = inflow, E = Evaporative loss, and ΔS = Storage change. In this study, the term "outflow" was used as a proxy for "release," which also included parallel diversions and other consumptive uses. The reservoir surface water extent areas A_{t-1} and A_t in figure 4.2 were extracted from visible/NIR imageries, corresponding heights h_{t-1} and h_t were extracted using Area-Elevation Curve (AEC), and finally, ΔS was calculated using equation (4.2). Details about the AEC development are discussed in Section 4.2.3.2.

$$\Delta S = \frac{A_{t-1} + A_t}{2} * (h_t - h_{t-1}) ------------------------ (4.2)$$

First, the ROI (previously explained in the Introduction section) of any reservoir is defined by following a reservoir size-dependent buffer distance shown in Table 4.1. The ROI is used to clip satellite observations for preparing the area-elevation relationship and to extract the time series of surface water area. Storage change of any reservoir can be computed using the reservoir water surface area/elevation time series and area-elevation relationship shown in Figure 4.2. This is a widely-used technique that has been reported to yield acceptable skill (Bonnema et al., 2016; Crétaux et al., 2011; Gao, 2015; Gao et al., 2012). Meteorological observations and land surface parameters are forced into a hydrological model to derive reservoir inflow. The inflow, evaporation, and storage change can then be used to infer the reservoir outflow using mass balance. Details about the datasets and specific methods are discussed in Sections 4.2.2, 4.2.3, and 4.2.4.

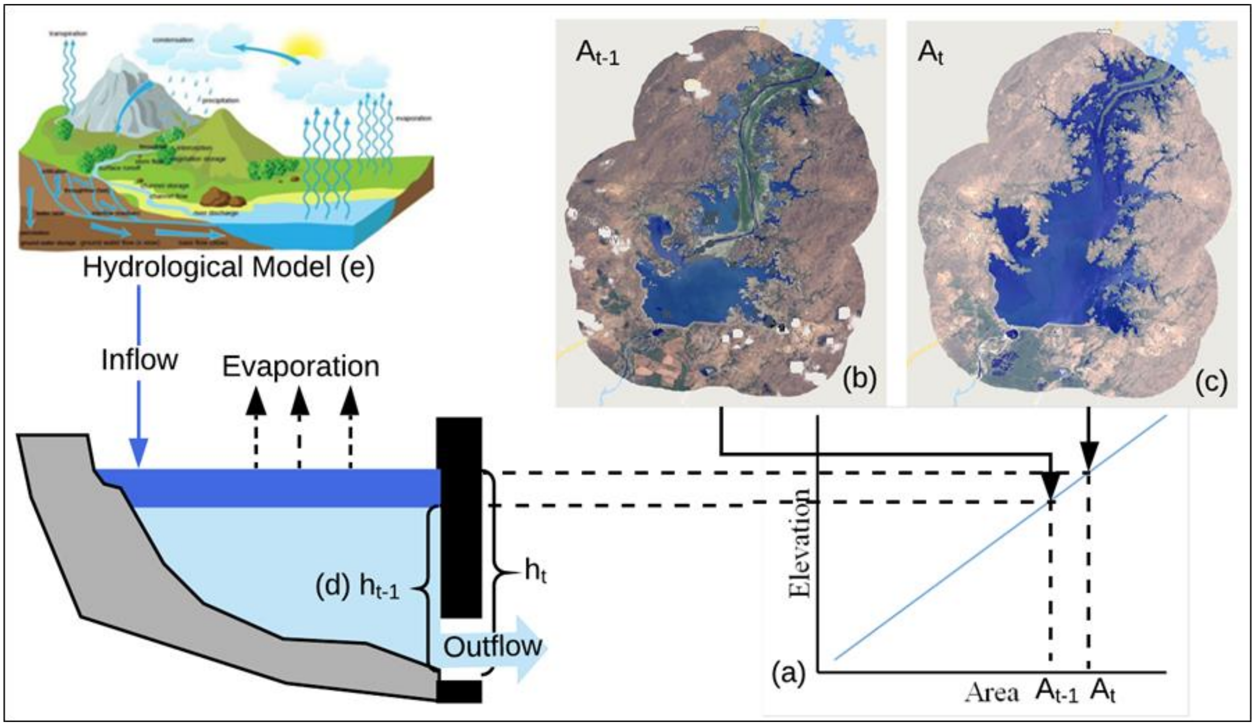

Figure 4.2 Concept of satellite data-based mass balance for reservoir monitoring. The different reservoir parameters and corresponding satellite datasets used are, (a) The Area-Elevation relationship Curve (AEC) derived from SRTM, (b) and (c) are from visible/NIR satellite imagery, (d) was derived from AEC, and (e) from satellite-based meteorological observations.

4.2.2 Datasets

The land elevation dataset used in this study was the Shuttle Radar Topography Mission (SRTM) 30 m resolution Digital Elevation Model (DEM) (Hennig et al., 2001). Three sensors were used to derive water-extent area time series, including (1) USGS Landsat 8 Collection 1 Tier 1 and Real-Time data Raw Scenes, (2) Sentinel-1 SAR GRID: C-band Synthetic Aperture Radar Ground Range Detected, and (3) Sentinel-2 MSI: Multispectral Instrument, Level-1C. In the gridded hydrological model, FAO Harmonized World Soil Database (Nachtergaele et al., 2009), USGS Global Land Cover Characteristics (GLCC), and Land Cover Database (Geological Survey, 1997) were used for land-surface parameters. CHIRPS precipitation (Funk et al., 2015), maximum and minimum temperature, and average wind speed at 10m height from NOAA NCEP/Climate

Prediction Center provided meteorological forcing data for this study. For routing the hydrological model outputs, global flow direction at 1/16 degree spatial resolution (Wu et al. 2011) was used.

4.2.3 Storage change calculation

The method followed in this study to calculate change in reservoir storage is shown in Figure 4.2. Major components mentioned in the mass balance equation are (a) ROI generation, (b) AEC extraction, (c) time-series processing of water extent area, (d) storage change calculation, (e) simulation of reservoir inflow from the hydrological model and evaporation from the reservoir, and (f) reservoir outflow calculation. Aside from hydrologic modeling (items e and f), all components are executed in the cloud using Google Earth Engine (GEE) to minimize internet bandwidth needed for downloading large datasets. GEE has been extensively used in different large-scale hydrological analyses (Biswas et al., 2019; Pekel et al., 2016; Zhao & Gao, 2018), which offers highly advanced and previously unachievable computational possibilities.

4.2.3.1 ROI delineation

After many trials over several reservoirs using multiple approaches, we classified the reservoirs according to the polygon defined in the GranD database. The polygon area was used to classify reservoirs into seven distinct classes to identify the appropriate buffering distance to create the ROI. Before deciding the buffering distance for each class, the frequency of occurrence map of the global surface water dataset (GSWD) prepared by Pekel et al. (2016) was used for visual comparison over 70–80 reservoirs. By following the maximum water extent of the GSWD dataset, a suitable buffer distance was decided (Table 4.1).

Table 4.1 Reservoir class, buffering distance, and computational scale in GEE

Reservoir Surface Area from GranD (Km^2)	Buffering Distance (m)
<2.0	500

2-10	750
10-50	1000
50-200	1250
200-500	1500
500-1000	1750
>1000	2000

4.2.3.2 Area-elevation curve extraction

Using the delineated ROI mentioned in Section 4.2.3.1 and SRTM DEM data, the Area Elevation Curve (AEC) was derived in two steps. First, the ROI of the selected reservoir was used to clip the SRTM DEM. The SRTM DEM elevation was used to generate the area-elevation relationship, which was valid for elevation above the water surface at the time of the SRTM overpass (which was in February 2000). The histogram of SRTM DEM was populated to count the number of cells corresponding to each of the elevation data. The area of individual elevation was then calculated and incremented to get incremental area. The steepest slope of the AEC was used to identify elevations corresponding to reservoir surface areas. Areas less than the area of water surface elevation were considered to be satellite noise and discarded from further analysis. Next, the relationship developed in the first step was extrapolated to the near-zero surface area in order to complete a virtual area-elevation relationship for elevations lower than the SRTM-observed water surface. During extrapolation, univariate spline was found to be the best estimator and was therefore used as the operational area-elevation relationship generator. Finally, these two area-elevation relationships were merged to create the complete area-elevation curve. The whole methodology of AEC development is summarized graphically in Figure 4.3. For more information on the area-elevation curve generation approach, readers are referred to the works of Bonnema et al. (2016) and Bonnema & Hossain (2017).

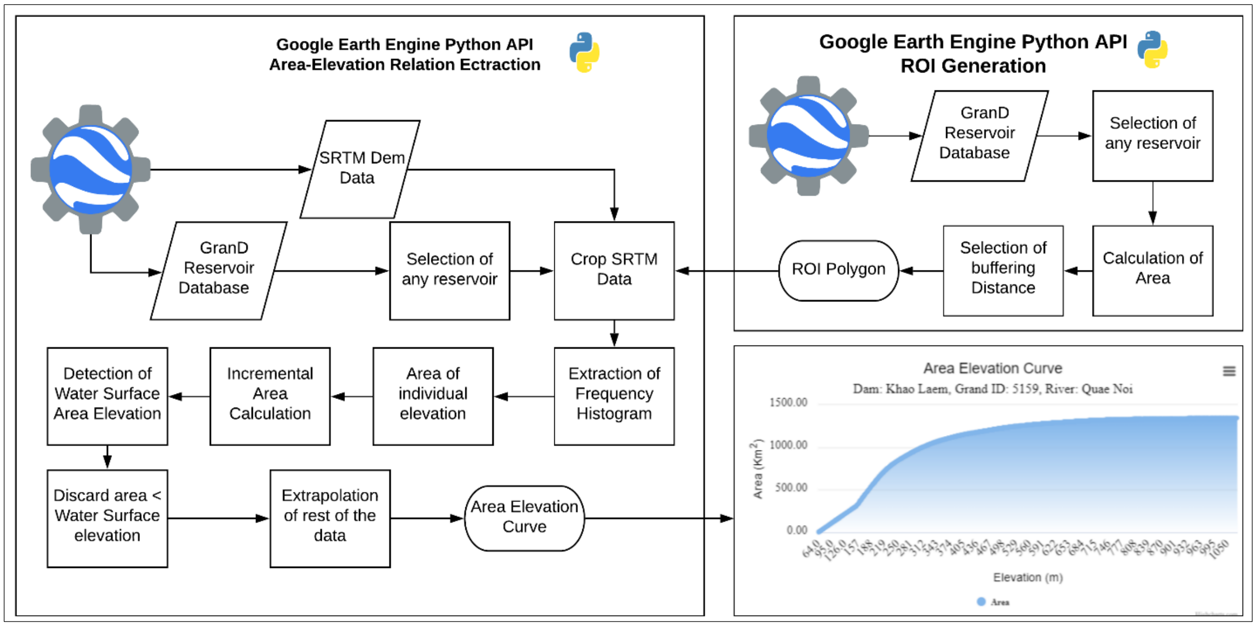

Figure 4.3 Reservoir ROI polygon delineation and AEC curve extraction procedure.

4.2.3.3 Surface water area extraction

The surface area time series and the AEC are prerequisites to calculating the storage change of any reservoir. First, the ROI polygon and AEC are prepared by following the approach mentioned in Sections 2.2.1 and 2.2.2. All imagery scenes are first filtered using a predefined date window and the ROI polygon, and then clipped using the ROI. In the case of Sentinel 2 and Landsat, cloudy pixels were removed from the ROI region of the scene. The area of scenes was calculated and filtered out for areas less than 80% of the ROI (after the removal of cloudy and partially covered scene). In the case of Sentinel 1, scenes were filtered based on polarization, look angle, and date window, and pixels with less than -16 dB backscatter value (Ahmad et al., 2019) were treated as water. For Landsat and Sentinel 2, different index-based methods were assessed, such as Normalized Difference Water Index-NDWI (McFeeters, 1996), Modified Normalized Difference Water Index-MNDWI (Xu, 2006), Water Index (Fisher et al., 2016), Advanced Water

Extraction Index (Feyisa et al., 2014), and Dynamic Surface Water Extent-DSWE (Jones, 2019). The extracted time series were then used to calculate the storage change time series (figure 4.4).

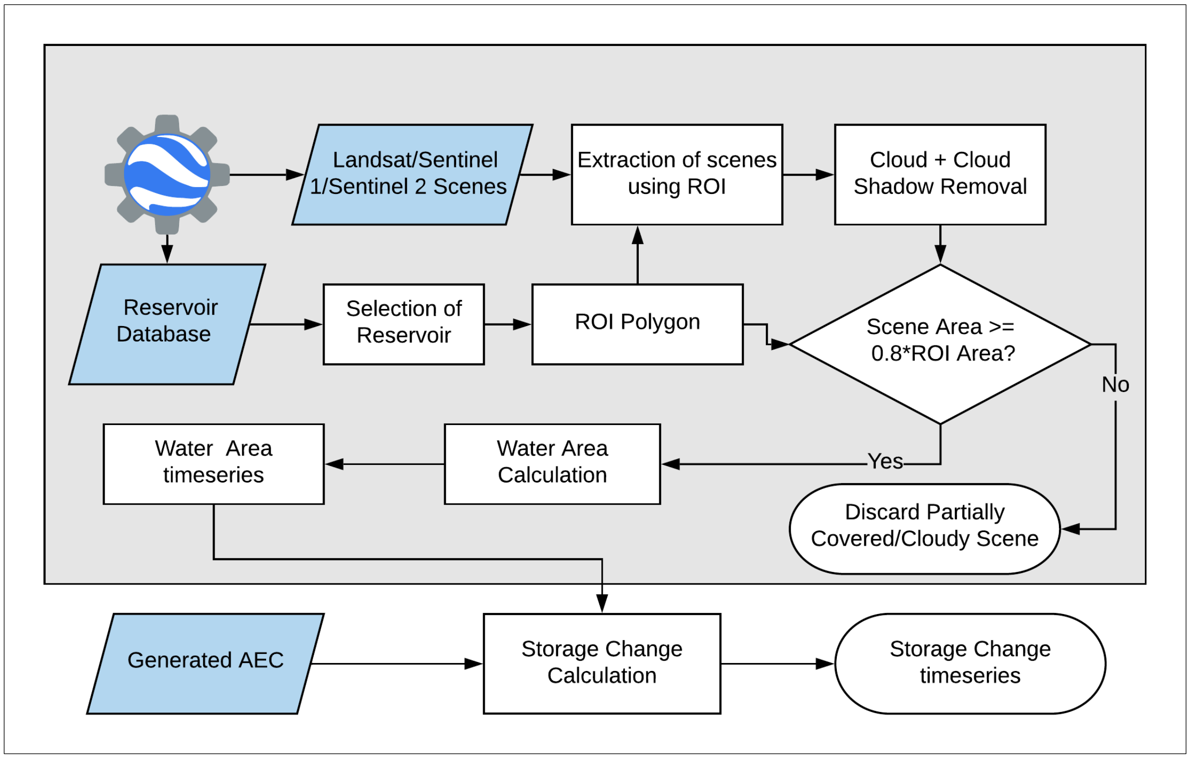

Figure 4.4 Surface water area time-series and storage change calculation workflow

4.2.3.4 Storage change calculation

The storage change time series was calculated from the surface time series of the water extent area and the AEC (Figure 4.4). For any pair of consecutive surface-water area data, corresponding elevations were computed from the AEC. Storage change was calculated from two consecutive heights and elevations using equation (4.2).

4.2.3.5 Simulation of reservoir inflow

The reservoir inflow was simulated using a hydrological model with streamflow routing capability. Variable Infiltration Capacity (VIC) model (Liang et al., 1994; Lohmann et al., 1998) was chosen for simulating the gridded surface runoff, evaporation, and baseflow in the upstream catchment area of the reservoir. Meteorological observations forced the model, along with land-surface parameters. For soil and land surface parameters, FAO land cover and World Harmonized Soil Dataset were used. Meteorological parameters used in this study were precipitation, maximum and minimum temperature, and average wind speed. All input forcings to the VIC model were prepared at 0.0625^0 by 0.0625^0 spatial resolution to match the Dominant River Tracing (DRT) flow direction at 0.0625^0 resolution (Wu et al., 2011). We chose the finest resolution of the hydrological model and DRT flow direction to cover the maximum number of reservoirs possible from the GranD database (Lehner et al., 2011).

There are several calibration parameters for the VIC model, which can be used to improve simulated streamflow. Some of these parameters (i.e., saturated hydraulic conductivity and the exponent of the unsaturated hydraulic conductivity curve) were estimated from soil properties by following the approach mentioned in Nijssen et al. (2001). Initially, the two calibration parameters (variable infiltration parameter and depth of the soil layer) were taken from Nijssen et al. (2001). We found that those critical parameters identified in Nijssen et al. (2001) were thoroughly investigated, based on climatic zone and geographical region, and presented the best available baseline study. These calibration parameters were resampled to a spatial resolution of 0.0625^0 by 0.0625^0 by using the cubic spline interpolation technique. The calibrated parameters were further updated wherever it was available to ensure better estimation of reservoir inflow by following more recent studies in several basins. For example, we used parameters for Ganges, Brahmaputra, Meghna basins from Siddique-E-Akbor et al. (2014), for Indus basin from Iqbal et al. (2017), for Mekong basin from Hossain et al. (2017) and for Nile basin from Eldardiry & Hossain (2019).

Upon completion of hydrological model simulation, outputs were forced into the Routing Model (Lohmann et al., 1998) along with the DRT flow direction (Wu et al., 2011) to simulate reservoir inflow. DRT flow-direction-derived flow accumulation was matched with satellite imagery and river networks manually in most of the reservoir locations. It was done by comparing the flow accumulation from the DRT flow direction to satellite imagery at different locations with the assistance of Google Earth (https://www.google.com/earth/).

4.2.3.6 Calculation of reservoir evaporation and outflow

The total net evaporation computed by the VIC hydrological model was used to compute the evaporation from the reservoirs. Users are referred to https://vic.readthedocs.io for a detailed description of total net evaporation calculation of VIC Model. Here, the VIC model grid closest to the dam location was identified, and the simulated total net evaporation at that grid cell was assumed to represent reservoir surface evaporation over a unit area. This amount of evaporation from the grid cell was multiplied by the reservoir surface area to calculate the evaporation from the reservoir. Equation (4.1) was used to calculate outflow from the reservoir. The inflow volume, storage change volume, and evaporation amount were used to calculate outflow volume between two consecutive storage changes. We have assumed the role of seepage and groundwater loss as minor, based on a previous study (Bonnema et al., 2016), and thus discarded them from the mass balance approach.

4.2.3.7 Consideration of upstream reservoirs

Where there is a series of reservoirs along a river and its tributaries and the inflow volume of the upstream reservoir is greater than 10% of the natural inflow to the downstream reservoir, the influence of the upstream reservoir on downstream inflow was considered. This was done by deriving the difference between the inflow and outflow of the upstream reservoir and adjusting for that for downstream reservoir inflow.

4.3 The interface of the Reservoir Assessment Tool (RAT) and operational reservoir monitoring

4.3.1 Graphical user interface (GUI)

The main window of the frontend is shown in figure 4.5, which can be accessed through http://depts.washington.edu/saswe/rat_beta. The detailed design of the frontend and salient features of the tool are discussed in the user manual of the tool and also available in the GitHub link (https://github.com/nbiswasuw/rat-reservoir_assessment_tool). Currently, 1,598 Dams from the GranD Database version 1.3 located in South America, Africa, and Southeast Asia are modeled operationally and visualized on the RAT frontend interface. All reservoir parameters (i.e., AEC, surface water extent, inflow, storage change, and outflow) were added to the frontend.

Figure 4.5 Frontend web interface of the RAT tool operational framework with the blue reservoir icons showing reservoir locations. The polylines are the river network downloaded from https://www.naturalearthdata.com. The upper right corner of the window allows users to toggle between selections of layers and to switch available basemaps from the lower right corner.

4.3.2 Monitoring of reservoirs

4.3.2.1 Monitoring of existing reservoirs

As more recent and frequent satellite observations on reservoir areas become available via GEE, the RAT framework automatically processes the data, runs the hydrological model, and post-processed model outputs to create updated estimates of outflow, inflow, storage change of the existing reservoirs. The water extent time series is extracted with the latest available scenes per the methodology used for water-extent area extraction, mentioned in Section 4.2.3.3. The available AEC data and water extent time series are processed to get the storage change time series. VIC model is simulated weekly (at a daily time step) to get the most recent inflow into the reservoirs. Finally, the outflow is calculated from the inflow and storage change. All of these time-series data are made available in the frontend for user access. The data and information interchange between the backend server and the frontend GUI of the tool is explained in figure 5.6. If the inflow into any reservoir is not calculated, the user can make a request through the frontend, which is explained next in Section 4.3.3.

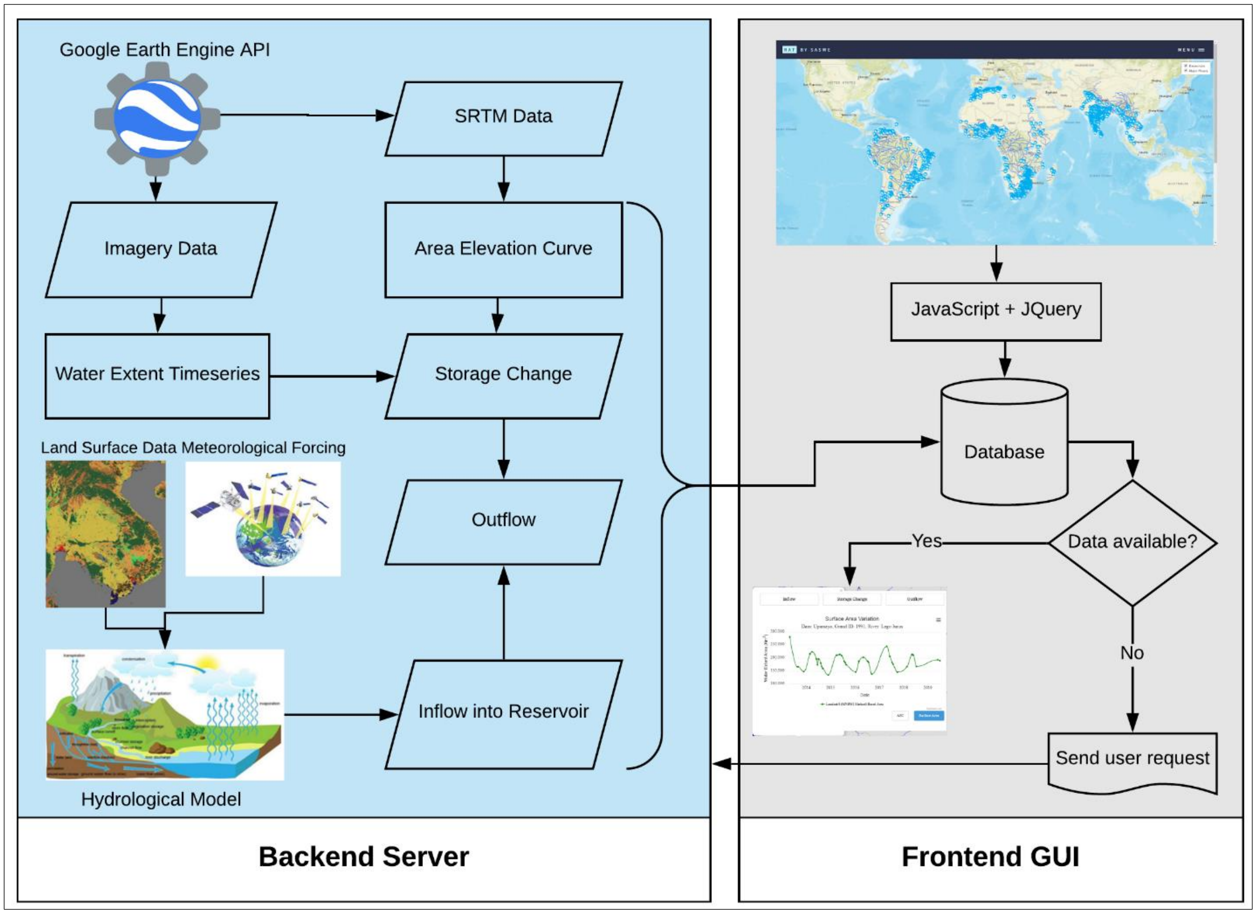

Figure 4.6 Data and information exchange between the backend server and the frontend interface. Left panel: Processing of different datasets and simulations. Right panel: summary of datasets that are made available in the frontend.

4.3.2.2 User request for adding new reservoirs to RAT

When data is not available over a reservoir location shown in the RAT framework, jQuery allows a user to push a request button (shown in Figure 16 of the RAT framework user manual). The user needs to specify the GranD ID of the reservoir when sending the request and other information, as mentioned in the user manual (see Figure 16 of the user manual). The form can also be accessed through this link: https://forms.gle/MUebn4bheie1b91J7. The request will push notifications to the administrator of the RAT framework to take further action. After being notified, the administrator can review the request to add the missing dam to the available list for calculation of reservoir state. During regular monitoring of reservoirs, the newly added reservoir will be considered for deriving all the parameters (including AEC extraction) and the user notified of the availability of data.

4.4 Results and discussion

The developed RAT software framework was applied in estimating reservoir storage change, inflow, and outflow. Reservoir Inflow and storage change were compared against in-situ measured data. The reservoir outflow was derived from the inflow and storage change using the mass balance approach discussed in section 4.2.1. Thus, it is assumed that accuracy of reservoir outflow is dependent on inflow and storage-change accuracy.

4.4.1 Accuracy of reservoir storage change

In-situ measurements of daily reservoir storage were web-scraped from the Central Water Commission (CWC - http://cwc.gov.in/) of India. This web-scraping is very similar in nature to a hydrologic platform development work described by Biswas & Hossain (2018). A map showing the reservoirs' locations along with their surface area (in different colors) and area-perimeter ratio (termed as irregularity index, shown in different colors) is shown in figure 4.7. To quantify the proposed framework's performance for different sizes of reservoirs, 77 reservoirs were classified according to their surface areas (from GranD database) in five different classes (very small, small, medium, large, and very large), as seen in Table 4.2.

To compare the simulated storage change based on reservoir shape, the reservoirs were classified according to the ratio of surface area to the perimeter (from GranD database), which is termed here as irregularity index. The categories based on area-perimeter ratio are highly irregular, very irregular, irregular, regular, very regular, and highly regular. Details about the classification based on the area-perimeter ratio are shown in Table 4.3. Three reservoirs, each with a distinctive irregularity index are shown in figure 4.8 to illustrate the differences in reservoir shapes based on the irregularity index.

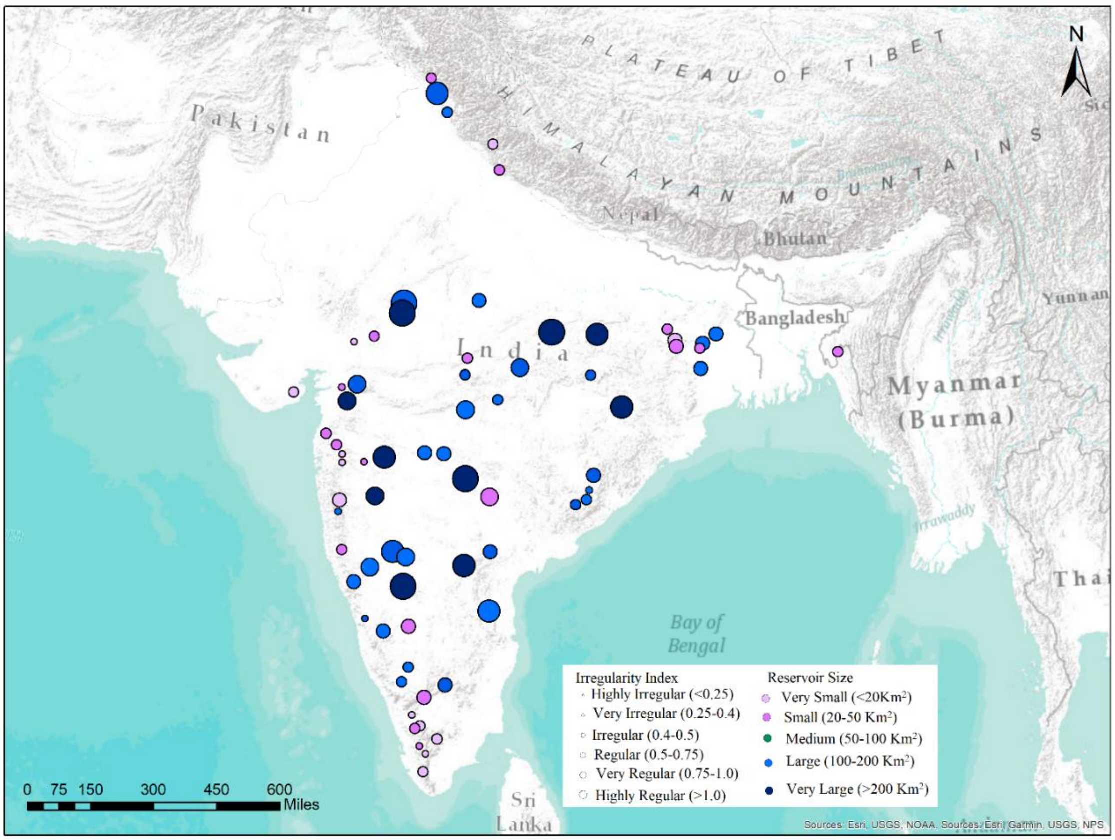

Figure 4.7 Validation stations along with the reservoir area, with their sizes color-coded and irregularity index as defined by A/P ratio (in parenthesis).

Table 4.2 Reservoir classifications according to size for validation of the RAT software tool

Classification	**GranD Area Range (Km^2)**	**Reservoir Count**

Very small	Less than 20	12
Small	20-50	20
Medium	50-100	20
Large	100-200	13
Very large	Greater than 200	12

Table 4.3 Reservoir classification according to irregularity index

Classification	**Irregularity Index (A/P, unit: Km^2/m)**	**Reservoir Count**
Highly irregular	Less than 0.25	13
Very irregular	0.25-0.40	25
Irregular	0.4-0.5	18
Regular	0. 5-0.75	9
Very regular	0.75-1.0	7
Highly regular	Greater than 1.0	5

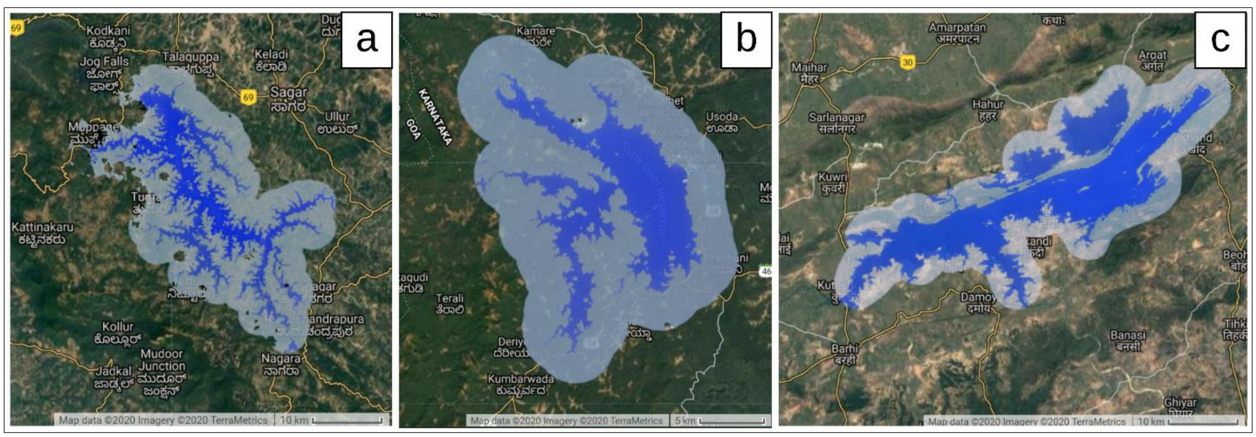

Figure 4.8 Reservoirs according to differing irregularity indices: (a) Highly Irregular Linganamakki Reservoir over Sharavathi River, India with A/P ratio 0.19 (Surface area 146.49 Km^2), (b) Regular- shaped Supa Reservoir over Kalinadi River, India with A/P ratio 0.51 (Surface area 94 km^2), (c) Highly regular Ban Sagar Reservoir over Sone River, India with A/P ratio of 1.8 (Surface area 384.3 Km^2).

The simulated storage change was compared against in-situ storage change of the individual reservoir on a monthly basis. Different sensors (Landsat 8, Sentinel 1 and 2) and different index-based methods (i.e., NDWI, MNDWI, WI, AWEI for Landsat 8 and Sentinel 2; Backscatter Coefficient for Sentinel 1) were tested to compare their accuracy. The correlation coefficient and the normalized root mean square error (NRMSE) were used to quantify the accuracy of individual methods and sensors for different reservoir classes. The sensors and methods are described in table 4.4.

Table 4.4 Sensors, temporal and spatial resolution, and applied methods

Sensor	Temporal and Spatial Resolution	Method	References
Landsat 8	15 days (30m)	NDWI	McFeeters (1996)
		MNDWI	Xu (2006)
		WI	Fisher et al. (2016)
		AWEI	Feyisa et al. (2014)
		DSWE	Jones (2019)
Sentinel 1	10 days (10m)	Backscatter Filter	Ahmad et al. (2019)
Sentinel 2	5 days (10m)	NDWI	McFeeters (1996)
		MNDWI	Xu (2006)
		WI	Fisher et al. (2016)
		AWEI	Feyisa et al. (2014)
		DSWE	Jones (2019)

The mean correlation coefficient and the normalized RMSE comparison of different reservoir sizes are shown in figure 4.9. All of the sensors and methods yield a correlation coefficient of more than 0.7 for all types of reservoirs. The correlation coefficient is highest for reservoirs with more than 200 km2 of surface area (very large reservoirs). For Landsat (marked as L8 in figure 4.9), all methods yielded a correlation coefficient of more than 0.8, which means more than 80% of the in-situ storage can be represented by the RAT framework. Except for very large reservoirs, the Normalized RMSE comparison revealed that Sentinel 2-generated storage changes are less accurate than those of Landsat or Sentinel 1, possibly because all of the indices were extensively tested for waterbody detection using Landsat data. Sentinel 1 provided better representation than Sentinel 2; however, the accuracy was less than that of Landsat. Although the data from Sentinel 1 was more accurate than that of all other sensors except Landsat, a few unrealistic estimations and a smaller number of samples resulted in a low score. Vegetated inundation, poor quality atmospheric composition during imagery acquisition, and incorrect identification of sand pixels as water are likely some of the underlying issues resulting in the low performance of Sentinel 1 (Martinis et al., 2015). In the case of very small, small, and medium reservoirs, Landsat performed better for all indices than the other two sensors. Among the different methods of Landsat 8, the DSWE method generated time series with continuous underestimation of water area and fewer records compared to the others. This was due to multiple filtering conditions. Additionally, GEE processing time was almost five times higher for DSWE than the calculations of other indices, making GEE a less practical method of global reservoir monitoring. MNDWI method was found to have limited skill for reservoirs located in steep terrains. Compared to all other methods, NDWI produced consistently better results with a simpler processing approach.

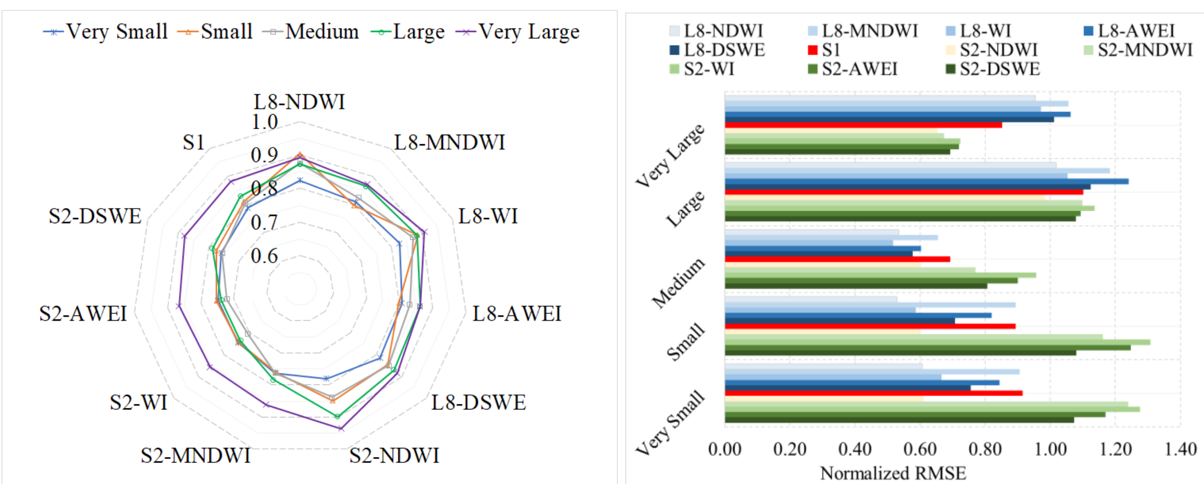

Figure 4.9 (left) Correlation Coefficient and (right) Normalized RMSE comparison of reservoirs of various sizes.

The storage change time series also was classified according to reservoir the irregularity index, which was used for very irregularly shaped reservoirs with extensive shorelines. The satellite imageries have limitations in detecting water pixels at the edges; thus, it was helpful to quantify the relative performance of the sensors and methods. The mean correlation coefficient and mean of the normalized RMSE for each of the classes were compared and shown in figure 4.10. The accuracy of every method and sensor decreased with the irregularity of the reservoirs. Landsat-based methods worked best for reservoirs in the irregular category. For regular shaped reservoirs, almost all methods yielded similar results. Highly irregular shaped reservoirs returned the lowest correlation coefficient, mostly due to water detection along the reservoirs' shorelines. Considering all the advantages and disadvantages of each of the sensors and methods, the Landsat 8-based NDWI method's performance was found to be most robust and consistent and was therefore selected for the operational RAT software framework.

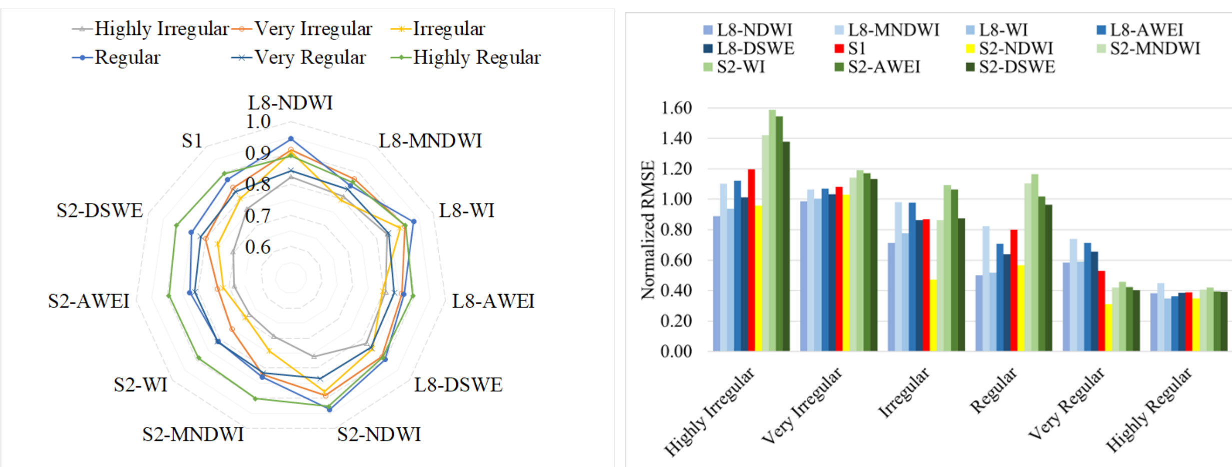

Figure 4.10 Correlation Coefficient (left side) and Normalized RMSE comparison of different reservoir classes defined according to the irregularity index (right side).

4.4.2 Validation of reservoir surface area estimation

The RAT framework's simulated reservoir surface area was compared with the latest published reservoir surface area dataset prepared by Zhao & Gao (2018). Zhao & Gao (2018) dataset provides the surface water extent area of the GranD database from 1984 to 2015 on a monthly scale. We compared the total reservoir surface area (from the NDWI method of Landsat 8 sensor and the DSWE method for Landsat 5) of all the RAT domain reservoirs to the total surface area of the same reservoirs estimated by Zhao & Gao (2018). The RAT framework was extensively validated for the Landsat 8 satellite imagery, and it was found that the NDWI method worked best in the case of the Landsat 8. Due to differences in sensor characteristics and differences in spectral band ranges, we found that the DSWE method worked best for the Landsat 5. For operational purposes, water areas generated from Landsat 5 (using the DSWE method) and Landsat 8 (using the NDWI method) were combined to produce monthly timeseries and then compared with Zhao and Gao (2018) data (figure 4.11). It was also found that reservoir surface area records were discontinuous for many reservoirs in the Zhao & Gao (2018) data during the years before 2000; consequently, comparison began with the year 2000. The proposed framework yielded a correlation coefficient of 0.92. Figure 4.11 shows that the reservoir surface area's seasonal variation is more clearly visible when the proposed framework-generated dataset was used. We should note that Zhao & Gao (2018) dataset is not available in near real-time scale for monitoring reservoir dynamics from the latest available satellite imagery.

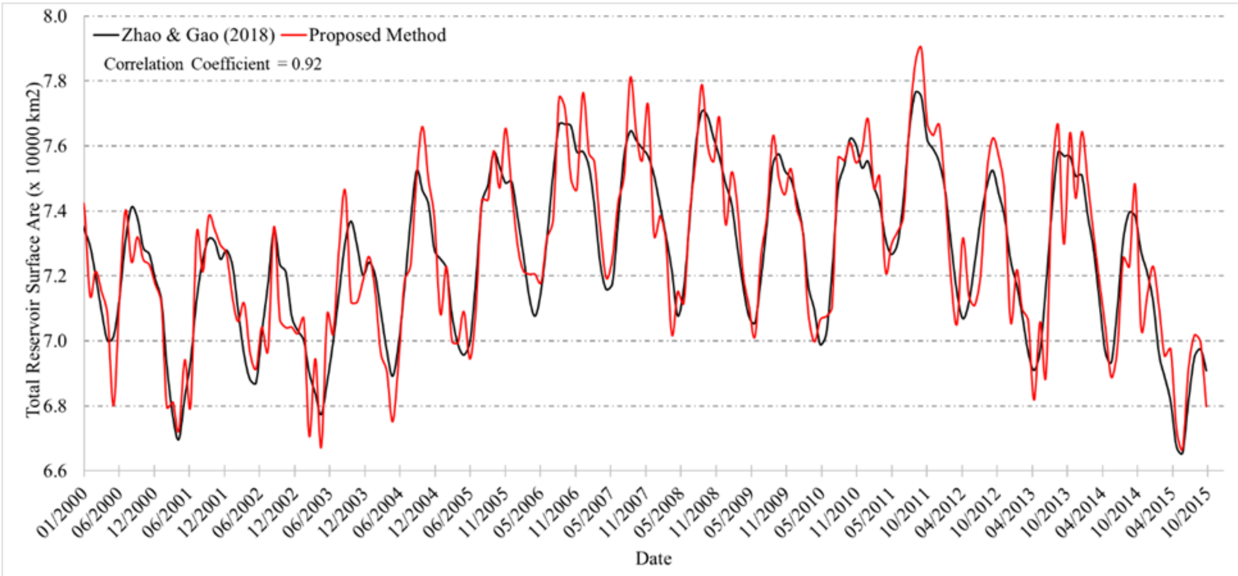

Figure 4.11 Comparison between the derived total reservoir surface area of all the reservoirs included in the RAT framework with Zhao & Gao (2018) generated reservoir surface area.

4.4.3 Validation of VIC hydrological model

Using the land surface parameters and meteorological forcing mentioned in Section 4.2.3.4, the VIC and Route model was simulated for the RAT domain (South America, Africa, and Southeast Asia). The simulated daily streamflow was first compared against ground-based daily discharge data collected through different sources. Information about validation stations is mentioned in table 4.5. The stations along with the respective basins are shown in the upper panel of figure 4.12.

Table 4.5 VIC hydrological model validation stations (BWDB: Bangladesh Water Development Board, Bangladesh; MRC: Mekong River Commission; CWC: Central Water Commission, India; GRDC: Global Runoff Data Center; PWAPDA: Pakistan Water and Power Development Authority; So-Hybam: HYBAM monitoring program, https://hybam.obs-mip.fr/)

Station	Basin	Longitude	Latitude	Data Source	Data Availability
Hardinge Bridge	Ganges	89.0273	24.0649	BWDB	2001-2019
Bahadurabad	Brahmaputra	89.7161	25.3363	BWDB	2001-2019
Kampong Cham	Mekong	105.4740	11.9855	MRC	2001-2019
Vijayawada	Krishna	80.6091	16.5049	CWC	2007-2019
Polavaram	Godavari	81.6547	17.2575	CWC	2001-2019
Pye	Irrawardy	95.2123	18.8075	GRDC	2001-2010

Hyderabad	Indus	68.3111	25.3727	PWAPDA	2014-2019
Katima Mulilo	Zambezi	24.2809	-17.4843	GRDC	2001-2018
Vioolsdrif	Orange	17.7295	-28.7611	GRDC	2001-2018
Lokoja	Niger	6.7571	7.7595	GRDC	2001-2006
Brazzaville	Congo	15.2817	-4.2904	So-Hybam	2001-2020
Obidos	Amazon	-55.5178	-1.9339	So-Hybam	2001-2018
Chapeton	Rio Parana	-60.3540	-31.6236	GRDC	2001-2014
Pichi Mahuida	Rio Colorado	-64.8295	-38.8261	GRDC	2001-2014
Primera Angostura	Rio Negro	-63.6744	-40.4452	GRDC	2001-2015
Bhairab Bazar	Meghna	90.9937	24.0441	BWDB	2001-2019
Serrinha	Amazon	-64.8077	-0.4891	So-Hybam	2001-2019
Tabatinga	Amazon	-69.9429	-4.2832	So-Hybam	2006-2016
Ocona	Rio Ocona	-72.6795	-16.7330	GRDC	2006-2018
La Pascana	Rio Tambo	-70.133	-18.4940	GRDC	2001-2018
Haindi	Saint Paul	-10.1238	6.5698	GRDC	2012-2019
Ruacana	Kunene	11.9861	-16.7715	GRDC	2001-2018
Beibrug	Limpopo	30.1731	-23.1643	GRDC	2001-2019
Prieska	Orange	22.7492	-30.0171	GRDC	2001-2018
Gamtoos Poort	Gamptoos	25.9853	-34.3954	GRDC	2001-2018

Time series comparisons of two stations are shown in the middle panel of figure 4.12. The left panel is Tabatinga station, located in the Amazon basin, where the correlation coefficient was less than 0.7, and the VIC model was not very accurate in representing low-flow and high-flow peaks. A similar case was observed at other stations. Timeseries comparison of Kampong Cham station located on the Mekong river (shown in the middle right corner) found accuracy was highest for the correlation coefficient. This basin performed exceptionally well due to subbasin scale calibration performed by Hossain et al. (2017). Nevertheless, the hydrological model showed dry season flow to be lower than the actual flow and overestimated the peaks. Summary statistics of all validation stations are shown in the lower panel of figure 4.12. In Southeast Asia’s stations, the correlation coefficients were more than 0.8, whereas the South American stations showed more than 0.6. Also, in some stations, NRMSE was higher with a good correlation coefficient due to the model's underperformance in capturing seasonality. We found that flow-direction modification improved the results significantly.

4.4.4 Comparison of streamflow with GRADES streamflow

We compared streamflow at different inflow locations with the Global Reach-level A priori Discharge Estimates for Surface Water and Ocean Topography modeled streamflow (GRADES; Lin et al., 2019). We compared our model’s estimated streamflow with the GRADES model's simulated streamflow at 44 randomly chosen locations along the river reaches within the RAT domain. The summary statistics are shown in figure 4.13. The average correlation coefficient of all the stations was 0.62, and the mean of normalized root mean square error was 0.49. Again, stations located in Southeast Asia performed better compared to the stations in the South America region. This is a clear indication that better calibration at regional and basin scales can improve simulated streamflow accuracy at the locations where our model underperformed.

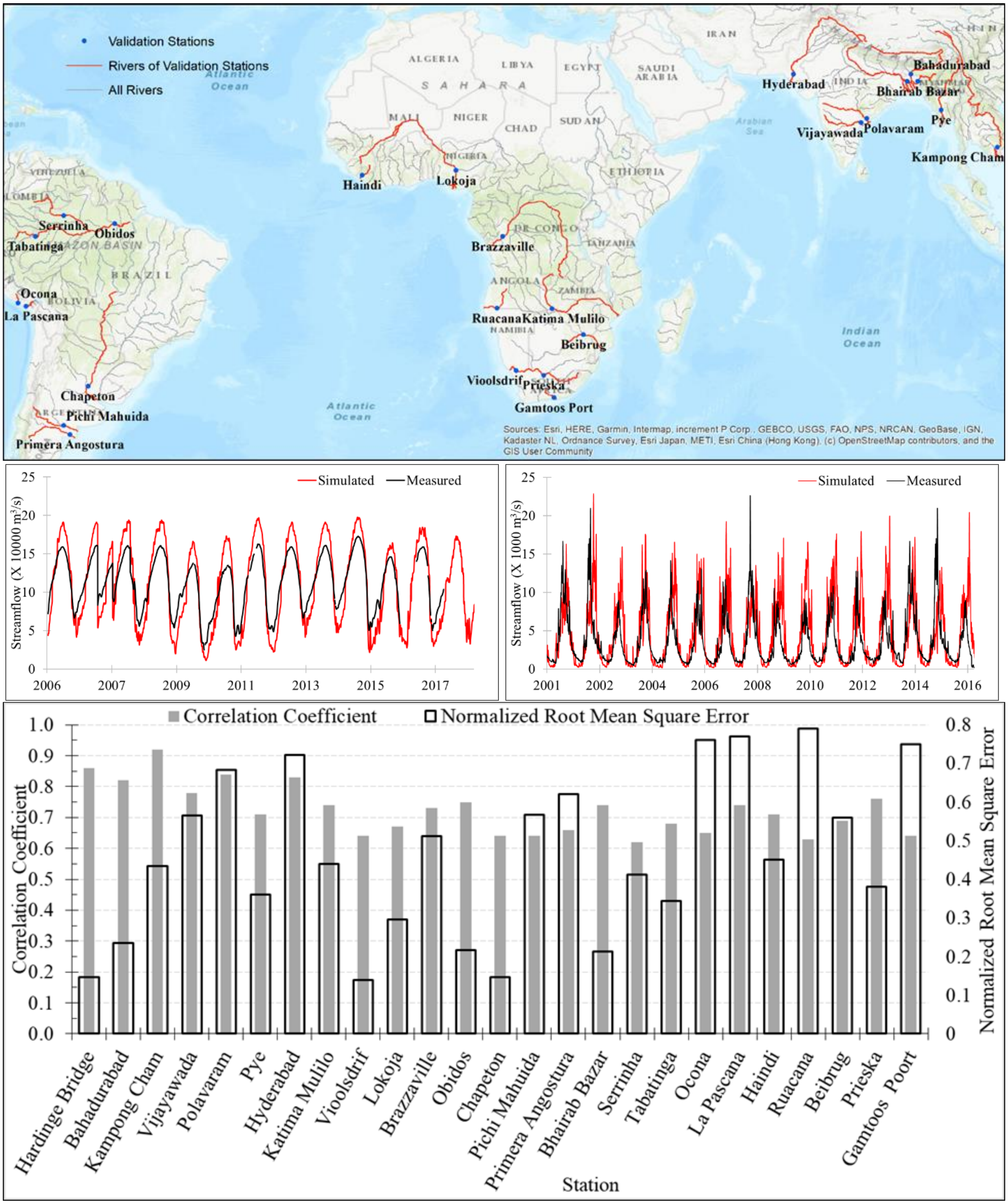

Figure 4.12 upper panel) VIC Model validation stations along with the respective basins, middle left) Streamflow timeseries of Tabatinga station of Amazon Basin, middle right) Streamflow Kampong Cham station of Mekong Basin, lower panel) Summary statistics of validation stations

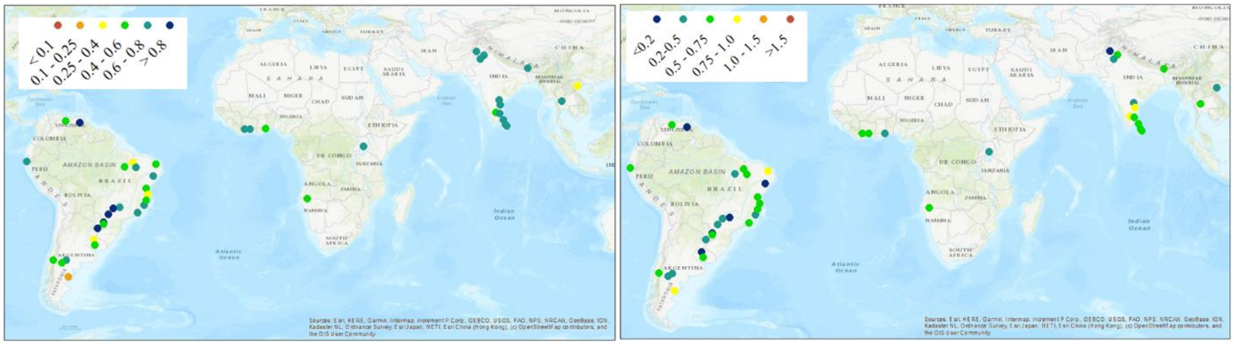

Figure 4.13 left) Correlation Coefficient and right) Normalized RMSE of different stations compared with GRADES simulated streamflow

4.5 Conclusion and Future Scope

To our knowledge, the online software framework for reservoir monitoring called RAT is the first of its kind. Given that the RAT tool is now publicly available for the world to use and benefit from, we believe the following are some examples of potential applications of this framework.

- By using this tool, long-term records denoting real-time behavior and operating rules at reservoirs can become publicly available.
- RAT can help users and the scientific community derive a global picture of reservoir monitoring, how they are being operated, and how they are likely impacting natural river flow and its variability as a function of climate, hydrologic regime, and socio-economic indicators.
- With further improvements in hydrological modeling using locally available ground observations, the RAT framework can be used with higher accuracy in local, regional, and global scale operational water resources management considering its near real-time data availability.

- The RAT framework can facilitate feasibility study of proposed/planned dams. It can be used to estimate the future reservoir capacity and inflow availability at any location, which is useful in optimizing reservoir benefits.
- The RAT framework presents future possibilities to study the impact of harnessing hydropower on river temperature, greenhouse gas emissions, aquatic habitats, land-use and land-cover change, and agriculture practices.
- The RAT tool can be used to minimize conflict between riparian countries (i.e., Egypt and Ethiopia over Nile Basin; China, India, and Bangladesh over Ganges-Brahmaputra-Meghna Basin; China, Laos, Thailand, Cambodia, Vietnam over Mekong Basin) as it can be considered an unbiased tool to all parties and provide data needed to drive fair and transparent water-sharing agreements.

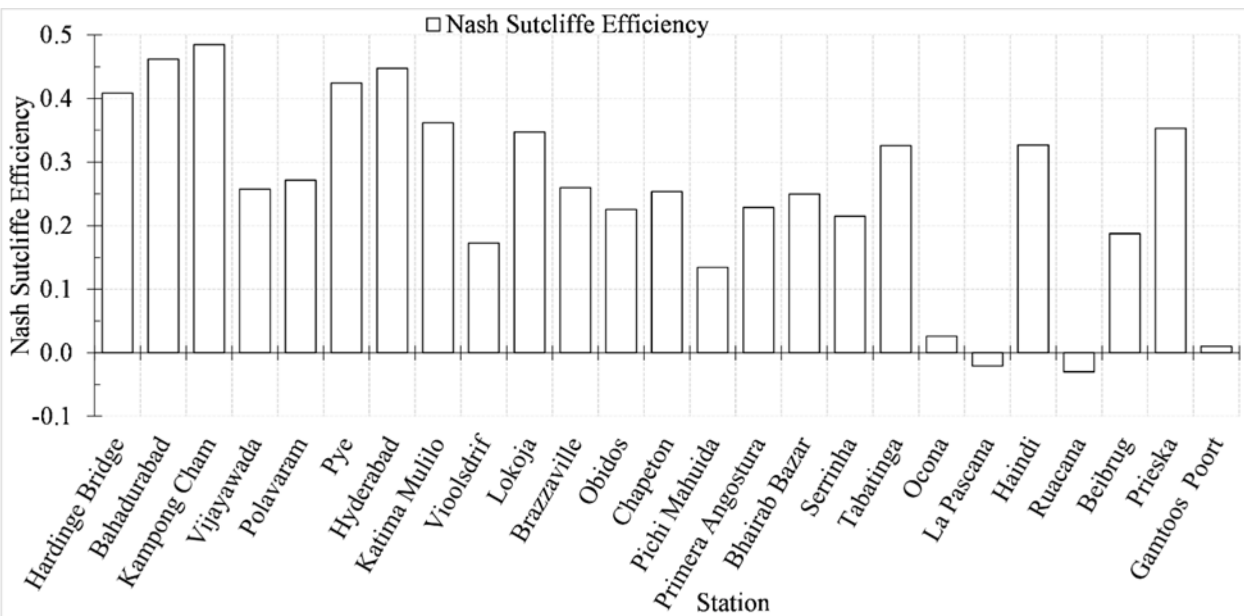

Figure 4.14 Nash-Sutcliffe efficiency of the streamflow validation stations (against in-situ streamflow) shown at 16-day aggregation in accordance with Landsat revisit period and reservoir management.

There are some future improvements that can be considered to make the framework more applicable in solving real-world water challenges. While the hydrological model validation showed promise, known uncertainties mandate that current results be carefully interpreted. Additionally, the VIC model used here will still need time to be improved and validated further at a more granular level. This need for improvement at many regions is evident when a superior goodness-of-fit such as Nash-Sutcliffe efficiency (figure 4.14) is compared with in-situ flow (accumulated over 16 days to match Landsat revisit time and for reservoir management). Improved reservoir inflow estimation can be made by using regional and basin-scale calibration, and validation of the hydrological model is one of them. The more complex method of water pixel identification from satellite imagery with artificial intelligence and the application of machine learning algorithms may yield better estimation of reservoir surface area. Reservoir bathymetry data from ground surveying or Lidar applications may be used to define the area-elevation curve more accurately. Lastly, reservoir outflow calculated in this study includes all types of diversions and consumptive water uses for various purposes, which may not be very accurate nor comparable to the actual reservoir releases. Thus, the simulated outflow should be compared with measured flow at in-situ locations immediately downstream of a reservoir.

The focus of our study here was on reservoirs and on methods of enabling the monitoring/prediction of reservoir states (surface area, storage change, inflow and outflow) at weekly to monthly scales of reservoir management. It should be noted that our study is not about developing a global hydrological modeling framework or even promoting an existing one for that matter. Our RAT framework is agnostic enough that the current hydrological model (VIC) can be replaced with other competing hydrological models. Our work to develop such an open and publicly available tool is driven by our mission to democratize water information on regulated river basins for all stakeholders and to facilitate more equitable water management. We believe that such a tool can level the playing field for stakeholder agencies and riparian nations that suffer from limited access to information on water availability due to hydro-politics, lack of in-situ infrastructure, or low adaptive capacity.

When the framework for reservoir monitoring was completed, then an example application of the framework in studying the impact of reservoirs on water availability was explored in the next chapter. In chapter 5, a multi-decadal analysis of reservoir storage variability and the potential drivers of the long-term reservoir storage was performed.

Chapter 5 A multi-decadal Analysis of Impact on Water availability due to Reservoir Operation in Ungauged Regions

Note: This chapter has been adapted from an article submitted to Journal of Hydrometeorology. At the time of writing, this article is under review.

Abstract

The limited amount of shared reservoir monitoring data around the world is insufficient to quantify the dynamic nature of reservoir operation with conventional ground-based methods. With the emergence of the global Reservoir Assessment Tool (RAT) driven by a multitude of earth-observing satellites and models, historical observation of reservoir operation spanning over three decades was made using open-source techniques. Reservoir storage variability was compared with trends of four critical hydrologic parameters (precipitation, runoff, evaporation, and Palmer Drought Severity Index) to understand the potential role of natural drivers in altering reservoir operating patterns. It was found that the reservoirs in Africa were losing storage at a rate of more than 1% per year of total storage capacity. Smaller reservoirs (with a capacity of less than 0.5 km^3) in South-East Asia were found to exhibit a sharp gain in the storage of 0.5% to 1% per year of total storage capacity. In most cases, drought was found to be the predominant driver of change in storage trends. In contrast, in certain places, precipitation trends were found to provide a better explanation along with human demand in the downstream due to population growth and economic development. Finally, large and recently-built reservoirs showed a more pronounced relationship with the hydrologic variables than those older than more than 30 years. This is possibly due to newer reservoirs being more dependent and sensitive to regulated surface water variability controlled by older dams in the upstream and long-term trends.

5.1 Introduction

Globally, reservoirs provide 30–40% of global irrigation water requirements, 17% of electricity generated, and various other services, including domestic and industrial water supply, recreation, fisheries, and flood control (Yoshikawa et al., 2014). In recent years, dam development has increased specifically in the developing countries to meet the demand for water and electricity for a growing population (Zarfl et al., 2014). According to Grill et al. (2015), the existing dams have altered 48% of the global rivers, which is predicted to increase to 93% if the planned dams are implemented by 2030. So, the construction of new dams will become more difficult in coming years with limited viable dam sites along the free-flowing reaches of rivers. Also, due to the negative impact of the impoundment created by older dams on the local population and river ecosystem, the construction of newer dams is going to become more questionable and difficult to justify around the world (Grill et al., 2015; Lehner et al., 2011; Nilsson et al., 2005).

Besides future challenges, several water supply failures have been reported in many parts of the world. For example, the Colorado River Basin of USA since 2000 (Udall & Overpeck, 2017), Sao Paulo in Brazil (Escobar, 2015), Cape Town in Africa (Sousa et al., 2018) are some examples of how existing dams can fail to meet water requirements for stakeholders. Given this current and emerging scenario of rivers becoming either more increasingly regulated or remaining historically regulated worldwide, it is now timely to study the dynamic behavior of existing reservoirs over multiple decades. A multi-decadal observation of reservoir operations can provide insights for a fairer distribution of the basin-wide resources, help water managers cope better with the climate change impacts, and fulfill the gap between future demand and available supply of water resources.

Despite the well-understood need to study multi-decadal reservoir dynamics for water management planning, very few studies have been performed to address this issue. Recently, Dawson et al. (2015) studied eleven reservoirs of Southern Great Plains using measured data of inflow, precipitation, and water withdrawal. They assessed long-term spatiotemporal characteristics of reservoir water quality and quantity of Brazos River and the Colorado River with a first-order trend without using any process-based models of the reservoir functions. Keys & Scott (2018) studied the volumetric variations in 10 large tropical reservoirs and lakes using Moderate Resolution Imaging Spectroradiometer (MODIS) satellite imagery and satellite radar altimetry which is not scalable to the smaller reservoirs due to the coarse resolution of MODIS imagery data. Duan & Bastiaanssen (2013) also proposed a method for long-term volumetric estimation of reservoir storage using satellite altimetry with satellite imagery, which is limited to the reservoirs having altimeter overpasses. Declining water storage capacity was studied by Wisser et al. (2013) using a simplified approach of sediment flux and installed reservoir capacity without having the exact information of reservoir operating information.

While past studies provide a platform for basic analysis of reservoir operating trends, some limitations remain. For example, the most common limitations of current studies are: 1) lack of scalability to regional or global scales due to location specific analysis without extensive validation); 2) use of simplistic methods based on multiple reservoir operating assumptions, rather than relying on observations, to define the relation between reservoir operation and its natural drivers; 3) lack of rigorous spatial-temporal characterization of reservoir dynamics at basin-continental scale. Such limitations are understandable if one tracks the evolution of the state of the art of reservoir operation modeling. An in-depth analysis of global reservoir dynamics has been absent until recently due to the lack of consistent spatiotemporal reservoir monitoring data. The most accurate way of getting consistent spatiotemporal information on reservoir dynamics is to get the in-situ or ground-based measurement of reservoir surface area, elevation, storage change, inflow, and outflow, which is nearly impossible for most reservoirs for several reasons. A vast majority of the world cannot afford the measurement of hydrological parameters due to budgetary constraints, especially in Africa, South and Southeast Asia, and South America (Solander et al., 2016). The institutional capacity of riparian nations for basin-wide cooperation is another major issue in sharing reservoir monitoring data. Even if reservoirs are observed using ground-based methods, the measurements are generally not shared publicly, to the best of our knowledge, due to the restrictions imposed by national governments (Alsdorf et al., 2007).

In the absence of necessary ground data for studying reservoir dynamics, the best way forward is to use publicly-available open-source physically-based models and satellite earth observations that are capable of representing the actual state of reservoir operation. Such a trend has recently been observed in studies based on a plethora of satellite observations and physical modeling systems (Bonnema et al., 2016; Bonnema and Hossain, 2017; Hossain et al., 2019; Biswas et al., 2020). In particular, we need to highlight the emergence of the Global Reservoir Assessment Tool, also known as RAT (Biswas et al., 2020, in press). Perhaps for the first time in literature, RAT has addressed the current limitations of reservoir operations monitoring in ungauged and developing regions. The RAT framework was developed to monitor 1598 reservoirs in South-East Asia, Africa, and South America in near-real-time at water management scales (i.e., bi-weekly) utilizing the advancements in cloud computing, land-surface modeling, and satellite remote sensing and big-data analytics.

The RAT framework's core concept was a satellite data-based mass balance approach, as shown in figure 4.2. The latest available visible and near-infrared (NIR) images (with cloud filtering) and area-elevation curve are used to calculate the storage change of any reservoirs. Reservoir inflow is simulated using a hydrological model forced with the latest available satellite-based meteorological variables (i.e., precipitation, maximum, minimum temperature, and average wind speed). Evaporative loss from the reservoir surface is calculated as well from the outputs of the hydrological model. Finally, reservoir outflow is calculated using reservoir inflow, storage change, and evaporation from the mass balance equation 4.1. The RAT framework can also derive an inferred operating rule curve for each of the reservoirs based on the long-term pattern of the operating information. All of the monitoring variables (i.e., reservoir inflow, storage change, evaporative loss, reservoir outflow, operating rule curve) are routinely updated based on the latest available satellite observations and continuous hydrologic modeling through the RAT framework at least once a month. The methods for estimating these variables including the mass balance approach are based on techniques with proven accuracy reported in recent studies (Bonnema et al., 2016; Bonnema and Hossain, 2017; Hossain et al., 2019; Biswas et al., 2020). The RAT framework, which can be publicly accessed from http://www.satellitedams.net or http://depts.washington.edu/saswe/rat_beta, is potentially useful in transboundary basins and data-scarce regions of the world (Rougé et al., 2018; Aldsorf et al., 2007).

There can be numerous applications of the RAT framework on a global scale to understand reservoirs and regulation of river flow and their impact on hydrology, eco-system function, bio-diversity, and socio-economic issues. In this study, the available spatially and temporally consistent record of reservoir monitoring from RAT was used to efficiently quantify the reservoirs' multi-decadal operating behavior according to underlying parameters (such as age, capacity, hydro-climatologic trends). This study's core objective is to quantify the long-term variability of the storage change of reservoirs and the identification of the potential natural drivers of this change. The storage variability was quantified based on the reservoir size, age, and occupying basins over the RAT domain (South America, Africa, and South-East Asia). The research question that this study tries to ask is, *How have the world's reservoirs been operated over the last three decades and what are the potential drivers of reservoir storage trends?* Hereafter, the words dam and reservoir will be used interchangeably to refer to the same dam-reservoir system.

5.2 Data and Methods

5.2.1 Datasets

The GranD Dam Database version 1.3 (Lehner et al., 2011) was used in this study, which is a georeferenced reservoir database and now available publicly for global-scale studies. It contains 7320 reservoirs with a cumulative storage capacity of about 6800 km3. From the Hydrosheds database (Lehner & Grill, 2013), 23 river basins were selected from South-East Asia, Africa, and South America regions with a minimum of 20 dams in a basin. We used RAT simulated outputs (i.e., reservoir surface water extent area timeseries, area-elevation relationship curve, and simulated storage change of the reservoirs) for the GranD reservoirs in South America, Africa, and South-East Asia. Landsat 5 and Global Surface Water Dataset (hereafter used as "GSWD"; Pekel et al., 2016) used to extend the reservoir surface water extent timeseries to 1985.

The ERA5-Land is a reanalysis dataset (available in Google Earth Engine Data Asset ID: ECMWF/ERA5_LAND/MONTHLY) that provides a consistent view of land evolution atmospheric variables over several decades at an enhanced spatial resolution of 0.1 degrees. ERA5-Land has been produced by replaying the land component of the ECMWF ERA5 climate reanalysis. This reanalysis combines model data with observations from across the world and is available at a monthly scale from 1981 to 2020. Precipitation, evaporation, and runoff were extracted from ERA5-Land data for analysis of reservoir storage change. Also, Palmer Drought Severity Index (PDSI), a commonly-used indicator for drought, was extracted from the TerraClimate data (available in Google Earth Engine Data Asset ID: IDAHO_EPSCOR/TERRACLIMATE; Abatzoglou et al., 2018) to compare drought severity with reservoir storage variability.

5.2.2 Methodology

The methodology performed in this study can be classified into two major steps, 1) preparation of long-term reservoir surface water extent area timeseries and storage change from RAT framework, and 2) extraction of variables over the selected basins from the ERA5-Land reanalysis data in google earth engine.

5.2.2.1 Preparation of long-term storage change data from RAT framework

During the development of the framework, RAT was extensively validated for Landsat 8. It was found that Normalized Difference Water Index (NDWI; McFeeters,1996) performed best among various methods for reservoir surface area estimation (Biswas et al., 2020). For this study, it was necessary to prepare a longer (multi-decadal) record, and thus we also incorporated Landsat 5 data to yield more than 30 years of the operating pattern from 1985. For the case of Landsat 5, several index-based methods were tested, and it was found that the Dynamic Surface Water Extent (DSWE; Jones, 2019) performed best. In figure 5.1, a flowchart is shown on how the index-based method was applied to generate the surface water extent timeseries from Landsat 5 data and merged to Landsat 8 based surface water extent area timeseries.

Firstly, the monthly average surface water extent was created for each of the reservoirs from the GSWD dataset. A monthly mosaic image of the available Landsat 5 (or 8) scenes over the reservoir was made by filtering cloudy pixels. Then, the image with more than 90% cloud contamination was discarded from the analysis. If the image consisted of less than 10% cloud cover, no correction method was applied to that image, and the water surface area was extracted by the applied DSWE algorithm for Landsat 5 and NDWI algorithm for Landsat 8. If the cloud cover is between 10% and 90%, the filtered out pixels are replaced with the monthly average GSWD raster data. This procedure was applied to generate long-term timeseries water extent data for any reservoir was prepared. These timeseries data was then converted into storage change timeseries using the area-elevation relationship described in Biswas et al. (2020).

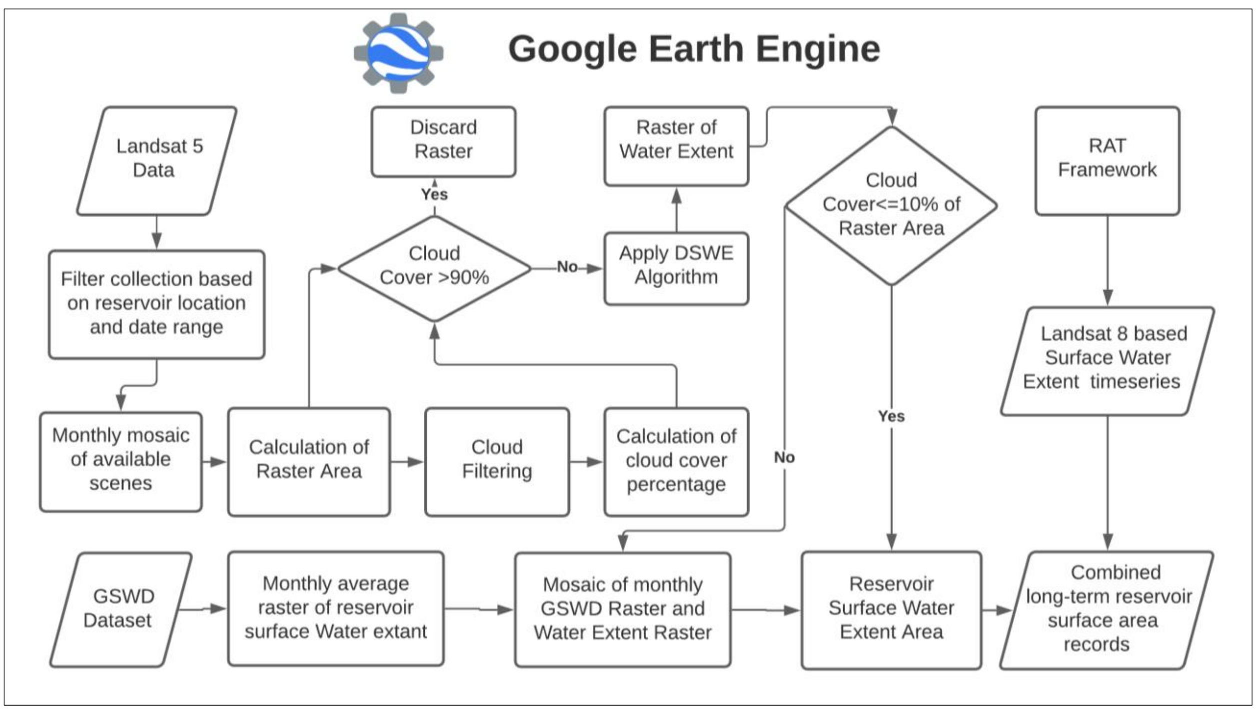

Figure 5.1 Methodology to extract monthly reservoir surface water extent timeseries by combining Landsat 5 and outputs from the RAT framework.

5.2.2.2 Extraction of hydrologic variables from ERA 5 atmospheric reanalysis data

Four key hydrologic variables (precipitation, runoff, evaporation, and Palmer Drought Severity Index) were extracted to compare the trends of reservoir storage change timeseries with potential natural drivers. For each of the river basins, these hydrologic parameters were extracted using Google Earth Engine. The boundary polygons of all the 23 basins were prepared and uploaded to Google Earth Engine to define the spatial processing extent of the reservoirs. Monthly precipitation, runoff, evaporation, and PDSI were then analyzed to check the correlation between the average storage change of the reservoirs within a river basin and the extracted parameters.

5.2.2.3 Long term trend analysis and correlation calculation between the datasets

All extracted hydrologic parameters were then averaged on a moving three year-window to remove seasonality. The derived hydrologic parameters were re-calculated as the anomaly from the long term mean to compare with the storage change. All of the analysis was performed from 1984 to 2020 on a monthly scale. During the comparison between the hydrologic parameters, Spearman's rank correlation coefficient was used. Spearman's rank correlation analysis is a non-parametric measure of rank correlation (statistical dependence between the rankings of two variables). It assesses how well the relationship between two variables can be described using a monotonic function. Usually, the Spearman rank correlation will be high when the individual data point has a similar rank between the two variables and low when the observations have a dissimilar rank between the two variables. Spearman's coefficient is appropriate for both continuous and discrete ordinal variables and has been used extensively in trend detection of hydrological variables (Yue et al., 2002; Chhipi-Shrestha et al., 2017; Diamantini et al., 2018).

5.3 Results

The selected river basins and the RAT domain are shown in figure 5.2. Among all the basins, seven basins were from South-East Asia, nine basins were from Africa, and six basins were selected from the South America region.

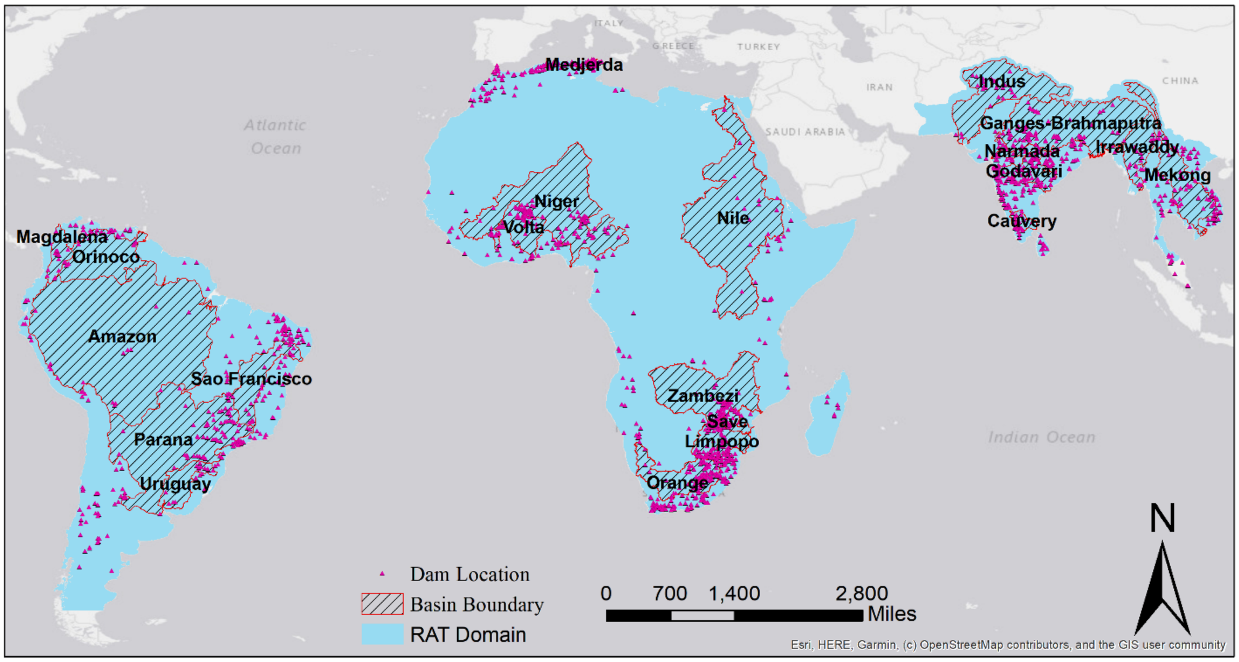

Figure 5.2 Selected river basins along with the RAT Domain

5.3.1 Classification of the dams

The GranD dams were first classified according to their size (capacity in units of million cubic meters, or 0.1 km^3, mentioned in the database). Hereafter the term for million cubic meters will be MCM. The dams were classified into three categories based on their size using the cumulative distribution function of the storage capacity of reservoirs. The information on the storage capacity of reservoirs was mentioned in the GranD database. The classification based on size was as follows, 1) Small (0-400 Million Cubic Meter), 2) Medium (400-1000 MCM), and Large (more than 1000 MCM). The distribution of the different sized dams in river basins is shown in figure 3 (left side). Dams were also classified based on the age of the dams (construction year of the dam mentioned in the GranD Database). They are 1) Old (more than 60 years old), 2) Medium-aged (40-60 years old), and 3) Recent (20-40 years old). In figure 5.3, the distribution of the dams based on the dam age is also shown (right side).

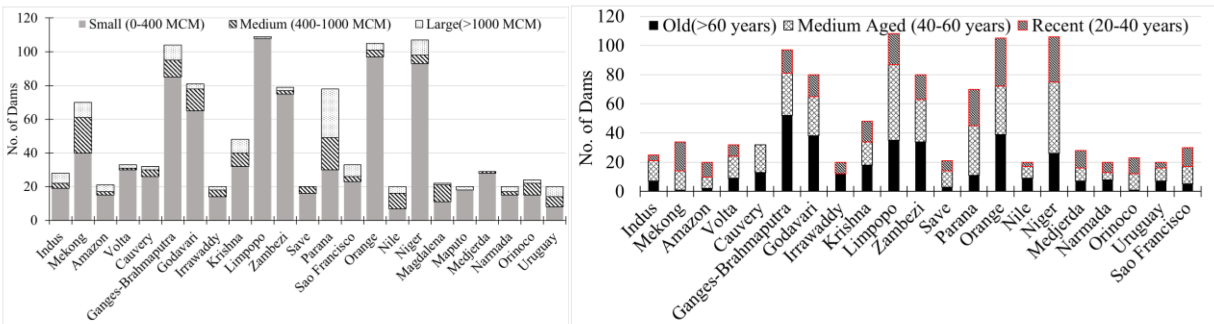

Figure 5.3 Dam distribution among the selected river basins based on the left) dam size and right) dam age

5.3.2 Long term trend of reservoir storage variability at different scales

The long-term trend of storage change of the reservoirs is shown in figure 5.4. Figure 5.4 shows that the dots' size represents dam size classification, and the color shows a long-term trend of storage change in the percentage of total reservoir storage capacity per year. The quantification of trends is also summarized in table 5.1. From the figure, it can be seen that many reservoirs in South America have been experiencing a positive trend in storage change (more than 0.1% per year of total reservoir capacity). A mixed behavior can be observed in the case of African reservoirs. More reservoirs have experienced a positive trend in the South-East Asia region compared to African reservoirs. The negative trend in storage change of the African reservoirs indicates that South America and South-EasAsia's reservoirs have been storing more water in recent years compared to the past.

Table 5.1 Quantification of the trend of reservoirs

Trend type	Threshold values (% of total capacity per year)	Region showing the trend
Highly negative	<-1.0	Eastern Africa
Negative	-1 ~ -0.1	Southern Africa
None	-0.1 ~ 0.1	-
Positive	0.1-1.0	South America
Highly Positive	>1.0	South-East Asia

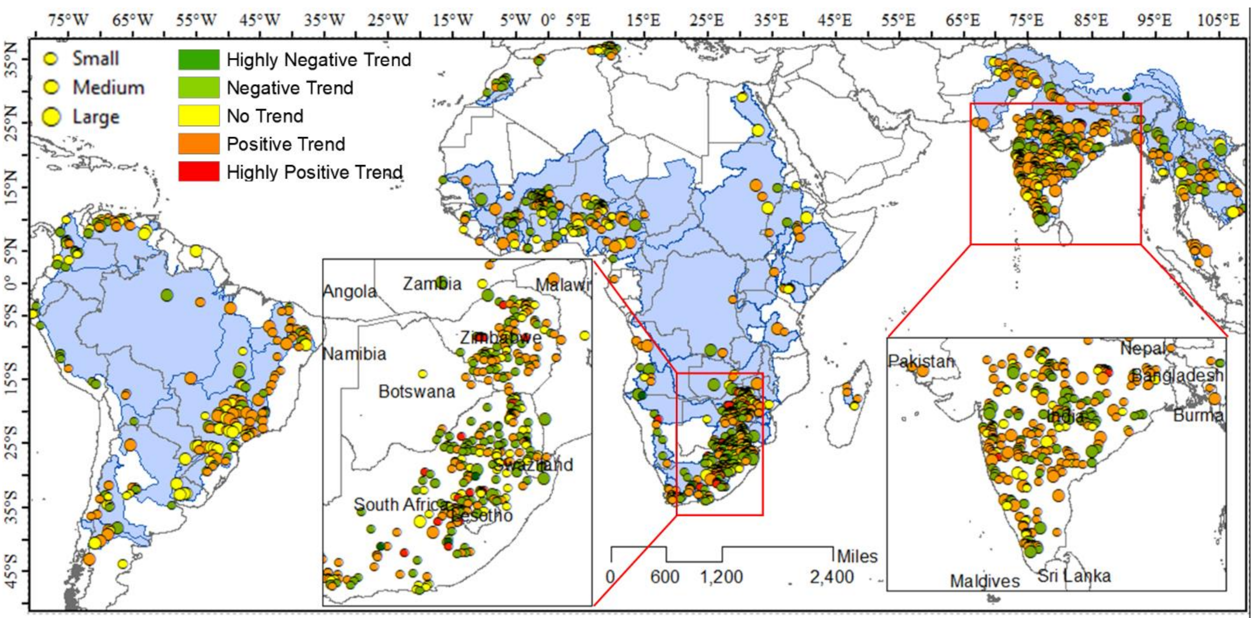

Figure 5.4 Trend of reservoir storage change included in the RAT framework. The left inset map shows South African reservoirs and the right inset map shows the South Asia region.

The cumulative storage change of different types of reservoirs in various river basins of the RAT domain is shown in figure 5.5 for a more visual and spatial comparison. Figure 5.5 shows that almost all types of reservoirs have experienced a net gain in storage in the South-East Asia region. In other words, these reservoirs have increased in their tendency to hedge or store strategically more rather than release. This could indicate accelerating hydropower development where higher storage equates to more hydropower (such as in the Mekong basin). More specifically, smaller reservoirs have experienced a highly positive trend in storage in the Ganges-

Brahmaputra Basin. Most of these dams have been constructed between 40-60 years (medium-aged reservoirs). This indicates that more water is being stored and then withdrawn laterally in recent times compared to the past. This may be attributed to the boom in agricultural activities after the green revolution of the 1970s to meet the gap between demand and supply of irrigation water need. Industrial development during the 1980s in that region might be a possible reason for more water abstraction via storage.

Figure 5.5 shows that older reservoirs in the South America region are showing a positive trend, all of which are small and large types of reservoirs. From the same figure, African basins are mostly experiencing a net loss in storage. Smaller reservoirs (old and medium-aged) have experienced a greater storage loss rate, which could imply that the reservoirs in those regions are either suffering from inflow reduction or an increase in downstream stakeholder release or a combination of both. Another potential reason for decreasing storage change in the Africa region might be the decrease in precipitation amount and evaporation increase from the reservoir surface.

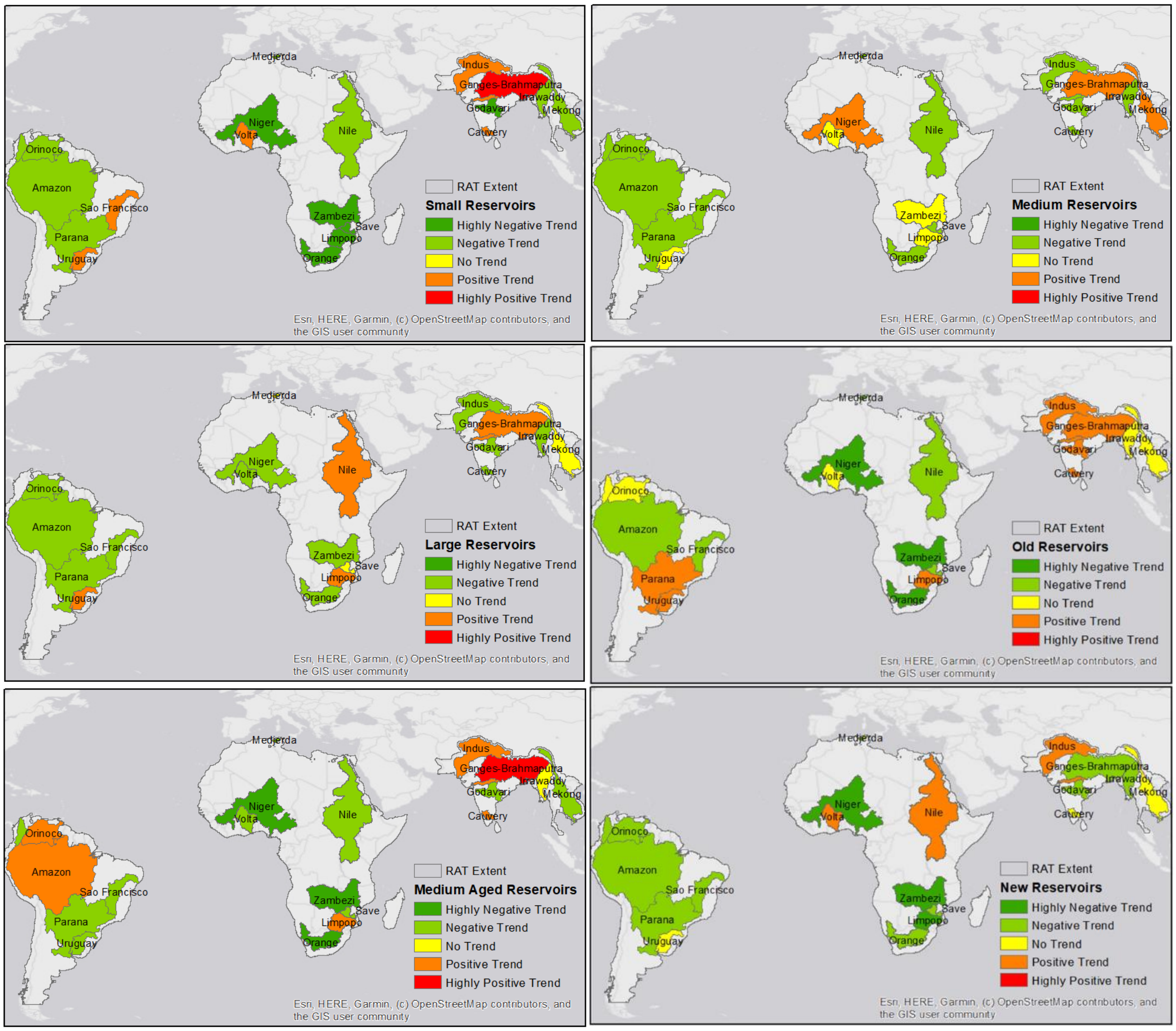

Figure 5.5 Storage change trend of different reservoirs of different river basins, upper left) Small reservoirs, upper right) Medium reservoirs, middle left) Large reservoirs, middle right) Old reservoirs, lower left) Medium aged reservoirs, lower right) Recent reservoirs

5.3.3 Comparison of storage change trends with the hydrologic trends

This study's second objective was performed by comparing the storage change trend with four key hydrologic parameters (i.e., precipitation, runoff, evaporation, and PDSI). All river basins and the variation in the spearman rank correlation coefficient are shown in figure 5.6. From figure 5.6, it can be seen that different sized dams have a unique correlation with each hydrologic parameters. For example, recent reservoirs of the Ganges-Brahmaputra basin have experienced a trend in storage change that follows the PDSI trend, whereas the correlation is negative for the old and medium-aged reservoirs. One potential reason for this could be that older reservoirs, by having lost more active storage through sedimentation, may have a higher tendency to store or hedge water more during droughts rather than release downstream. Also, in the South-East Asian reservoirs, the correlation of hydrologic parameters was not as pronounced as the other two regions (South America and Africa region). In general, Mekong, Orinocco, Zambezi, Orange, and Medjerda river basins have experienced storage change trends negatively correlated to PDSI. In most cases, recent reservoirs have experienced a stronger correlation than the medium-aged and old reservoirs. In the case of the Zambezi river basin, where negative correlations for PDSI, runoff, and precipitation and positive correlation with evaporation varies consistently with the age of the dams. This probably indicates that the recent reservoirs are now being operated more precisely by keeping in mind the limited water availability within the basin for other stakeholders. A similar pattern can be observed in other basins also.

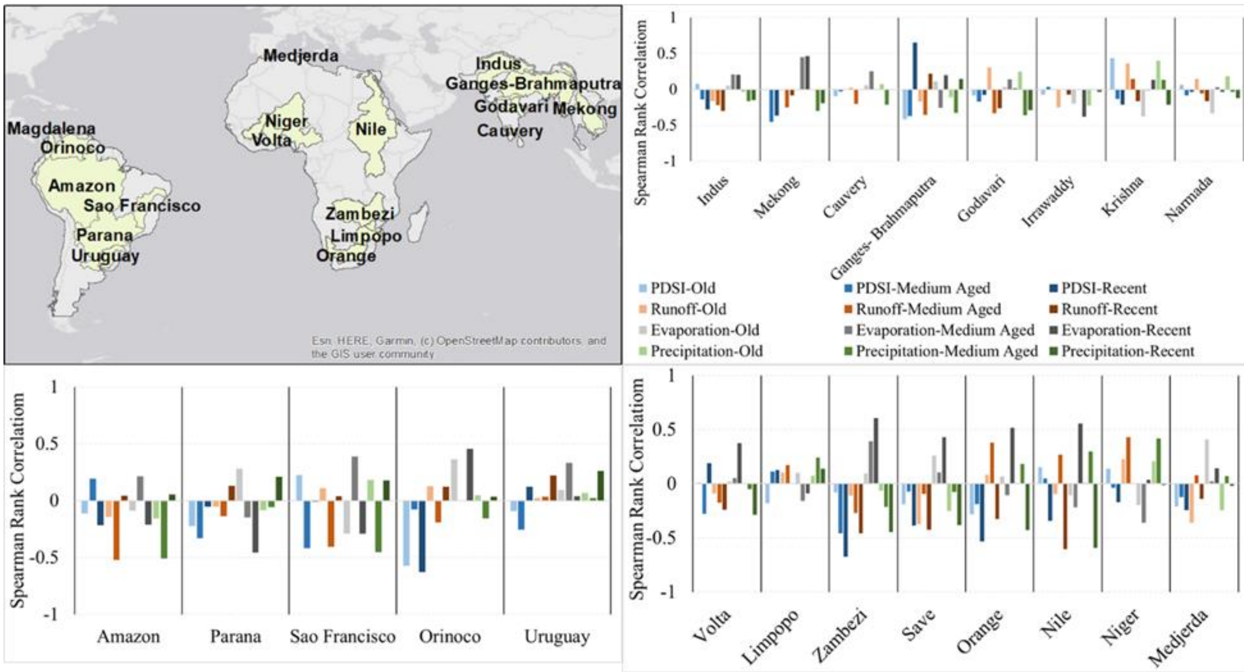

Figure 5.6 Spearman Rank Correlation Coefficient (between reservoir storage change and hydrologic parameters) comparison plot of the basins based on reservoir age. Upper left) Selected river basins, Upper right) Basins of South-East Asia, lower left) South American basins and lower right) African river basins.

River basins were also compared based on the size classes of reservoirs (figure 5.7). Different classes of reservoirs showed a more consistent pattern of storage change trends compared to the classes based on the dam age. Almost all river basins yielded a negative correlation with the PDSI except for a few reservoirs. Parana and Orinocco river basin have experienced storage increase during drought years by yielding the highest negative correlation with the PDSI. Narmada, Sao Francisco, Orinocco, and Zambezi basin showed a positive correlation with evaporation. A wide range of relationships was found in the case of South-East Asian reservoirs. For example, the Ganges-Brahmaputra basin shows a positive correlation with almost all hydrologic parameters. On the other hand, Mekong and Cauvery Basins showed an insignificant relationship with hydrologic parameters.

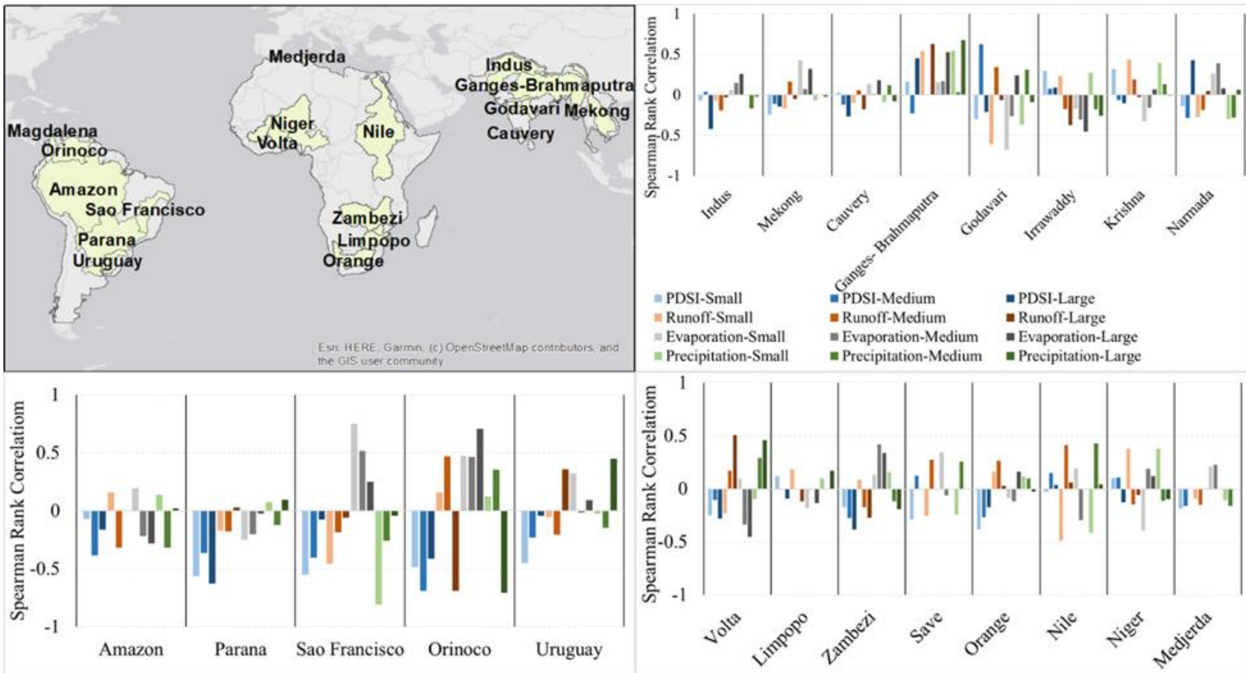

Figure 5.7 Spearman Rank Correlation Coefficient (between reservoir storage change and hydrologic parameters) comparison plot of the basins based on reservoir size. Upper left) Selected river basins, Upper right) Basins of South-East Asia, lower left) South American basins and lower right) African river basins.

From figures 5.5, 5.6, and 5.7, it is clear that the reservoirs in Africa region have experienced a decreasing trend in storage, with most of them showing a positive relationship with evaporation. This indicates that a recent increase in global temperature or hydro-climatic change may have directly affected the reservoir storage via increasing evaporation from the reservoir surface. Another combination of relationships can be seen in figure 5.8, where two river basins showed opposite relation with the PDSI. This also implies the spatial variability of the relationship for the different types of dams in different basins.

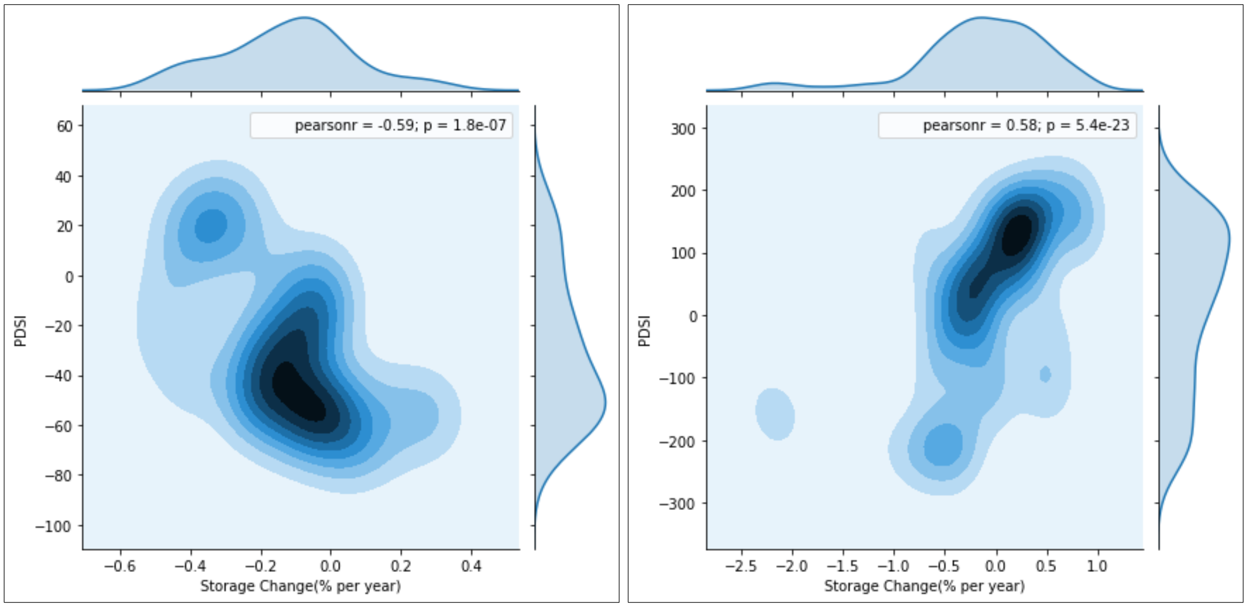

Figure 5.8 Kernel Density Estimation (KDE) plot of the storage change (% of the capacity of reservoirs per year) and hydrologic parameters which show opposite relationships; upper left) PDSI for the Parana River Basin, right) Godavari Basin

The Spearman rank correlation coefficient's variation is shown in figure 5.9 using a box plot comparison for the different sized and aged reservoirs. The variation of relationship with different hydrologic parameters for different reservoir classes is apparent from the box plot. From the left side of figure 5.9, it can be seen that the range of correlation decreases with the size of the reservoirs. However, some of the basins showed a very high correlation (both negative and positive) for large reservoirs, as shown by the presence of the box plot's outliers. In the case of comparison among the basins based on the dam age (shown on the right side of figure 5.9), it can be seen that the correlations are more pronounced in recent reservoirs compared to old reservoirs. This may indicate that the variability in hydrologic parameters is being considered in the operation of recently constructed dams (in other words, the operating rule curves are more aligned to recent changes in hydrologic variables).

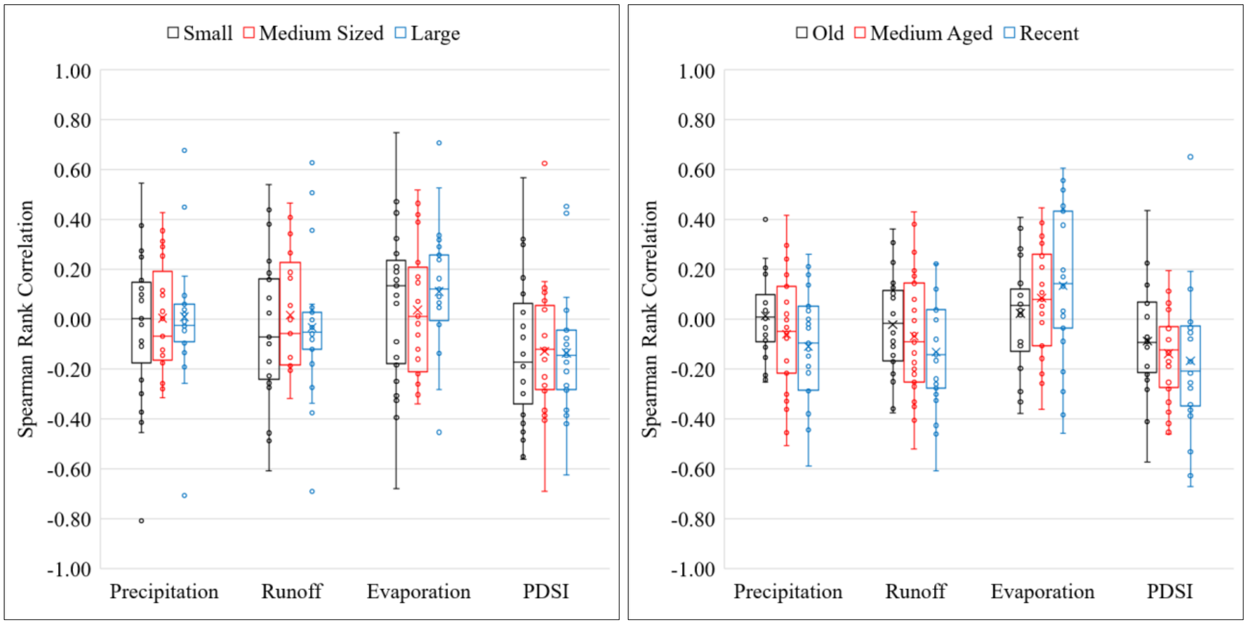

Figure 5.9 Box plot comparison of the spearman rank correlation coefficient between different types of reservoirs and

5.4 Conclusion

This study quantified the impact of multi-decadal reservoir operation on water availability in the ungauged regions of South/Southeast Asia, Africa, and South America. The data used in this study was prepared using a reservoir modeling framework called RAT, which consists of physically-based hydrological modeling and the latest available satellite observations. Multi-decadal observations of reservoir operations generated from the RAT framework was used to study the reservoir storage variability and identify the potential drivers of storage trend. The storage variability of the reservoirs was further quantified based on the dam size and age. The key findings of this study are as follows:

- Smaller reservoirs showed high variation in storage change trends compared to the medium and large reservoirs.

- Overall, South-East Asian reservoirs have been experiencing a net gain in storage, possibly due to more significant hedging and lesser downstream release driven by hydropower production plans.
- African reservoirs of all ages showed a highly negative trend in storage change, possibly due to the decrease in inflow and an increase in evaporation from the reservoir surface.
- The newer dams showed a more evident correlation with hydrologic parameters compared to the older reservoirs. This implies that newer reservoirs are likely being operated more realistically by following the recent alterations in the variability of hydrologic parameters.

Some potential future improvements can be considered from this study. A more comprehensive dam database (i.e., GOODD Database: Mulligan et al., 2020) can be used as a future study to perform a more detailed representation of reservoir variability. This study demonstrated one of the many potential applications of the RAT tool. This study's findings can facilitate better planning and management of existing dams and help the decision-makers in planning and construction of newer dams. Dam operators can make a more informed decision on adaptive reservoir management with revised reservoir operation based on this study's findings or integrate the RAT framework in their tools. The long-term observations of reservoir monitoring data have been made publicly accessible through http://www.satellitedams.net/ so that users, dam operators, decision-makers, and the scientific community can benefit from this study as well as from the publicly available RAT framework.

Chapter 6 Conclusion and Recommendation

The focus of this study was to use multi-mission satellite data to form a compound eye view. This compound eye view can help to minimize the dependency on the ground-based measurements and can also reduce the uncertainty associated with depending on a single satellite. It was shown that this technique could improve the conventional practice in operational water management, especially in the case of the data-scarce region and developing nations of the world. The whole study is broken into three major components, 1) monitoring, 2) forecasting, and 3) quantifying human impacts.

To address the study's monitoring component, a river monitoring system was established using multiple satellite data. The questions answered in this chapter are, a) how much improvement in river monitoring can be achieved using ancillary satellite platforms? And b) under what geophysical conditions do the use of information from ancillary satellite platforms maximize monitoring accuracy? More than 150 potential virtual stations were found over South and South-East Asia (more than 3500 locations worldwide) in response to the above questions. It was found that river morphology can consistently improve the estimation of heights in morphologically active rivers by 70% compared to the conventional methods. Also, SAR imagery platform based river morphology worked better than the Landsat visible imagery-based methods in estimating river heights.

The forecasting component of operational water management was studied as the second part of the study. Two key questions were answered in this part of the study. They are, a) what is the optimal combination of scale, time-step, and complexity for topographic and hydrometeorological data to produce forecasts? And b) what is the baseline accuracy of a forecasting system achievable using NWP weather forecasts? A fully end-to-end operational flash flood forecasting framework was developed by selecting the best combination of topographic and hydrometeorological observations for forecasting flash floods in the Northeast region of Bangladesh. The framework was able to produce a skillful flash flood early warning for up to 5 day lead time with an accuracy of more than 60% (more than 70% for up to 3-day lead time). Computation efficiency, scalability, and the framework's economic feasibility made it globally applicable in similar hydrologic-hydrodynamic conditions.

Regarding the human impact quantification component, the question answered was, can we build a reasonably skillful global monitoring framework for predicting the hydrologic impact of existing and planned reservoirs? A web-based framework was developed for near-realtime monitoring and impact analysis of 1598 reservoirs in South America, Africa, and South-East Asia. Different reservoir parameters (i.e., inflow, outflow, storage change) were calculated using satellite observations and a mass balance approach. The framework simulated storage change were compared with ground-based measurements of 77 reservoirs and found over 75% accuracy. At 25 different stations over large river basins across the domain, the framework simulated streamflow was compared with the in-situ streamflow and showed more than 60% accuracy.

Using the outputs from the RAT framework, long-term variability of the reservoirs studied. Multi-decadal observation of reservoir operation was used to quantify reservoir storage variability based on reservoir size, age, and hydro-climatic variability. Reservoir variability was compared with trends of four critical hydrologic parameters (precipitation, runoff, evaporation, and Palmer Drought Severity Index) to understand the role of natural drivers. It was found that the reservoirs in Africa were losing storage at a rate of more than 1% per year of the installed capacity. Also, in most cases, the drought index was found to be the predominant driver of change in storage.

There are some potential future improvements which can be considered as the future scope of this research. Study on the monitoring component of operational water management can be further explore through application of machine learning and deep learning approach. Deep learning, Artificial Neural Network (ANN), and other data based approaches can be applied to improve the accuracy of estimated river heights from satellite altimeter. Accuracy of the forecast of river levels/inundation discussed in the forecasting component can be further be improved by using more accurate topographic data sources (such as Lidar, surveyed DEM). Downscaling of the GFS forecast data can be a better source of the hydrologic and hydrodynamic modelling framework. Recent version of HecRAS software has the capability of ingesting spatial precipitation data which will improve the model accuracy in generating forecasts. The RAT framework generated outflow need to be validated against measured data to illustrate the model performance and to identify the error propagation through the modeling efforts. Sediment influxes can be incorporated into the framework while studying the impact on the reservoir storage variability. Gravity Recovery and Climate Experiment (GRACE) satellite-observed Total Water Storage can also be considered while comparing the long-term changes in storage variability of the reservoirs. Finally, satellite based observations of river temperature can provide another valuable information regarding the reservoir impacts.

Research completed in this dissertation has demonstrated that multi-mission satellite has a lot to offer in operational water management. The dissertation study filled the gap between ongoing scientific research and the operationalization of the unprecedented amount of untapped earth observation resources with the goal of moving the needle for societal application in the right direction. Water managers and policymakers could use the user-ready and user-oriented research presented in this dissertation for decision making and policy analysis. In transboundary basins, satellite observations can also be considered unbiased to all the parties and provide data needed to drive a fair and transparent water-sharing agreement. Future allocation of water resources will be more difficult due to growing demand and climate change impacts. This dissertation will help the scientific and hydrologic community cope with the projected future state of the climate, water demand, and land cover change, thus facilitating a more sustainable water resources management. The benefits of using multimission satellite observations over the conventional methods are shown in figure 5.1.

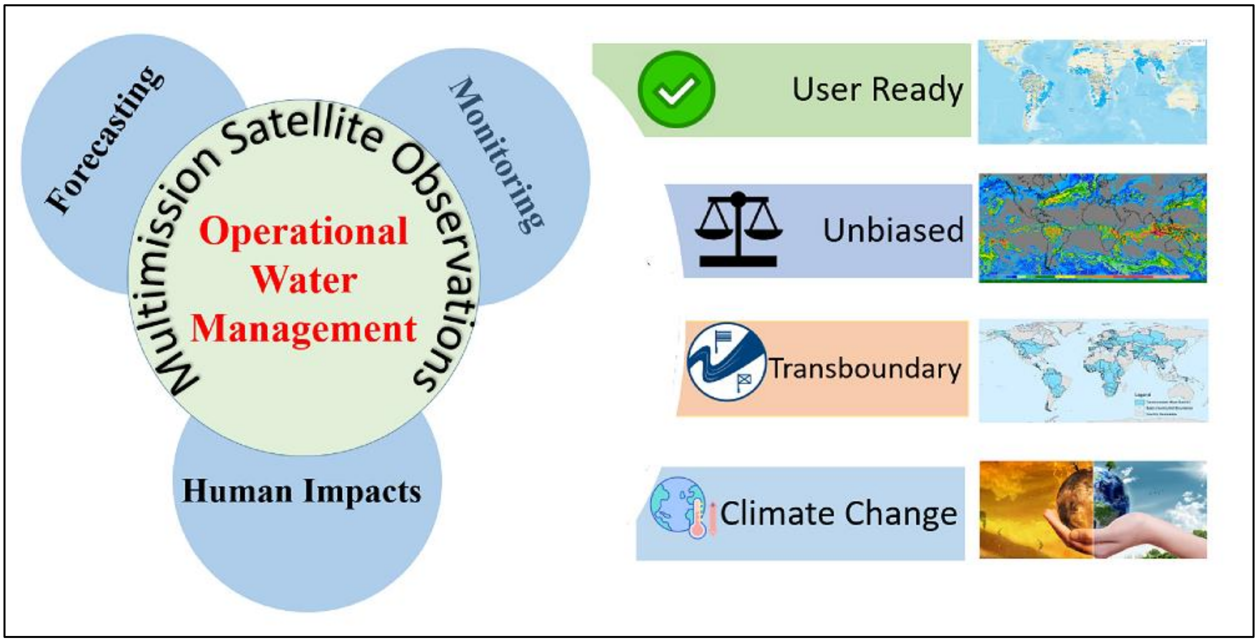

Figure 6.1 Benefits of multi-mission satellite observations

Bibliography

Abatzoglou, J. T., Dobrowski, S. Z., Parks, S. A., & Hegewisch, K. C. (2018). TerraClimate, a high-resolution global dataset of monthly climate and climatic water balance from 1958–2015. Scientific data, 5, 170191. https://doi.org/10.1038/sdata.2017.191

Abuzied, S. M., & Mansour, B. M. (2019). Geospatial hazard modeling for the delineation of flash flood-prone zones in Wadi Dahab basin, Egypt. Journal of Hydroinformatics, 21(1), 180-206. https://doi.org/10.2166/hydro.2018.043

Ahmad, S. K., Hossain, F., Eldardiry, H., & Pavelsky, T. M. (2019). A Fusion Approach for Water Area Classification Using Visible, Near Infrared and Synthetic Aperture Radar for South Asian Conditions. IEEE Transactions on Geoscience and Remote Sensing, 58(4), 2471-2480. https://doi.org/10.1109/TGRS.2019.2950705

Alsdorf, D. E., Rodriguez, E., & Lettenmaier, D. P. (2007). Measuring surface water from space. *Reviews of Geophysics*, *45*(2), 1–24. https://doi.org/10.1029/2006RG000197.1.

Andreadis, K. M., Schumann, G. J. P., & Pavelsky, T. (2013). A simple global river bankfull width and depth database. Water Resources Research, 49(10), 7164–7168. https://doi.org/10.1002/wrcr.20440

Aonashi, K., Awaka, J., Hirose, M., Kozu, T., Kubota, T., Liu, G., Shige, S., Kida, S., Seto, S., Takahashi, N., and Takayabu, Y. (2009). GSMaP Passive Microwave Precipitation Retrieval Algorithm : Algorithm Description and Validation. Journal of the Meteorological Society of Japan. 87A:119–136. https://doi.org/10.2151/jmsj.87a.119

Ashley, S., Ashley, W. (2008). Flood Fatalities in the United States. Journal of Applied Meteorology and Climatology. 47(3), 805–818. https://doi.org/10.1175/2007jamc1611.1

Berry, P. A. M., Garlick, J. D., Freeman, J. A., & Mathers, E. L. (2005). Global inland water monitoring from multi-mission altimetry. Geophysical Research Letters, 32(16), 1–4. https://doi.org/10.1029/2005GL022814

Biancamaria, S., Hossain, F., Lettenmaier, D.P. (2011). Forecasting transboundary river water elevations from space. Geophys. Res. Lett. 38, L11401. https://doi.org/10.1029/2011GL047290

Bierkens, M. F. P., Bell, V. A., Burek, P., Chaney, N., Condon, L., David, C. H., de Roo, A., Döll, P., Drost, N., Famiglietti, J. S., Flörke, M., Gochis, D. J., Houser, P., Hut, R., Keune, J., Kollet, S., Maxwell, R., Reager, J. T., Samaniego, L., Sudicky, E., Sutanudjaja, E. H., van de Giesen, N., Winsemius, H., and Wood, E. F. (2015). Hyper-resolution global hydrological modelling: what is next?, Hydrol. Process., 29, 310– 320. https://doi.org/10.1002/hyp.10391.

Birkett, C.M. (1995). The contribution of TOPEX/POSEIDON to the global monitoring of climatically sensitive lakes. J. Geophys. Res.: Oceans 100, 25179–25204.

Birkett, C. M. (1998). Monitoring of Large Rivers and Wetlands (B), 34(5), 1223–1239.

Birkett, C.M., Beckley, B. (2010). Investigating the performance of the JASON-2/OSTM radar altimeter over lakes and reservoirs. Marine Geodesy 33 (S1), 204–238. https://doi.org/10.1080/01490419.2010.488983.

Biswas, N. K., & Hossain, F. (2018). A scalable open-source web-analytic framework to improve satellite-based operational water management in developing countries. Journal of Hydroinformatics, 20 (1), 49–68. https://doi.org/10.2166/hydro.2017.073.

Biswas, N. K., Hossain, F., Bonnema, M., Okeowo, M. A., & Lee, H. (2019). An altimeter height extraction technique for dynamically changing rivers of South and South-East Asia. *Remote Sensing of Environment*, *221*, 24–37. https://doi.org/10.1016/j.rse.2018.10.033

Biswas, N. K., Hossain, F., Bonnema, M., Aminul Haque, A. M., Biswas, R. K., Bhuyan, A., & Hossain, A. (2020). A computationally efficient flash flood early warning system for a mountainous and transboundary river basin in Bangladesh. Journal of Hydroinformatics, 22(6), 1672-1692. https://doi.org/10.2166/hydro.2020.202

Biswas, N.K., Hossain, F., Bonnema, M., Lee, H., Chishtie, F. (2020). A Global Reservoir Assessment Tool for Predicting Hydrologic Impact and Operating Pattern of Existing and Planned Reservoirs, Environmental Modeling and Software (In revision).

Bonnema, M., & Hossain, F. (2017). Inferring reservoir operating patterns across the Mekong Basin using only space observations. *Water Resources Research*, *53*(5), 3791–3810. https://doi.org/10.1002/2016WR019978

Bonnema, M., Sikder, S., Miao, Y., Chen, X., Hossain, F., Ara Pervin, I., Mahbubur Rahman, S. M., and Lee, H. (2016), Understanding satellite-based monthly-to-seasonal reservoir outflow estimation as a function of hydrologic controls. Water Resources Research, 52(5), 4095–4115. https://doi.org/10.1002/2015WR017830.

Borga, M., Gaume, E., Creutin, J. D., & Marchi, L. (2008). Surveying flash floods: gauging the ungauged extremes Re-Analysis of Radar-Based Precipitation Estimates of the Flash-Flood Producing Storm. *Process*. https://doi.org/10.1002/hyp.7111

Bunn, S. E., & Arthington, A. H. (2002). Basic principles and ecological consequences of altered flow regimes for aquatic biodiversity. Environmental management, 30(4), 492-507. https://doi.org/10.1007/s00267-002-2737-0.

Calmant, S., & Seyler, F. (2006). Continental surface waters from satellite altimetry. Comptes Rendus - Geoscience, 338(14–15), 1113–1122. https://doi.org/10.1016/j.crte.2006.05.012

Carpenter, T., Sperfslage, J., Georgakakos, K., Sweeney, T., Fread, D. (1999) National threshold runoff estimation utilizing GIS in support of operational flash flood warning systems. Journal of Hydrology 224(1-2):21–44. https://doi.org/10.1016/s0022-1694(99)00115-8

Chen, S., Yu, P. (2007), Real-time probabilistic forecasting of flood stages. Journal of Hydrology, 340(1-2):63–77. https://doi.org/10.1016/j.jhydrol.2007.04.008

Chhipi-Shrestha, G., Hewage, K., & Sadiq, R. (2017). Water–energy–carbon nexus modeling for urban water systems: system dynamics approach. Journal of Water Resources Planning and Management, 143(6), 04017016. https://doi.org/10.1061/(ASCE)WR.1943-5452.0000765

Chiang, Y.M., Hsu, K., Chang, F., Hong, Y., Sorooshian, S. (2007). Merging multiple precipitation sources for flash flood forecasting. Journal of Hydrology. 340(3-4), 183–196. https://doi.org/10.1016/j.jhydrol.2007.04.007

Chipman, J. W. (2019). A multisensor approach to satellite monitoring of trends in lake area,water level, and volume. *Remote Sensing*. https://doi.org/10.3390/rs11020158

Crétaux, J. F., Jelinski, W., Calmant, S., Kouraev, A., Vuglinski, V., Bergé-Nguyen, M., ... & Maisongrande, P. (2011). SOLS: A lake database to monitor in the Near Real Time water level and storage variations from remote sensing data. Advances in space research, 47(9), 1497-1507. https://doi.org/10.1016/j.asr.2011.01.004.

Crochemore, L., Ramos, M. H., & Pappenberger, F. (2016). Bias correcting precipitation forecasts to improve the skill of seasonal streamflow forecasts. *Hydrology and Earth System Sciences*. https://doi.org/10.5194/hess-20-3601-2016

Crop Explorer for Major Crop Regions - United States Department of Agriculture. (n.d.). Retrieved February 26, 2018, from https://ipad.fas.usda.gov/cropexplorer/global_reservoir/

Dawson, D., VanLandeghem, M. M., Asquith, W. H., & Patiño, R. (2015). Long-term trends in reservoir water quality and quantity in two major river basins of the southern Great Plains. Lake and reservoir management, 31(3), 254-279. https://doi.org/10.1080/10402381.2015.1074324

Degu, A. M., Hossain, F., Niyogi, D., Pielke Sr, R., Shepherd, J. M., Voisin, N., & Chronis, T. (2011). The influence of large dams on surrounding climate and precipitation patterns. Geophysical Research Letters, 38(4). Geophysical Research Letters, 38(4). https://doi.org/10.1029/2010GL046482.

Diamantini, E., Lutz, S. R., Mallucci, S., Majone, B., Merz, R., & Bellin, A. (2018). Driver detection of water quality trends in three large European river basins. Science of the Total Environment, 612, 49-62. https://doi.org/10.1016/j.scitotenv.2017.08.172

Döll, P., Fiedler, K., & Zhang, J. (2009). Global-scale analysis of river flow alterations due to water withdrawals and reservoirs. Hydrology and Earth System Sciences, 13(12), 2413-2432. https://doi.org/10.5194/hess-13-2413-2009.

Döll, P., Kaspar, F., & Lehner, B. (2003). A global hydrological model for deriving water availability indicators: model tuning and validation. Journal of Hydrology, 270(1-2), 105-134. https://doi.org/10.1016/S0022-1694(02)00283-4.

Duan, Z., & Bastiaanssen, W. G. M. (2013). Estimating water volume variations in lakes and reservoirs from four operational satellite altimetry databases and satellite imagery data. Remote Sensing of Environment, 134, 403-416. https://doi.org/10.1016/j.rse.2013.03.010

Ehsani, N., Fekete, B. M., Vörösmarty, C. J., & Tessler, Z. D. (2016). A neural network based general reservoir operation scheme. Stochastic environmental research and risk assessment, 30(4), 1151-1166. https://doi.org/10.1007/s00477-015-1147-9.

Eldardiry, H., & Hossain, F. (2019). Understanding reservoir operating rules in the transboundary nile river basin using macroscale hydrologic modeling with satellite measurements. Journal of Hydrometeorology, 20(11), 2253-2269. https://doi.org/10.1175/JHM-D-19-0058.1

England, J.F., Velleux, M.L., Julien, P.Y. (2007). Two-dimensional simulations of extreme floods on a large watershed. Journal of Hydrology. 347(1-2), 229–241. https://doi.org/10.1016/j.jhydrol.2007.09.034

Escobar, H. (2015). WATER SECURITY: Drought triggers alarms in Brazil's biggest metropolis. Science, 347(6224). https://doi.org/10.1126/science.347.6224.812

FAO (Food and Agriculture Organization of the United Nations). 2007. Dams and agriculture in Africa. Prepared by the AQUASTAT programme. Rome, Italy: FAO. 14p. (accessed on August 19, 2020).

Fatichi, S., Vivoni, E. R., Ogden, F. L., Ivanov, V. Y., Mirus, B., Gochis, D., Downer, C.W., Camporese, M., Davison, J.H., Ebel, B., & Jones, N. (2016). An overview of current applications, challenges, and future trends in distributed process-based models in hydrology. Journal of Hydrology, 537, 45-60. https://doi.org/10.1016/j.jhydrol.2016.03.026.

Feyisa, G. L., Meilby, H., Fensholt, R., & Proud, S. R. (2014). Automated Water Extraction Index: A new technique for surface water mapping using Landsat imagery. Remote Sensing of Environment, 140, 23-35. https://doi.org/10.1016/j.rse.2013.08.029.

Fisher, A., Flood, N., & Danaher, T. (2016). Comparing Landsat water index methods for automated water classification in eastern Australia. Remote Sensing of Environment, 175, 167-182. https://doi.org/10.1016/j.rse.2015.12.055.

Flesch, T.K., Reuter, G.W. (2012). WRF Model Simulation of Two Alberta Flooding Events and the Impact of Topography. Journal of Hydrometeorology. 13(2), 695–708. https://doi.org/10.1175/jhm-d-11-035.1

Flood Situation Report (2017) ReliefWeb, 19 Apr. 2017, retrieved from reliefweb.int/. Accessed on 19 April 2019

Frappart, F., Calmant, S., Cauhope ´, M., Seyler, F., Cazenave, A. (2006). Preliminary results of ENVISAT RA-2 derived water levels validation over the Amazon basin. Rem. Sens. Environ. 100 (2), 252–264. https://doi.org/10.1016/j.rse.2005.10.027.

Funk, C., Peterson, P., Landsfeld, M., Pedreros, D., Verdin, J., Shukla, S., Husak, G., Rowland, J., Harrison, L., Hoell, A. & Michaelsen, J. (2015). The climate hazards infrared precipitation with stations- a new environmental record for monitoring extremes. Scientific data, 2, 150066. https://doi.org/10.1038/sdata.2015.66.

Gao, H. (2015). Satellite remote sensing of large lakes and reservoirs: from elevation and area to storage. Wiley Interdisciplinary Reviews: Water, 2(2), 147–157. https://doi.org/10.1002/wat2.1065

Gao, H., Birkett, C., & Lettenmaier, D. P. (2012). Global monitoring of large reservoir storage from satellite remote sensing. Water Resources Research, 48(9), 1–12. https://doi.org/10.1029/2012WR012063.

Gebregiorgis, A., & Hossain, F. (2011). How much can a priori hydrologic model predictability help in optimal merging of satellite precipitation products?. Journal of Hydrometeorology, 12(6), 1287-1298. https://doi.org/10.1175/JHM-D-10-05023.1.

Geological Survey, U. S. (1997). Global land cover characteristics data base. Http://Edc2.Usgs.Gov/Glcc/Globe_Int.Php.

Georgakakos, K.P. (1986). On the design of national real-time warning systems with capability for site-specific flash flood forecasts. Bulletin of American Meteorological Society. 67, 1233–1239. https://doi.org/10.1175/1520-0477(1986)067<1233:OTDONR>2.0.CO;2

Gerlak, A. K., Lautze, J., & Giordano, M. (2011). Water resources data and information exchange in transboundary water treaties. *International Environmental Agreements: Politics, Law and Economics*, *11*(2), 179–199. https://doi.org/10.1007/s10784-010-9144-4

Ghoneim E, Foody GM (2011) Assessing flash flood hazard in an arid mountainous region. Arabian Journal of Geosciences 6(4):1191–1202. https://doi.org/10.1007/s12517-011-0411-7

Gorelick, N., Hancher, M., Dixon, M., Ilyushchenko, S., Thau, D., & Moore, R. (2017). Google Earth Engine: Planetary-scale geospatial analysis for everyone. *Remote Sensing of Environment*, *202*. https://doi.org/10.1016/j.rse.2017.06.031

Govender, M., Chetty, K., & Bulcock, H. (2007). A review of hyperspectral remote sensing and its application in vegetation and water resource studies. *Water SA*. https://doi.org/10.4314/wsa.v33i2.49049

Grill, G., Lehner, B., Lumsdon, A. E., Macdonald, G. K., Zarfl, C., & Reidy Liermann, C. (2015). An index-based framework for assessing patterns and trends in river fragmentation and flow regulation by global dams at multiple scales. *Environmental Research Letters*. https://doi.org/10.1088/1748-9326/10/1/015001

Hall, A. C., Schumann, G. J. P., Bamber, J. L., Bates, P. D., & Trigg, M. A. (2012). Geodetic corrections to Amazon River water level gauges using ICESat altimetry. Water Resources Research, 48(6), 1–6. https://doi.org/10.1029/2011WR010895

Hanasaki, N., Kanae, S., & Oki, T. (2006). A reservoir operation scheme for global river routing models. Journal of Hydrology, 327(1-2), 22-41. https://doi.org/10.1016/j.jhydrol.2005.11.011.

Hapuarachchi, H. A. P., Wang, Q. J., & Pagano, T. C. (2011). A review of advances in flash flood forecasting. *Hydrological Processes*, *25*(18), 2771–2784. https://doi.org/10.1002/hyp.8040

Hennig, T. A., Kretsch, J. L., Pessagno, C. J., Salamonowicz, P. H., & Stein, W. L. (2001). The shuttle radar topography mission. In Lecture Notes in Computer Science (including subseries Lecture Notes in Artificial Intelligence and Lecture Notes in Bioinformatics). https://doi.org/10.1007/3-540-44818-7_11.

Hong, Y., Hsu, K.L., Sorooshian, S., Gao, X. (2004). Precipitation Estimation from Remotely Sensed Imagery Using an Artificial Neural Network Cloud Classification System. Journal of Applied Meteorology. 43(12), 1834–1853. https://doi.org/10.1175/jam2173.1

Hossain, F., Sikder, S., Biswas, N., Bonnema, M., Lee, H., Luong, N. D., Hiep, N.H. Du Duong, B., & Long, D. (2017). Predicting water availability of the regulated Mekong river basin using satellite observations and a physical model. Asian Journal of Water, Environment and Pollution, 14(3), 39-48. https://doi.org/10.3233/AJW-170024

Hossain, F., Serrat-Capdevila, A., Granger, S., Thomas, A., Saah, D., Ganz, D., … Akanda, A. S. (2016). A global capacity building vision for societal applications of earth observing systems and data: Key questions and recommendations. *Bulletin of the American Meteorological Society*, *97*(7), 1295–1299. https://doi.org/10.1175/BAMS-D-15-00198.1

Hossain, F., Bonnema, M., Biswas, N.K., Ahmad, S., Duong, B., & Luong, N. D. (2019). When floods cross borders, satellite data can help, Eos, 100.

Hsiao, L.F. et al. (2013). Ensemble forecasting of typhoon rainfall and floods over a mountainous watershed in Taiwan. Journal of Hydrology. 506, 55–68. https://doi.org/10.1016/j.jhydrol.2013.08.046

Huang, C., Chen, Y., Zhang, S., & Wu, J. (2018). Detecting, Extracting, and Monitoring Surface Water From Space Using Optical Sensors: A Review. *Reviews of Geophysics*, *56*(2), 333–360. https://doi.org/10.1029/2018RG000598

Huang, X., Xie, H., Zhang, G., & Liang, T. (2013). A novel solution for outlier removal of ICESat altimetry data: A case study in the Yili watershed, China. Frontiers of Earth Science, 7(2), 217–226. https://doi.org/10.1007/s11707-013-0362-2

Iqbal, N., Hossain, F., Lee, H., & Akhter, G. (2017). Integrated groundwater resource management in Indus Basin using satellite gravimetry and physical modeling tools. Environmental monitoring and assessment, 189(3), 128. https://doi.org/10.1007/s10661-017-5846-1

Jasper, K., Gurtz, J., Lang, H. (2002). Advanced flood forecasting in Alpine watersheds by coupling meteorological observations and forecasts with a distributed hydrological model. Journal of Hydrology. 267(1-2), 40–52. https://doi.org/10.1016/s0022-1694(02)00138-5

Jones, J. W. (2019). Improved automated detection of subpixel-scale inundation-revised Dynamic Surface Water Extent (DSWE) partial surface water tests. Remote Sensing, 11(4), 374. https://doi.org/10.3390/rs11040374.

Kansakar, P., & Hossain, F. (2016). A review of applications of satellite earth observation data for global societal benefit and stewardship of planet earth. *Space Policy*. https://doi.org/10.1016/j.spacepol.2016.05.005

Keys, T. A., & Scott, D. T. (2018). Monitoring volumetric fluctuations in tropical lakes and reservoirs using satellite remote sensing. Lake and Reservoir Management, 34(2), 154-166. https://doi.org/10.1080/10402381.2017.1402226

Khan, O., Mwelwa-Mutekenya, E., Crosato, A., & Zhou, Y. (2014). Effects of dam operation on downstream river morphology: the case of the middle Zambezi River. In Proceedings of the Institution of Civil Engineers-Water Management (Vol. 167, No. 10, pp. 585-600).

Kim, G., Barros, A. (2001). Quantitative flood forecasting using multisensor data and neural networks. Journal of Hydrology. 246(1-4), 45–62. https://doi.org/10.1016/s0022-

1694(01)00353-5

Kratzert, F., Klotz, D., Brenner, C., Schulz, K., & Herrnegger, M. (2018) Rainfall–runoff modelling using long short-term memory (LSTM) networks. Hydrol. Earth Syst. Sci, 22(11), 6005-6022.

Kubota, T., Shige, S., Hashizume, H., Aonashi, K.. Takahashi, N., Seto, S., Hirose, M., Takayabu, Y.N., Ushio, T., Nakagawa, K. (2007). Global Precipitation Map Using Satellite-Borne Microwave Radiometers by the GSMaP Project: Production and Validation. IEEE Transactions on Geoscience and Remote Sensing. 45(7),2259–2275. https://doi.org/10.1109/tgrs.2007.895337

Lauri, H., De Moel, H., Ward, P. J., Räsänen, T. A., Keskinen, M., & Kummu, M. (2012). Future changes in Mekong River hydrology: Impact of climate change and reservoir operation on discharge. *Hydrology and Earth System Sciences*. https://doi.org/10.5194/hess-16-4603-2012

Lee, H. (2008). Radar Altimetry Methods for Solid Earth Geodynamics Studies. Ph.D. Dissertation at Ohio State University, (489). Retrieved from http://www.geology.osu.edu/~jekeli.1/OSUReports/reports/report_489.pdf%5Cnpapers://29803081-7a18-4199-a903-38c6fcf8334a/Paper/p10465

Lee, H., Zhang, Y., Seo, D. J., & Xie, P. (2015). Utilizing satellite precipitation estimates for streamflow forecasting via adjustment of mean field bias in precipitation data and assimilation of streamflow observations. *Journal of Hydrology*. https://doi.org/10.1016/j.jhydrol.2015.08.057

Lee, H., Shum, C., Yi, Y., Ibaraki, M., Kim, J.-W., Braun, A., Kuo, C.- Y., Lu, Z. (2009). Louisiana wetland water level monitoring using retracked TOPEX/POSEIDON altimetry. Mar. Geodesy 32, 284–302. https://doi.org/10.1080/01490410903094767.

Lee, Y. H., Singh, V. (1999), Tank Model Using Kalman Filter. Journal of Hydrologic Engineering 4(4), 344–349. https://doi.org/10.1061/(asce)1084-0699(1999)4:4(344)

Lehner, B., Liermann, C. R., Revenga, C., Vörömsmarty, C., Fekete, B., Crouzet, P., … Wisser, D. (2011). High-resolution mapping of the world's reservoirs and dams for sustainable river-flow management. *Frontiers in Ecology and the Environment*, *9*(9), 494–502. https://doi.org/10.1890/100125

Lehner, B., & Grill, G. (2013). Global river hydrography and network routing: baseline data and new approaches to study the world's large river systems. Hydrological Processes, 27(15), 2171-2186. https://doi.org/10.1002/hyp.9740

Liang, X., Lettenmaier, D. P., Wood, E. F., & Burges, S. J. (1994). A simple hydrologically based model of land surface water and energy fluxes for general circulation models. Journal of Geophysical Research: Atmospheres, 99(D7), 14415-14428. https://doi.org/10.1029/94jd00483.

Liang, Q. and Smith, L.S. (2015) A high-performance integrated hydrodynamic modelling system for urban flood simulations, Journal of Hydroinformatics, 17 (4), pp. 518-533.

Liguori, S., Rico-Ramirez, M., Schellart, A., Saul, A. (2012). Using probabilistic radar rainfall nowcasts and NWP forecasts for flow prediction in urban catchments. Atmospheric Research 103, 80–95. https://doi.org/10.1016/j.atmosres.2011.05.004

Lin, P., Pan, M., Beck, H. E., Yang, Y., Yamazaki, D., Frasson, R., ... & Gleason, C. J. (2019). Global reconstruction of naturalized river flows at 2.94 million reaches. Water resources research, 55(8), 6499-6516.

Liu, C. (2016). Analysis of Sentinel-1 SAR data for mapping standing water in the Twente region, 37. Retrieved from www.itc.nl/library/papers_2016/msc/wrem/cliu.pdf

Liu, J., Wang, J., Pan, S., Tang, K., Li, C., Han, D. (2015). A real-time flood forecasting system with dual updating of the NWP rainfall and the river flow. Natural Hazards 77(2):1161–1182. https://doi.org/10.1007/s11069-015-1643-8

Lohmann, D., Raschke, E., Nijssen, B., & Lettenmaier, D. P. (1998). Regional scale hydrology: I. Formulation of the VIC-2L model coupled to a routing model. Hydrological sciences journal, 43(1), 131-141. https://doi.org/10.1080/02626669809492107.

Lugg, A., & Copeland, C. (2014). Review of cold water pollution in the Murray–Darling Basin and the impacts on fish communities. Ecological Management & Restoration, 15(1), 71-79. https://doi.org/10.1111/emr.12074.

Marcé, R., George, G., Buscarinu, P., Deidda, M., Dunalska, J., De Eyto, E., … Jennings, E. (2016). Automatic High Frequency Monitoring for Improved Lake and Reservoir Management. *Environmental Science and Technology*, *50*(20), 10780–10794. https://doi.org/10.1021/acs.est.6b01604

Martinis, S., Kuenzer, C., Wendleder, A., Huth, J., Twele, A., Roth, A., & Dech, S. (2015). Comparing four operational SAR-based water and flood detection approaches. International Journal of Remote Sensing, 36(13), 3519-3543. https://doi.org/10.1080/01431161.2015.1060647.

Maswood, M. and Hossain, F. (2016). Advancing River Modeling in Ungauged River Basins using Remote Sensing: The Case of Ganges-Brahmaputra-Meghna Basins. Journal of River Basin Management, 14(1), pp. 103-117. doi:10.1080/15715124.2015.1089250.

McFeeters, S. K. (1996). The use of the Normalized Difference Water Index (NDWI) in the delineation of open water features. International journal of remote sensing, 17(7), 1425-1432. https://doi.org/10.1080/01431169608948714.

Medina, C.E., Gomez-Enri, J., Alonso, J.J., Villares, P. (2008). Water level fluctuations derived from ENVISAT radar altimeter (RA-2) and in situ measurements in a subtropical waterbody: Lake Izabal (Guatemala). Rem. Sens. Environ. 112 (9), 3604–3617. doi:10.1016/j. rse.2008.05.001.

Meigh, J. R., McKenzie, A. A., & Sene, K. J. (1999). A grid-based approach to water scarcity estimates for eastern and southern Africa. Water Resources Management, 13(2), 85-115. https://doi.org/10.1023/A:1008025703712.

Michailovsky, C.I., McEnnis, S., Berry, P.A.M., Smith, R., Bauer- Gottwein, P. (2012). River monitoring from satellite radar altimetry in the Zambezi River basin. Hydrol. Earth Syst. Sci.

16, 2181–2192. doi:10.5194/hess-16-2181-2012.

Mishra, V., & Shah, H. L. (2018). Hydroclimatological Perspective of the Kerala Flood of 2018. Journal of the Geological Society of India, 92(5), 645-650. https://doi.org/10.1007/s12594-018-1079-3.

Muala, E., Mohamed, Y. A., Duan, Z., & van der Zaag, P. (2014). Estimation of reservoir discharges from Lake Nasser and Roseires Reservoir in the Nile Basin using satellite altimetry and imagery data. Remote Sensing, 6(8), 7522–7545. doi:10.3390/rs6087522

Mulligan, M., van Soesbergen, A., & Sáenz, L. (2020). GOODD, a global dataset of more than 38,000 georeferenced dams. Scientific Data, 7(1), 1-8. https://doi.org/10.1038/s41597-020-0362-5

Nachtergaele, F., Van Velthuizen, H., Verelst, L., Batjes, N., Dijkshoorn, K., Van Engelen, V., ... & Petri, M. (2008). Harmonized world soil database–Food and Agriculture Organization of the United Nations.

Neitsch, S. L., Arnold, J. G., Kiniry, J. R., Srinivasan, R., & Williams, J. R. (2001). Soil and water assessment tool (SWAT) user's manual version 2000. Grassland. Soil, and Water Research Laboratory & Blackland Research Center, USDA-ARS: Temple, TX.

Nijssen, B., & Lettenmaier, D. P. (2004). Effect of precipitation sampling error on simulated hydrological fluxes and states: Anticipating the Global Precipitation Measurement satellites. *Journal of Geophysical Research D: Atmospheres*. https://doi.org/10.1029/2003jd003497

Nijssen, B., O'donnell, G. M., Hamlet, A. F., & Lettenmaier, D. P. (2001). Hydrologic sensitivity of global rivers to climate change. Climatic change, 50(1-2), 143-175. https://doi.org/10.1023/A:1010616428763.

Nijssen, B., O'Donnell, G. M., Lettenmaier, D. P., Lohmann, D., & Wood, E. F. (2001). Predicting the discharge of global rivers. Journal of Climate, 14(15), 3307-3323. https://doi.org/10.1175/1520-0442(2001)014<3307:PTDOGR>2.0.CO;2.

Nilsson, C., Reidy, C. A., Dynesius, M., & Revenga, C. (2005). Fragmentation and flow regulation of the world's large river systems. Science, 308(5720), 405-408. https://doi.org/10.1126/science.1107887

Okamoto, K., Ushio, T., Iguchi, T., Takahashi, N., Iwanami, K. (2005). The global satellite mapping of precipitation (GSMaP) project. Proceedings. 2005 IEEE International Geoscience and Remote Sensing Symposium. IGARSS'05. https://doi.org/10.1109/igarss.2005.1526575

Okamoto, K., Takahashi, N., Iwanami, K., Shige, S., Kubota, T. (2008). High precision and high resolution global precipitation map from satellite data. 2008 Microwave Radiometry and Remote Sensing of the Environment. https://doi.org/10.1109/micrad.2008.4579485

Okeowo, M. A., Lee, H., Hossain, F., & Getirana, A. (2017). Automated Generation of Lakes and Reservoirs Water Elevation Changes from Satellite Radar Altimetry. IEEE Journal of Selected Topics in Applied Earth Observations and Remote Sensing, 10(8), 3465–3481. doi:10.1109/JSTARS.2017.2684081

Parry, L. (2013). Think the weather bad's here? Spare a thought for these Indian villagers who live in the wettest place in the world with 40 FEET of rain a year, Daily Mail, UK. 2013. Available online: http://www.dailymail.co.uk/news/article-2471421/Indias-Mawsynram-villagers-live-wettest-place-world-40-FEET-rain-year.html. Accessed on 24 March 2019

Pekel, J. F., Cottam, A., Gorelick, N., & Belward, A. S. (2016). High-resolution mapping of global surface water and its long-term changes. Nature, 540(7633), 418. https://doi.org/10.1038/nature20584.

Piotrowski, A., Napiórkowski, J.J., Rowiński, P. (2006). Flash-flood forecasting by means of neural networks and nearest neighbour approach-a comparative study. Nonlinear Processes in Geophysics. 13(4), 443–448. https://doi.org/10.5194/npg-13-443-2006

Pokhrel, Y., Hanasaki, N., Koirala, S., Cho, J., Yeh, P. J.-F., Kim, H., … Oki, T. (2012). Incorporating Anthropogenic Water Regulation Modules into a Land Surface Model. *Journal of Hydrometeorology*, *13*(1), 255–269. https://doi.org/10.1175/JHM-D-11-013.1

Pokhrel, Y. N., Koirala, S., Yeh, P. J. F., Hanasaki, N., Longuevergne, L., Kanae, S., & Oki, T. (2015). Incorporation of groundwater pumping in a global L and Surface Model with the representation of human impacts. Water Resources Research, 51(1), 78-96. https://doi.org/10.1002/2014WR015602

Ponchaut, F., Cazenave, A. (1998). Continental lake level variations from Topex/Poseidon (1993–1996). C.R. Acad. Sci. Ser. IIA Earth Planet. Sci. 326 (1), 13–20.

Quddus, M. (2009). Crop production growth in different agro-ecological zones of Bangladesh. Journal of the Bangladesh Agricultural University. 7(2), 351–360. https://doi.org/10.3329/jbau.v7i2.4746

Rao, Y.V.R., Hatwar, HR., Salah, A.K., Sudhakar, Y. (2007). An Experiment Using the High Resolution Eta and WRF Models to Forecast Heavy Precipitation over India. Pure and Applied Geophysics. 164(8-9), 1593–1615. https://doi.org/10.1007/s00024-007-0244-1

Roberts, N., Cole S, Forbes, RM, Moore, RJ., Boswell, D. (2009). Use of high-resolution NWP rainfall and river flow forecasts for advance warning of the Carlisle flood, north-west England. Meteorological Applications. 16(1), 23–34. https://doi.org/10.1002/met.94

Rougé, C., Tilmant, A., Zaitchik, B., Dezfuli, A., & Salman, M. (2018). Identifying key water resource vulnerabilities in data-scarce transboundary river basins. Water Resources Research, 54(8), 5264-5281. https://doi.org/10.1029/2017WR021489

Sajikumar, N., & Thandaveswara, B. S. (1999) A non-linear rainfall–runoff model using an artificial neural network. Journal of hydrology, 216(1-2), 32-55.

Sangati, M. (2009). Flash Flood Analysis and Modelling. Risk Management. Dissertation, Università Degli Studi Di Padova

Santos da Silva, J., Calmant, S., Seyler, F., Rotunno Filho, O. C., Cochonneau, G., & Mansur, W. J. (2010). Water levels in the Amazon basin derived from the ERS 2 and ENVISAT radar altimetry missions. Remote Sensing of Environment, 114(10), 2160–2181. doi:10.1016/j.rse.2010.04.020

Schwatke, C., Dettmering, D., Bosch, W., & Seitz, F. (2015). DAHITI - An innovative approach for estimating water level time series over inland waters using multi-mission satellite altimetry. Hydrology and Earth System Sciences, 19(10). doi:10.5194/hess-19-4345-2015

Schulla, J., Jasper, K. (2000). Model description of WaSiM-ETH, IAC ETH Zu¨rich, p166.

Sharma, S., Siddique, R., Reed, S., Ahnert, P., & Mejia, A. (2019). Hydrological model diversity enhances streamflow forecast skill at short-to medium-range timescales. *Water Resources Research*. https://doi.org/10.1029/2018WR023197

Sheffield, J., Wood, E. F., Pan, M., Beck, H., Coccia, G., Serrat-Capdevila, A., & Verbist, K. (2018). Satellite Remote Sensing for Water Resources Management: Potential for Supporting Sustainable Development in Data-Poor Regions. *Water Resources Research*. https://doi.org/10.1029/2017WR022437

Shih, D.S., Chen, C.H., Yeh, G.T. (2014). Improving our understanding of flood forecasting using earlier hydro-meteorological intelligence. Journal of Hydrology. 512, 470–481. https://doi.org/10.1016/j.jhydrol.2014.02.059

Shiklomanov, A. I., Lammers, R. B., & Vörösmarty, C. J. (2002). Widespread decline in hydrological monitoring threatens Pan-Arctic research. *Eos*. https://doi.org/10.1029/2002EO000007

Siddique-E-Akbor, A. H. M., Hossain, F., Sikder, S., Shum, C. K., Tseng, S., Yi, Y., … Limaye, A. (2014). Satellite Precipitation Data–Driven Hydrological Modeling for Water Resources Management in the Ganges, Brahmaputra, and Meghna Basins. *Earth Interactions*, *18*(17), 1–25. https://doi.org/10.1175/EI-D-14-0017.1

Sikder, M. S., & Hossain, F. (2015). Understanding the geophysical sources of uncertainty for satellite interferometric (SRTM)-based discharge estimation in river deltas: The case for Bangladesh. *IEEE Journal of Selected Topics in Applied Earth Observations and Remote Sensing*. https://doi.org/10.1109/JSTARS.2014.2326893

Sikder, M. S., Hossain, F. (2016). Assessment of the weather research and forecasting model generalized parameterization schemes for advancement of precipitation forecasting in monsoon-driven river basins. Journal of Advances in Modeling Earth Systems. 8(3), 1210–1228. https://doi.org/10.1002/2016ms000678

Sikder, M. S., & Hossain, F. (2019). Improving operational flood forecasting in monsoon climates with bias-corrected quantitative forecasting of precipitation. *International Journal of River Basin Management*. https://doi.org/10.1080/15715124.2018.1476368

Sikder, M. T., & Elahi, K. M. (2013). Environmental degradation and global warming-consequences of Himalayan mega dams. American Journal of Environmental Protection, 2(1), 1-9. https://doi.org/10.11648/j.ajep.20130201.11.

Simons, F., Busse, T., Hou, J., Özgen, I., and Hinkelmann, R. (2014) A model for overland flow and associated processes within the Hydroinformatics Modelling System, Journal of Hydroinformatics, 16 (2), pp. 375-391. https://doi.org/10.2166/hydro.2013.173

Solander, K. C., Reager, J. T., & Famiglietti, J. S. (2016). How well will the Surface Water and

Ocean Topography (SWOT) mission observe global reservoirs?. Water Resources Research, 52(3), 2123-2140. https://doi.org/10.1002/2015WR017952.

Solander, K. C., Reager, J. T., Thomas, B. F., David, C. H., & Famiglietti, J. S. (2016). Simulating human water regulation: The development of an optimal complexity, climate-adaptive reservoir management model for an LSM. Journal of Hydrometeorology, 17(3), 725-744. https://doi.org/10.1175/JHM-D-15-0056.1.

Sousa, P. M., Blamey, R. C., Reason, C. J., Ramos, A. M., & Trigo, R. M. (2018). The 'Day Zero'Cape Town drought and the poleward migration of moisture corridors. Environmental Research Letters, 13(12), 124025. https://doi.org/10.1088/1748-9326/aaebc7

Sulistioadi, Y. B., Tseng, K.-H., Shum, C. K., Hidayat, H., Sumaryono, M., Suhardiman, A., Setiawan, F., and Sunarso, S. (2015). Satellite radar altimetry for monitoring small rivers and lakes in Indonesia. Hydrology and Earth System Sciences, 19(1), 341–359. doi:10.5194/hess-19-341-2015

Sweeney, T.L. (1992). Modernized areal flash flood guidance. NOAA Technical report NWS HYDRO 44, Hydrologic Research Laboratory, National Weather Service, NOAA, Silver Spring, MD, October, 21pp.

Swenson, S., & Wahr, J. (2009). Monitoring the water balance of Lake Victoria, East Africa, from space. Journal of Hydrology, 370 (4-Jan). https://doi.org/10.1016/j.jhydrol.2009.03.008.

Thu, H. N., & Wehn, U. (2016). Data sharing in international transboundary contexts: The Vietnamese perspective on data sharing in the Lower Mekong Basin. *Journal of Hydrology*. https://doi.org/10.1016/j.jhydrol.2016.02.035

Tourian, M. J., Elmi, O., Chen, Q., Devaraju, B., Roohi, S., & Sneeuw, N. (2015). A spaceborne multisensor approach to monitor the desiccation of Lake Urmia in Iran. *Remote Sensing of Environment*. https://doi.org/10.1016/j.rse.2014.10.006

Tourian, M. J., Tarpanelli, A., Elmi, O., Qin, T., Brocca, L., Moramarco, T., & Sneeuw, N. (2016). Spatiotemporal densification of river water level time series by multimission satellite altimetry. Water Resources Research, 52(2), 1140–1159. doi:10.1002/2015WR017654

Tucker, C. J., & Choudhury, B. J. (1987). Satellite remote sensing of drought conditions. *Remote Sensing of Environment*. https://doi.org/10.1016/0034-4257(87)90040-X

Udall, B., & Overpeck, J. (2017). The twenty-first century Colorado River hot drought and implications for the future. Water Resources Research, 53(3), 2404-2418. https://doi.org/10.1002/2016WR019638

Ushio, T., Kubota, T., Shige, S., Okamoto, K., Aonashi, K., Inoue, T., Takahashi, N., Iguchi, T., Kachi, M., Oki, R., Morimoto, T., Kawasaki, Z. (2009). A Kalman Filter Approach to the Global Satellite Mapping of Precipitation (GSMaP) from Combined Passive Microwave and Infrared Radiometric Data. Journal of the Meteorological Society of Japan. 87A, 137–151. https://doi.org/10.2151/jmsj.87a.137

Vachaud, G., Passerat de Silans, A., Balabanis, P., & Vauclin, M. (1985). Temporal stability of spatially measured soil water probability density function. Soil Science Society of America

Journal, 49(4), 822-828. https://doi.org/10.2136/sssaj1985.03615995004900040006x

Verbunt, M., Zappa, M., Gurtz, J., Kaufmann, P. (2006). Verification of a coupled hydrometeorological modelling approach for alpine tributaries in the Rhine basin. Journal of Hydrology. 324(1-4), 224–238. https://doi.org/10.1016/j.jhydrol.2005.09.036

Voisin, N., Li, H., Ward, D., Huang, M., Wigmosta, M., & Leung, L. R. (2013). On an improved sub-regional water resources management representation for integration into earth system models. Hydrology and Earth System Sciences, 17(9), 3605-3622. https://doi.org/10.5194/hess-17-3605-2013.

Vörösmarty, C., Hinzman, L., Peterson, B., Bromwich, D., Hamilton, L., Morison, J., … Webb, R. (2002). Arctic-champ: A program to study arctic hydrology and its role in global change. *Eos*. https://doi.org/10.1029/2002EO000167

Wang, W. C., Chau, K. W., Qiu, L., & Chen, Y. B. (2015) Improving forecasting accuracy of medium and long-term runoff using artificial neural network based on EEMD decomposition. Environmental research, 139, 46-54.

Ward, F. A. (2013). Forging sustainable transboundary water-sharing agreements: Barriers and opportunities. *Water Policy*. https://doi.org/10.2166/wp.2012.003

WCD. (2000). Dams and development: a new framework for decision-making. Earthscan Publications, London, UK.

Wisser, D., Frolking, S., Hagen, S., & Bierkens, M. F. (2013). Beyond peak reservoir storage? A global estimate of declining water storage capacity in large reservoirs. Water Resources Research, 49(9), 5732-5739. https://doi.org/10.1002/wrcr.20452

Woldemichael, A. T., Hossain, F., Pielke, R., & Beltrán-Przekurat, A. (2012). Understanding the impact of dam-triggered land use/land cover change on the modification of extreme precipitation. *Water Resources Research*. https://doi.org/10.1029/2011WR011684

Wu, H., Kimball, J. S., Mantua, N., & Stanford, J. (2011). Automated upscaling of river networks for macroscale hydrological modeling. Water Resources Research, 47(3). https://doi.org/10.1029/2009WR008871.

Wu, J., Liu, H., Wei, G., Song, T., Zhang, C., & Zhou, H. (2019). Flash flood forecasting using support vector regression model in a small mountainous catchment. *Water (Switzerland)*. https://doi.org/10.3390/w11071327

Xu, H. (2006). Modification of normalised difference water index (NDWI) to enhance open water features in remotely sensed imagery. International journal of remote sensing, 27(14), 3025-3033. https://doi.org/10.1080/01431160600589179

Yatheendradas, S., Wagener, T., Gupta, H., Unkrich, C., Goodrich, D., Schaffner, M., & Stewart, A. (2008). Understanding uncertainty in distributed flash flood forecasting for semiarid regions. *Water Resources Research*. https://doi.org/10.1029/2007WR005940

Yoon, Y., Kumar, S. V., Forman, B. A., Zaitchik, B. F., Kwon, Y., Qian, Y., … Mukherjee, A. (2019). Evaluating the uncertainty of terrestrial water budget components over high mountain

Asia. *Frontiers in Earth Science*. https://doi.org/10.3389/feart.2019.00120

Yoshikawa, S., Cho, J., Yamada, H. G., Hanasaki, N., & Kanae, S. (2014). An assessment of global net irrigation water requirements from various water supply sources to sustain irrigation: rivers and reservoirs (1960–2050). Hydrology and Earth System Sciences, 18(10), 4289-4310. https://www.doi.org/10.5194/hess-18-4289-2014

Yue, S., Pilon, P., & Cavadias, G. (2002). Power of the Mann–Kendall and Spearman's rho tests for detecting monotonic trends in hydrological series. Journal of hydrology, 259(1-4), 254-271. https://doi.org/10.1016/S0022-1694(01)00594-7

Zarfl, C., Lumsdon, A. E., Berlekamp, J., Tydecks, L., & Tockner, K. (2014). A global boom in hydropower dam construction. *Aquatic Sciences*, *77*(1), 161–170. https://doi.org/10.1007/s00027-014-0377-0

Zhang, S., & Gao, H. (2016). A novel algorithm for monitoring reservoirs under all-weather conditions at a high temporal resolution through passive microwave remote sensing. *Geophysical Research Letters*. https://doi.org/10.1002/2016GL069560

Zhao, G., & Gao, H. (2018). Automatic Correction of Contaminated Images for Assessment of Reservoir Surface Area Dynamics. *Geophysical Research Letters*, *45*(12), 6092–6099. https://doi.org/10.1029/2018GL078343